



Dipl.-Ing. Daniel Franz Treffer, Bsc

Pharmaceutical Hot Melt Extrusion - Novel Tools for Screening and Processing

DOCTORAL THESIS

to achieve the university degree of
Doktor der technischen Wissenschaften

submitted to

Graz University of Technology

Supervisor

Univ.-Prof. Dipl.-Ing. Dr. techn. Johannes Khinast

Institute of Process and Particle Engineering
Graz University of Technology

AFFIDAVIT

I declare that I have authored this thesis independently, that I have not used other than the declared sources/resources, and that I have explicitly indicated all material which has been quoted either literally or by content from the sources used. The text document uploaded to TUGRAZonline is identical to the present doctoral thesis.

16.12.16

Date



Signature

Dipl.-Ing. Daniel Franz Treffer, BSc.

Pharmaceutical Hot Melt Extrusion - Novel Tools for Screening and Processing

Dissertation

First assessor

Univ.-Prof. Dipl.-Ing. Dr. techn. Johannes Khinast
Institute of Process and Particle Engineering
Graz University of Technology
Research Center Pharmaceutical Engineering GmbH

Second assessor

Univ.-Prof. Dipl.-Ing. Dr. techn. Matthäus Siebenhofer
Institute of Chemical Engineering and Environmental Technology
Graz University of Technology

Copyright ©2016 Daniel Treffer

All rights reserved. No part of the material protected by this copyright notice may be reproduced or utilized in any form or by any means, electronically or mechanical, including photocopying, recording or by any information storage and retrieval system with written permission from the author.

Acknowledgement

This work was carried out during the years 2011-2016 at the Institute of Process and Particle Engineering at Graz University of Technology as well as at the Research Centre of Pharmaceutical Engineering (RCPE). The combination of both institutes provided an excellent breeding ground for my work. I would like to show my greatest appreciation to Professor Johannes Khinast for giving me an interesting and broad research topic and the unrestricted opportunity to develop myself. My gratitude is extended to Dr. Thomas Klein for his continuous support with his entrepreneurial abilities during the start-up of my company MeltPrep GmbH, which is based on the findings of this thesis. I acknowledge Professor Matthäus Siebenhofer for being the second assessor of my thesis and Assistant Professor Heidrun Gruber-Wölfler for being the chairwomen of my PhD defense.

Equally, I owe a great debt to Johann Grubbauer, who transformed my sketchy ideas into working prototypes. The fruitful discussions with him influenced my personal way of approaching challenges and led to countless simple solutions of formerly complex problems in the experimental parts of this work. My special thanks go to Andreas Eitzlmayr, Theresa Hörmann, Wolfgang Eberl, Christian Witz, Peter Neugebauer, Sarah Zellnitz, Simone Eder, Johannes Gursch, Otto Scheibelhofer, Daniel Markl, Josip Matic, and Alexander Troiss for their intense exchange of expertise during our studies, and I am very pleased to count them to my friends. I would like to thank all industrial partners in my research projects. In particular, I would like to thank Christian Makert, Reinhardt-Karsten Mürb, and Stefan Deiss, for their endless support and the industrial conversion of the thermally decoupled extrusion die plate.

I am indebted to all my colleagues at the RCPE and at the University Institute for their support and inspiration during my work. I would like to thank the teams from the laboratory and the technical center at RCPE, as well as the administration teams of both organizations. Furthermore, I would like to thank all students that I met and (co-)supervised during my work. I remember fondly all the inspiring discussions with them, in particular with Theresa Hörmann, Alexander Troiss, Daniela Fiedler, Simon Rustige, Michael Essl, Clemens Smola, Martin Landfahrer, Rosemarie Scharf,

Martina Kautsch and Hannes Bauer. In addition, I am grateful for all the unforgettable social gatherings with colleagues, students and friends during my time as a student.

I would also like to thank the Austrian Funding Agencies (Federal Ministries BMVIT and BMWFV, Styrian Funding Agency (SFG), FFG and the Austria Wirtschaftsservice GmbH (AWS)) for their financial support of my research.

Furthermore, I would like to thank Magdalena Makk for proof reading many parts of my thesis.

Last but definitely not least I would like to thank my family for their continuous support on the over 31 years long way leading up to this achievement.

Thank you all!

Daniel Treffer

Kurzfassung

Die pharmazeutische Schmelzextrusion ist eine Schlüsseltechnologie zur Herstellung von modernen Arzneiformen. Viele der neuen Wirkstoffe sind als Reinstoff nur schlecht für den Körper resorbierbar und erfordern die Verarbeitung hin zu festen Dispersionen mit geeigneten Trägermaterialien. Die Schmelzextrusion ist ein vielversprechender Prozess zur Verbesserung der Resorptionsfähigkeit. Der Prozess wurde aus der Kunststoffindustrie für pharmazeutische Anwendungen adaptiert, die Rahmenbedingungen der pharmazeutischen Anwendung stellen allerdings auch andere Anforderungen an die Prozesstechnik: die Materialien sind vor allem in frühen Entwicklungsstadien teuer, die Produktionsmengen sind klein, und die Ausgangsstoffe sind oft nur als feinste Pulver verfügbar, welche zumeist sensitiv gegenüber thermischer und mechanischer Belastung sind. Die notwendigen Stoffdaten zur Prozessauslegung stehen, aufgrund der starken Wechselwirkungen zwischen den Formulierungsbestandteilen nicht zur Verfügung.

Die vorliegende Arbeit untersucht zwei offene Herausforderungen bei der Übertragung der Prozesstechnik von der Kunststoffindustrie in die Pharmaindustrie.

(1) Wie können die Materialeigenschaften, im speziellen die rheologischen Eigenschaften von Formulierungen aus unterschiedlichen Substanzen präzise und mit geringen Materialeinsatz bestimmt werden? Die klassischen Probenvorbereitungsmethoden sind langwierig, verursachen dadurch Degradation, und sind nur bedingt auf feine Pulver anwendbar. Deshalb wurde ein neues Vakuumkompressionsverfahren entwickelt, welches Pulver verlustfrei, schnell und dadurch auch degradationsfrei in homogene Probekörper überführt. Die Probenkammer wird durch PTFE Trennfolien geformt und bietet den einzigartigen Vorteil, dass sich die Geometrie der Kammer an das Probenvolumen während des Prozesses anpassen kann. Dadurch können Dichteänderungen, welche sich im Laufe des Kompaktierens, des Schmelzens und des anschließenden Erstarrens ergeben, kompensiert werden. Das neue Verfahren wurde zur Bestimmung der rheologischen Eigenschaften von degradationssensitiven Polymeren getestet und bietet Vorteile hinsichtlich der Genauigkeit der Messwerte und deren Reproduzierbarkeit.

(2) Wieso kleben manche Formulierungen am Prozessequipment an und verhindern dadurch die störungsfreie Verarbeitung? Als Downstream-Equipment zur Schmelzextrusion kommt oft der Trockenheißabschlag zum Einsatz. Dieser Prozess schneidet das austretende Material im hochviskosen Zustand, dadurch entstehen rundliche Pellets. Bislang war der Prozess jedoch nur auf nicht klebrige Substanzen und somit auch nur auf einen geringen Anteil der Formulierungen anwendbar. Im ersten Schritt wurde die Ursache für das Ankleben der Schmelze am Schneidewerkzeug untersucht und die zu hohe Kontakttemperaturen als entscheidendes Problem identifiziert. In der Literatur gab es keine Untersuchungen zum Klebeverhalten unter nicht-isothermen Bedingungen, deshalb wurde dieser Bereich genauer betrachtet und die Kontakttemperatur-Klebe-Hypothese aufgestellt. Diese besagt, dass die Kontakttemperatur zwischen Extrudat und Schneidewerkzeug unterhalb des Erweichungspunktes des Extrudats liegen muss, damit benetzen des Werkzeuges und das Ausbilden hoher Adhäsionskräfte vermieden werden kann. Die Hypothese mit kontrollierten nicht-isothermen Klebrigkeitstests bestätigt. Mit dieser Erkenntnis wurde der Wärmehaushalt eines Trockenheißabschlags analysiert. Die Messer sind typischerweise thermisch an die Extrusionskanäle gekoppelt und somit auf Temperaturen oberhalb des Erweichungspunktes. Der Wärmehaushalt wurde geändert und die Extrusionskanäle thermisch vom Schneidewerkzeug getrennt. Dies ermöglicht das Absenken der Messertemperaturen, ohne dass die Extrusionskanäle einfrieren. Die Verarbeitung von klebrigen Substanzen wurde dadurch erstmals ermöglicht. Des Weiteren, wurde ein bildgebendes Analysesystem zum Monitoring der Pelletabmessungen implementiert.

Abstract

The pharmaceutical hot melt extrusion (HME) is a key technology for the production of modern dosage forms. In their pure form, a lot of the new active pharmaceutical ingredients of drugs are very hard to absorb by the human body. Therefore, to ensure a better bodily absorption, they are processed, together with a polymeric substrate, to form solid dispersions. HME is a promising process for the improvement of resorption capacity. The process, which has origins in the plastics industry, was adapted for pharmaceutical use. However, the overall conditions of pharmaceutical usage demand other requirements from the process technology: the materials are expensive, especially in the early production stages, the production output is small, and the raw materials are often only available in the form of fine powders, which on top of that, are in the most cases sensitive towards thermal and mechanical stress. Because of the strong interactions between the formulation ingredients, the required material data for process design is not available.

This thesis investigates two unsettled challenges posed by the application of the process technology from the plastics industry into the pharmaceutical industry.

(1) How can material properties, especially rheological characteristics of formulations consisting of different substances, be determined precisely and using little material input? The conventional methods used for specimen preparation need long set-up times, thereby causing degradation, and are only of limited suitability for fine powders. Thus, a new Vacuum Compression Molding (VCM) process was developed, which converts powders lossless and quickly, and therefore also without degradation, into homogeneous specimens. The sample chamber is formed by PTFE foils, and provides the unrivalled advantage of being able to adapt the chamber's geometry to the sample volume during the process. Thereby, changes in density, which occur during the compacting, melting and subsequent solidifying, can be compensated. The new process was tested on the rheological properties of polymers sensitive to degradation, and provides advantages in regard to the accuracy of measurements, as well as their reproducibility.

(2) Why do some formulations stick to the process equipment and thereby reduce the interference-free processing? A die face pelletizer (DFP) is often used as downstream equipment for HME; in this process the emerging material is cut in a highly viscous state. Thereby, almost spherical pellets are formed. However, up to now, the process was only applicable for non-sticky substances and therefore only for a small percentage of formulations. In the first step, the cause of the sticking of the melt unto the cutting tool was investigated, in which the too high contact temperatures were identified as the crucial problem. There was no research to be found in the literature about stickiness under non-isothermal conditions, therefore this area was scrutinized, and a hypothesis linking contact temperature and stickiness was made. This hypothesis states that the contact temperature between the extrudate and the cutting tool must lie below the softening temperature of the extrudate, to avoid a wetting of the tool and thereby a development of high adhesive forces. The hypothesis was supported by controlled, non-isothermal probe tack experiments. Using this insight, subsequently the heat balance of a conventional DFP was analyzed. The cutting tools typically are linked thermally to the extrusion channels and are thereby inevitably on temperatures above the softening temperature. The heat balance was changed and the extrusion channels thermally unlinked from the cutting tool.

This enabled a decrease of the cutting tool temperatures, without freezing of the extrusion channels. Thus, for the first time, the processing of sticky substances was made possible. Furthermore, an analyzing imaging method for the monitoring of the pellet dimensions was implemented.

Table of contents

Acknowledgement	i
Kurzfassung	iii
Abstract	v
Table of contents.....	vii
1 Introduction	7
1.1 Objectives and Challenges in the Field	8
1.2 Content of the Dissertation:	9
1.3 References	12
2 A Novel Tool to Standardize Rheology Testing of Molten Polymers for Pharmaceutical Applications.....	13
2.1 Introduction	14
2.2 Materials and Methods	18
2.2.1 Materials.....	18
2.2.2 Vacuum Compression Molding	18
2.2.3 Sample Preparation Cycle	19
2.2.4 Melt Rheology.....	21
2.2.5 Data Fitting.....	22
2.2.6 Time-Temperature Superposition	23
2.3 Results and Discussion	25
2.3.1 VCM Samples	25
2.3.2 Rheological Measurements	26
2.4 Conclusions	32

2.5	References	33
3	Why Hot Melt Do Not Stick to Cold Surfaces?.....	36
3.1	Introduction	37
3.2	Experimental.....	39
3.2.1	Material & Sample Preparation.....	39
3.2.2	Differential Scanning Calorimetry (DSC).....	39
3.2.3	Non-isothermal Probe Tack Experiments	40
3.3	Results and Discussion	42
3.3.1	Contact Temperature Tack Hypothesis	42
3.3.2	Heat Transfer Analysis.....	43
3.3.3	Non-isothermal Probe Tack Test.....	46
3.4	Conclusions	50
3.5	References	51
4	Enhanced Air-Cooled Die Face Pelletizing of Sticky Formulations Using a Thermally-Decoupled Die Plate.....	54
4.1	Introduction	55
4.2	Materials and Methods	60
4.2.1	Materials.....	60
4.2.2	Extrusion Line Setup.....	60
4.2.3	Heat Transfer Analysis.....	60
4.3	Results and Discussion	62
4.3.1	Energy Balance - Modeling and Simulation	62
4.3.2	Prototype	66

4.3.3	Pelletizing Experiments.....	67
4.4	Conclusions	68
4.5	References	69
5	In-line Implementation of an Image-based Particle Size Measurement Tool to Monitor Hot-melt Extruded Pellets	71
5.1	Introduction	72
5.2	Materials and methods.....	75
5.2.1	Materials.....	75
5.2.2	Methods.....	75
5.2.3	Implementation.....	78
5.3	Results and discussion	81
5.3.1	Applicability to pellet analysis	81
5.3.2	Implementation evaluation.....	82
5.3.3	Application to in-line process monitoring.....	86
5.3.4	Application in process development	90
5.4	Conclusion	92
5.5	Acknowledgements	93
5.6	Reference	94
6	Findings and Future Directions	97
6.1	Findings	97
6.2	Future Directions	99
6.3	References	101
7	Appendix	102

7.1	List of Figures.....	102
7.2	List of tables	106
7.3	List of publications	107
7.3.1	Peer reviewed papers.....	107
7.3.2	Book Chapters:	107
7.3.3	Patent Applications:	108
7.3.4	Conference Talks:	108
7.3.5	Posters:	110
7.3.6	Degree Thesis:.....	111
7.4	Curriculum Vitae	112

*“A person who never made a mistake never tried
anything new.”*

Albert Einstein

1 Introduction

Hot melt extrusion (HME) has attracted great interest in the pharmaceutical industry over the last decades. It is a continuous process to produce solid dispersions or solid suspensions via a so-called fusion method, where a formulation comprising an active pharmaceutical ingredient (API), thermoplastic carriers, and additional excipients (e.g. plasticizers) are processed at elevated temperatures [1]. Solid dispersions are typically used to overcome problems, such as poor API solubility, or to develop modified-release or abuse-resistant drug products [2]. Figure 1.1 shows a typical scheme of a HME Process, which combines several process steps into one process. In the pharmaceutical field, it is usually performed with co-rotating twin-screw extruders [3]. The input materials melt, due to a combination of shear forces generated by the extrusion screws and the heat transfer from the heat exchangers in the barrel walls [4]. The process must be temperature controlled in such a way that the softening temperature of a formulation is exceeded but the degradation temperatures of the formulation ingredients are not reached. The materials are intensively mixed to form homogeneous molten strands at the end of the extruder, called die. The products or intermediates are formed in the downstream process.

Figure 1.2 gives an overview of the available downstream options. Most of the marketed HME drug products are shaped in classical manufacturing processes, such as tablet compaction or capsule filling [5]. Extrusion supplies these processes with the suitable intermediates (powders, pellets) either by strand cutting, die face pelletizing or cooling calandring. In some cases, for example the intermediates are also being milled to achieve better tableability.

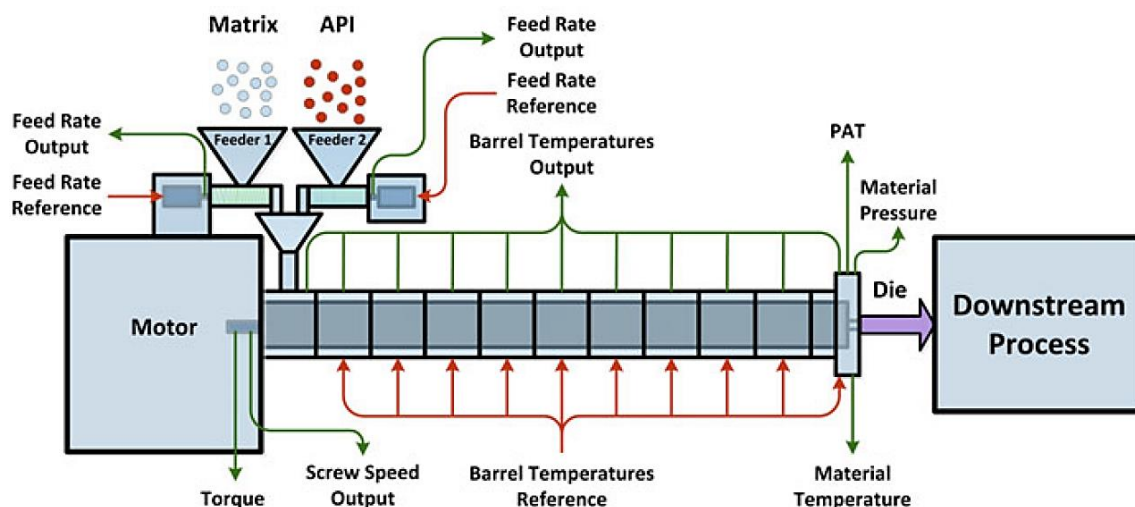


Figure 1.1: Illustration of the HME Process (reproduced with kind permission [3])

Due to the development of downstream equipment in the last years, the thermoplastic character of HME formulations also enables a direct shaping to the final dosage form via injection molding (IM) [6], shaping calanders, or film extrusion. Based on the strands or pellets generated by HME, 3D printing is also a fascinating way to generate (new) dosage forms.

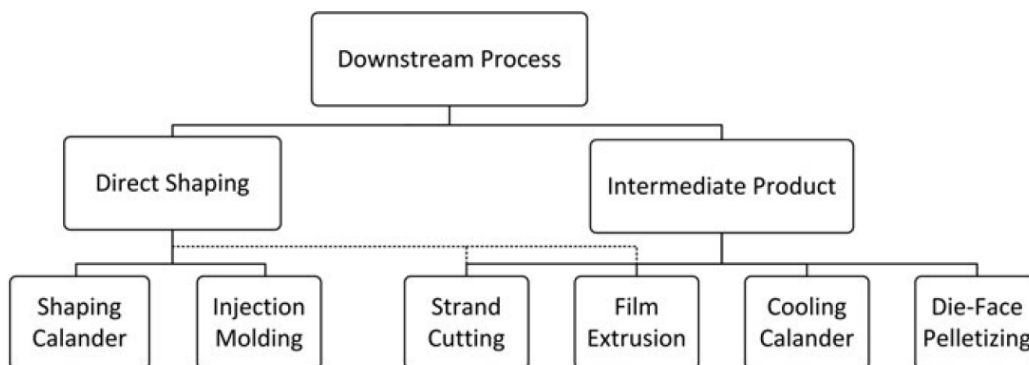


Figure 1.2: Overview of common downstream processes (reproduced with kind permission [3])

1.1 Objectives and Challenges in the Field

The challenges for process engineers in the pharmaceutical HME are manifold. The substances are expensive, often very sensitive to heat and shear forces, and on top of that the field is quite new and just recently gained interest as an opportunity to overcome the challenge presented by solubility. Equipment and methodologies are in many cases directly adopted from the plastics

industry, often with unsatisfying results. Therefore, the industry strongly requests novel tools to meet the specific pharmaceutical requirements in the formulation development and downstream processing.

1.2 Content of the Dissertation:

The work focuses on different topics and challenges, with which engineers are faced with during the development of a new product based on the HME technology. All topics are considered and treated from a process engineering perspective. The following section gives an overview and shows the connections between the research topics, which at first sight may appear very diverse.

The first publication [7] deals with the determination of accurate material properties of sensitive material, which is required for basic process design tasks. Process engineering requires specific material properties; however, these are simply not available for pharmaceutical formulations, as each development has its specific composition and self-conducted measurements are often the only way to finding reliable material properties. Moreover, the substances are often sensitive against heat and shear forces, and simply put, not well suited for a preparation using the standard approaches applied in the plastics industry. A novel approach, vacuum compression molding (short: VCM), has been developed to create proper samples from a sensitive powdery base material. It uses PTFE coated glass fiber foils to form an adaptable and fully enclosed sample chamber, in which the base material is molten and compressed under vacuum. The result is a homogeneous and degradation free sample body, even when using very sensitive materials, which can be used for different types of analyses. The publication (chapter 2) shows the novel process for the sample preparation, as well as a case study on the accurate determination of rheological data. Remarkably, the sample bodies are not exclusively applicable for rheological characterizations; they can also be applied for a broad range of other material property measurements, e.g. solid state characterization, dissolution behavior, surface properties etc., which are frequently requested for formulation, or process development tasks. The novel VCM process is patent pending [8] and was successfully transferred from the RCPE GmbH to its spin-off MeltPrep GmbH in January 2016.

Using the novel sample preparation method, one of the major challenges usually occurring during melt processing was investigated in depth. Many formulations in the pharmaceutical industry are commonly termed as sticky formulations. They tend to adhere to the processing equipment, thereby preventing the processing itself. One limitation, which initiated the research, was the pelletizing downstream processing to HME. Hot die face pelletizing is often requested, as it provides the advantage that the pellets are almost spherical, since the cutting takes place at temperatures above the solidification point of a thermoplastic formulation. Because the pellets are in molten state during the cutting process, surface tension and other viscous forces are responsible for their afterward spherical shape. However, this process was limited to commonly known non-sticky formulations, and what's more, the knowledge whether a formulation was sticky or non-sticky, could only be attained empirically. This fact, that empiricism was state of the art, was a highly motivating driving force for gaining a better understanding in that field. Therefore, the second publication investigates the fundamentals of the sticking of hot melts to processing equipment [9]. One simple observation in the laboratory was, that hot melts, even the commonly known as sticky ones, do not stick to cold surfaces. This led to a novel model to predict non-isothermal sticking behavior, which is based on heat transfer properties and material flowability.

Building on the work and the fundamental understandings above, about what limited the downstream processing, our work led us to a novel interface between an extruder and a pelletizer, the thermally decoupled die plate, which is further described in the third section (chapter 4) of this dissertation. During our work, the heat balance of the processing equipment was modified to ensure that the temperatures of the processing equipment meet the requirements identified in the previous chapter. Then, the new design was simulated and subsequently a prototype was manufactured, which in turn was successfully tested in the laboratory with different commonly known sticky substances. The concept resulted in a patent pending [10].

The last publication focuses on the monitoring of pellet properties [11]; whether it being a classical down streaming into a tablet via capsule filling, or tablet compaction. Uniform pellet properties are required to obtain consistent properties of the final dosage form. For example, the pellet size

strongly effects the dissolution properties, due to a changing surface to volume ratio. In addition, the pellet size distribution effects the flowability and dosing accuracy in subsequent processing steps. For this reason, an image based particle size measurement tool (Eyecon by Innopharma labs) was implemented in the HME line at the RCPE GmbH. Different in-line implementation approaches were developed and subsequently evaluated regarding their measurement accuracy. The system provides real time information, allowing the implementation of control algorithms to off-specification production of pellets.

The following chapters (2-5) contain the full papers of the above outlined research. Chapters 2, 3 and 5 were published in peer reviewed journals and chapter 4 is intended for publication. For details about the full list of publications generated within the course of this thesis, please see the publication list at the end of this dissertation.

1.3 References

- [1] J. Breitenbach, "Melt extrusion: from process to drug delivery technology.," *Eur. J. Pharm. Biopharm.*, vol. 54, no. 2, pp. 107–117, Sep. 2002.
- [2] M. A. Repka, N. Langley, and J. DiNunzio, *Melt Extrusion - Materials, Technology and Drug Product Design*, 1st ed. New York: American Association of Pharmaceutical Scientists, 2013.
- [3] D. Treffer, P. Wahl, D. Markl, G. Koscher, E. Roblegg, and G. J. Khinast, "Hot Melt Extrusion as a Continuous Pharmaceutical Manufacturing Process," in *Melt Extrusion: Materials, Technology and Drug Product Design*, M. A. Repka, N. Langley, and J. DiNunzio, Eds. aapspress, 2013.
- [4] K. Kohlgrüber, *Co-Rotating Twin-Screw Extruder*. Carl Hanser Verlag GmbH & CO. KG, 2007.
- [5] M. Maniruzzaman, J. S. Boateng, M. J. Snowden, and D. Douroumis, "A review of hot-melt extrusion: process technology to pharmaceutical products.," *ISRN Pharm.*, vol. 2012, no. 2, pp. 436763–436769, 2012.
- [6] K. Eggenreich, S. Windhab, S. Schrank, D. Treffer, H. Juster, and G. Steinbichler, "Injection molding as a one-step process for the direct production of pharmaceutical dosage forms from primary powders," *Int. J. Pharm.*, vol. 505, no. 1–2, pp. 341–351, 2016.
- [7] D. Treffer, A. Troiss, and J. Khinast, "A novel tool to standardize rheology testing of molten polymers for pharmaceutical applications," *Int. J. Pharm.*, vol. 495, no. 1, pp. 474–481, 2015.
- [8] D. Treffer, J. Grubbauer, G. Koscher, T. Klein, and J. Khinast, "Apparatus, method and system for moulding a thermoplastic material by vacuum compression moulding," WO2015197830 A1, 2014.
- [9] D. Treffer and J. G. Khinast, "Why Hot Melts Do Not Stick to Cold Surfaces," *Polym. Eng. Sci.*, 2016.
- [10] D. Treffer, J. Khinast, J. Grubbauer, A. Eitzlmayr, G. Koscher, and T. Klein, "Hot viscous raw material leaving a cooler perforated body cooling a cutter," 2013.
- [11] D. Treffer, P. R. Wahl, T. R. Hörmann, D. Markl, S. Schrank, I. Jones, P. Cruise, R.-K. Mürb, G. Koscher, E. Roblegg, and J. G. Khinast, "In-line implementation of an image-based particle size measurement tool to monitor hot-melt extruded pellets," *Int. J. Pharm.*, vol. 466, no. 1–2, pp. 181–189, 2014.

*“I have not failed. I’ve just found 10,000 ways
that won’t work.”*

Thomas Edison

2 A Novel Tool to Standardize Rheology Testing of Molten Polymers for Pharmaceutical Applications¹

Abstract:

Melt rheology provides information about material properties that are of great importance for equipment design and simulations, especially for novel pharmaceutical manufacturing operations, including extrusion, injection molding or 3d printing. To that end, homogeneous samples must be prepared, most commonly via compression or injection molding, both of which require costly equipment and might not be applicable for shear- and heat-sensitive pharmaceutical materials. Our study introduces a novel vacuum compression molding (VCM) tool for simple preparation of thermoplastic specimens using standard laboratory equipment: a hot plate and a vacuum source. Sticking is eliminated by applying Polytetrafluoroethylene (PTFE) coated separation foils. The evacuation of the tool leads to compression of the sample chamber, which is cost-efficient compared to conventional methods, such as compression molding or injection molding that require special equipment. In addition, this compact design reduces the preparation time and the heat load. The VCM tool was used to prepare samples for a rheological study of three pharmaceutical polymers (Soluplus®, Eudragit®E, EVA Rowalit® 300-1/28). The prepared samples were without any air inclusions or voids, and the measurements had a high reproducibility. All relative standard deviations were below 3%. The obtained data were fitted via the Carreau-Yasuda model and time-temperature superposition was applied.

¹ This chapter is based on: D. Treffer, A. Troiss, and J. Khinast, “A novel tool to standardize rheology testing of molten polymers for pharmaceutical applications,” *Int. J. Pharm.*, vol. 495, no. 1, pp. 474–481, 2015.

2.1 Introduction

Understanding melt rheology is important in order to design processing equipment for polymer processing. However, the variety of thermoplastic formulations used in different industries is extremely large. Thus, literature and databases cannot possibly describe the associated material properties. Self-conducted rheological measurements are often the only way to obtain the data relevant for products and process design. For example, in the pharmaceutical field understanding of the rheology of melts has become increasingly important. This is due to the emergence of innovative manufacturing methods, including hot melt extrusion (HME) for the production of solid dispersions ([1-4]), injection molding ([5-6]) and 3d printing ([7-8]). These processes are in the development phase for pharmaceutical applications by many research groups, and thus, melt rheology needs to be analyzed to evaluate the processing behavior. A recent review on melt rheology and its pharmaceutical applications is given by [9].

It is well known that sample preparation and methodology strongly influence the measurement result. However, most studies do not provide sufficient detail of the preparation methods and the testing setup. Thus, literature results are sometimes elusive as artefacts or degradation caused by the preparation may influence the measured material properties. Standardized methods for sample preparation do not exist. For example, in rotational rheology a tested sample is placed into a gap of the measurement device and deformed under controlled conditions. The resulting forces are recorded, and on that basis the material properties are identified. This approach averages the material properties over the entire material in the measurement device. Thermoplastic materials are usually placed onto the rheometer's base plate as a solid material and molten to obtain a short time-temperature history. Due to the temperature rise and the phase change, entrapped air or moisture inclusions of hygroscopic substances within the sample expand and can occupy a significant volume, resulting in an unusable foaming sample. Even if the gas inclusions are small and the data may look reasonable they refer to a multiphase sample consisting of the gas inclusions and the thermoplastic material. These results may deviate strongly from the properties of pure thermoplastic material.

There is a variety of techniques for preparing sample bodies that are suitable for rotational rheological analysis. Many thermoplastic materials have high viscosities (>100 Pas) in a molten state. Thus, the challenge is to produce homogenous samples without air pockets or moisture inclusions in a melting or solidification cycle of such highly viscous materials. There are two major ways of removing the amount of embedded gas during a melting cycle (devolatilization):

First, the sample can be melted under atmospheric conditions, with the air bubbles rising due to the differences in density and escaping from the upper surface of the sample body. Since the viscosity is high, the terminal speed of the trapped air bubbles is very low and an increase in temperature is the only way for obtaining reasonable devolatilization rates. However, in many cases keeping the sample at a high temperature for a long time may lead to its degeneration, affecting the analysis result.

Second, air pockets may be prevented by melting the sample in a vacuum. The starting material is placed into a hermetically sealed chamber at room temperature and subsequently molten. Since no air is present between the material's particles during the melting, they are molten as a homogenous sample. The critical influencing factors with that regard are the speed of evacuation of the sample chamber, the obtainable heating/cooling rates and a possible sublimation or evaporation of the sample.

The production is often performed in a hot-press equipped with a vacuum chamber, in which different cycle temperatures and pressures can be applied. The sample material is placed into spacers between separating foils, e.g., Teflon® coated glass-fiber foil. The plates are heated and pressed against the sample material and the spacer to form specimens. Several authors describe their sample preparation as a combination of milling, drying, compression molding and cutting [10–21].

In many cases, the specimens are produced using injection molding [16], [22-23]. A plasticizing unit melts the starting material, e.g., pellets or powders. Melting in the chamber is performed either via thermal conduction or with a rotating screw (i.e., via dissipation). The melt is subsequently

pushed through a gate into a mold consisting of two parts, where it solidifies, and is released by taking the mold apart. To generate specimens manually operated machines are typically applied. Some automated systems are available that generate the melt in a micro compounder and transfer it directly to a piston-injection molding machine.

Solvent casting is a rather untypical method for preparing melt rheology specimens. A polymeric sample is dissolved in a suitable solvent, filled into a suitable pan and dried for sufficiently long time. The samples are cut from the sheet and loaded into a rheometer. This approach generally requires long preparation times and is prone to error since the residual solvent may significantly affect the results. Other approaches, which involve transferring the molten material from the plasticizing unit directly into the measurement gap, are also feasible but require special equipment (e.g., a conical twin-screw extruder) in addition to the rheometer.

Wolff and Münstedt [24] investigated the influence of gas inclusion in polymeric samples and found that G' (storage modulus) is strongly affected by the presence of gas bubbles at low deformation frequencies. Deviations from a typical terminal behavior (slope = 2) are caused by the bubble relaxation process, superimposed on the polymeric relaxation. Bubbles tend to significantly minimize their interfacial area, increasing G' . This effect was also noticed in hydrophobic materials (e.g., silicone oils) due to water adsorption on the sample's surface.

Stadler [25] provides an excellent description of problems associated with rheological measurements. However, this study does not address sample preparation, insertion and trimming, although consistent sample quality has a major effect on reproducibility.

Freislinger and Staudinger [26] introduced a fully-automated rheometer for high-throughput screening with robotic equipment for sample loading and trimming. This approach standardized a major source of error: making trimming (i.e., the removal of excess material) identical in each case increases the reproducibility.

Dijkstra [21] studied the impact of several parameters on the rheological characterization of polyamide melts. He compared capillary and oscillatory rheology. The measurements showed

strong dependence on rheometer type, specimen humidity, preparation method and time-temperature history of both: drying and measurement run. He concluded that without standardization large deviations are obtained and proposed an extrapolation method for capillary rheometry to obtain comparable results for samples with various moisture contents.

In the current work, we introduce vacuum compression molding as a cost-efficient and fast method for sample preparation with consistent quality for rheological measurements. It reduces the applied heat load and mechanical stress on the sample material, decreasing the tendency towards degradation. Compared to other systems it enables short cycle times due to minimized chamber volume and therewith minimized thermal inertia. Three materials were chosen to demonstrate the new method. The samples were subsequently analyzed via rotational rheology and evaluated in terms of reproducibility.

2.2 Materials and Methods

2.2.1 Materials

A cationic copolymer based on dimethylaminoethyl methacrylate, butyl methacrylate and methyl methacrylate marketed as Eudragit® E100 (EE) was donated by Evonik Industries (Darmstadt, Germany). Ethylene-vinyl acetate (EVA) Rowalit® 300-1/28, 0-300 μm with a vinyl-acetate content of 28% was purchased at Rowak AG (Zürich, Switzerland). Polyvinyl caprolactame-polyvinyl acetate-polyethylene glycol graft copolymer, PVCL-PVAc-PEG, commercialized as Soluplus® (S+) was donated by BASF (Ludwigshafen, Germany).

2.2.2 Vacuum Compression Molding

The new vacuum compression molding (VCM) tool used for specimen preparation is shown in Figure 2.1. It has a cylindrical design and consists of a main body, a base plate, a lid, a piston and separation foils. The lid and the base plate have O-ring seals that provide a gas-tight closure when connected to the main body. Completely enclosed by the separation foils, the sample is loaded as a powdery material into the sample chamber. The vacuum connector on the lid links the tool to a vacuum source. The pressure inside VCM is lower than the surrounding atmospheric pressure, causing a compressive force that is transferred via the piston, slightly compacting the sample material. The tool is then placed on a pre-heated hot plate. The heat is transferred across the base plate to the sample, forming a homogeneous bubble-free specimen. The tool is subsequently cooled down and disassembled, and the sample wrapped in the separation foil was released. Sticking issues associated with polymers at metal interfaces are resolved by applying the separation foils that is simply peeled off from the sample disc and could be reused several times.

The maximum compression force depends on the geometric dimension of the compression tool. In this study, the ratio between the piston and lid diameter was 3.2, meaning that a compression pressure of 3.2 bar was transferred to the sample upon the total evacuation of the VCM tool. Note that this pressure was transferred directly to the sample. Because the height of the sample chamber is variable and can be adapted to the sample amount and operating conditions, different sample

heights are achievable in one mold since the sample thickness can easily be altered by the filling weight. During conventional compression molding, the compression forces are transferred between the molding parts and the separation layers and only a small fraction reaches the actual sample. Moreover, since the sample volume is fixed and cannot be adjusted to the filled amount, under-filled regions or cavities may occur within the sample.

A compression pressure of 3.2 bar is sufficient to fuse homogeneous samples of highly viscous materials (>100Pas) without a yield point. Materials with yield points exceeding the compact pressure will not form homogeneous samples and will require higher compaction pressures. In such cases, VCM tools with sufficient lid-to-piston diameter ratio are required. However, higher compaction pressures or low viscosities (<100 Pas) may cause leaking through the joints of the release foils. If a more precise control of the compaction pressure is required, a double acting lid with controlled vacuum levels can be applied (not shown nor used in this study).

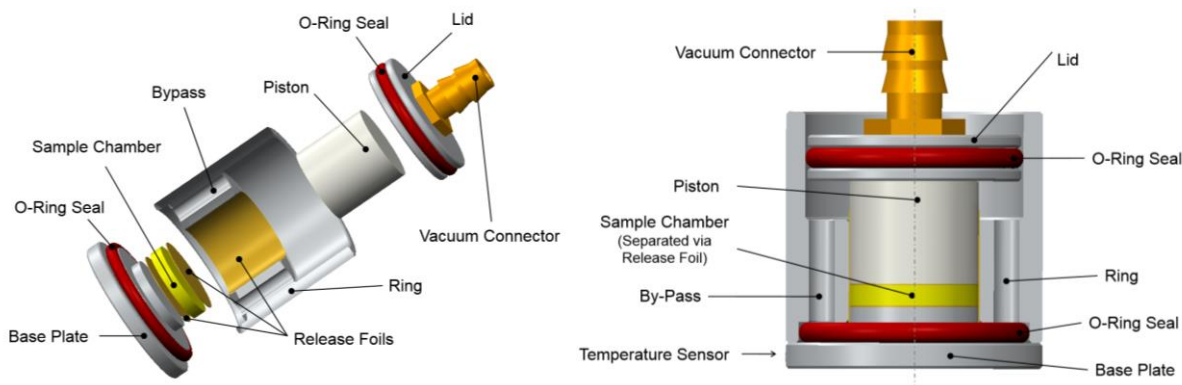


Figure 2.1: Sectional view of the vacuum compression tool; left: 3d explosion view, right: assembled front view.

2.2.3 Sample Preparation Cycle

The preparation cycle requires a hot plate, a vacuum pump and a cooler as illustrated in Figure 2.2. The VCM system applies vacuum before melting is performed. Some of the moisture is removed during the compression and evacuation phases. However, a sample may take a long time to dry well enough to achieve an adequate sample quality. Since the combination of pre-dried powder and

a short evacuation and compaction is generally the most time-efficient way to prepare high-quality samples, the raw materials were stored at constant conditions to maintain constant material properties of the starting materials. The preparation cycle consisted of five steps:

1. assembling and filling,
2. evacuation and compaction
3. heating
4. cooling
5. disassembling

During assembling, the separation foil is introduced into the ring along the lateral surface. Next, the base plate is fitted into the ring and the lower end-face separation foil is inserted. Subsequently, the weighed power material is transferred into the sample chamber. The sample weight is calculated based on the material's density to obtain specimens of 2 mm in height. The sample material is then covered with the second end-face separation layer and the piston is inserted from above. The first step, assembling and filling, is completed by securing the lid. The VCM is then connected to a vacuum pump, compacting the sample material at approximately 3.2 bar (step 2). The evacuation phase was chosen to last 5 minutes in order to remove moisture that may have been introduced during the material's handling and to ensure the best sample quality. The vacuum remains in place until the end of the cooling phase. After 5 minutes, the VCM tool is placed onto the preheated temperature controlled plate for the heating step (step 3). The temperature is set to be between the degradation and softening points of the tested substance. The heating time is 5 minutes to ensure complete melting of the sample material. The temperature is recorded in the base plate to monitor the preparation cycle (refer Figure 2.1 for the sensor's location).

The cooling rate can be altered via several cooling approaches (step 4). The slowest cooling can be achieved by simply turning off the hot plate after the melting and allow natural convection to cool the VCM tool gently. This approach allows the material to relax its internal stresses due to the volume contraction. Slightly faster cooling can be performed by removing the VCM tool from the

hot plate and putting it on a cooled solid metal plate, i.e., drawing the heat out via conduction and natural convection. Higher cooling rates can be obtained by combining conduction and forced convection. A forced convection cooler, as shown in Figure 2.2, consists of a base plate with circularly-arranged air nozzles above the VCM tool. The cooling is obtained both via conduction towards the base plate and forced convection. The forced convection cooling rate can be controlled using the air volume stream and the cooling air temperature.

During the cooling phase, the VCM tool is still assembled and preferentially evacuated. When higher cooling rates are requested, the entire tool is flushed with cold liquids. Cooling during sample preparation is performed for 5 minutes via the forced convection cooler and compressed air.

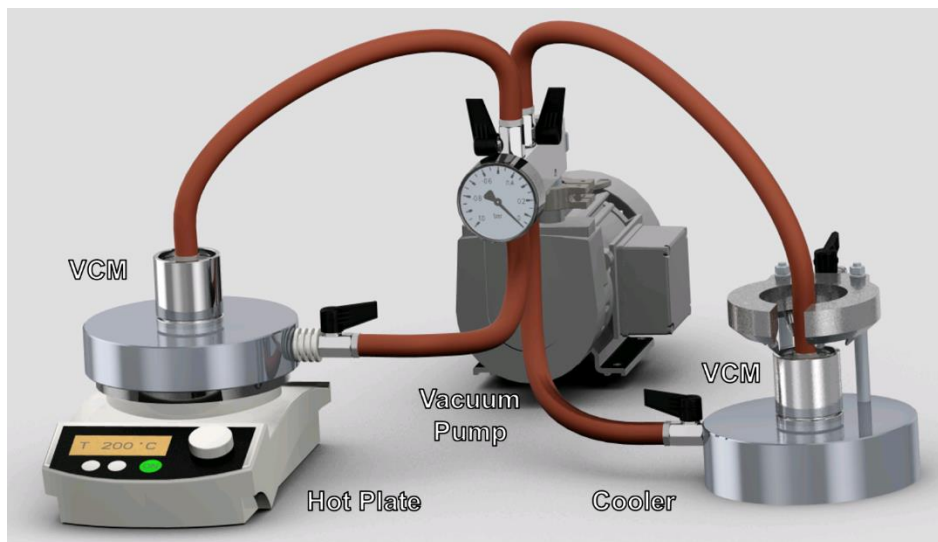


Figure 2.2: VCM Setup

2.2.4 Melt Rheology

The measurements are performed in an oscillatory rheometer (MCR 301, Anton Paar GmbH) equipped with a 25 mm plate-plate system and a heating hood (ETD 400, Anton Paar GmbH, Austria) to ensure accurate temperature distributions throughout the measurements. The measurements comprised flow curves (complex viscosity vs. angular frequency) at three

temperatures well above the glass transition temperature and within the linear viscoelastic range (LVE). The LVE range was tested with amplitude sweeps, and a deflection of 1% was found suitable for the purposes of all rheological measurements. All measurements were conducted in triplicate in order to test reproducibility. All data were presented in complex notation (η^* , ω) since the applicability of the Cox-Merz rule was not tested for the formulations.

Measurements were carried out with both, i.e., samples produced by a conventional preparation method and the novel VCM preparation method. Direct powder melting was chosen for the conventional approach. The powder was placed on the rheometer's base plate and heated and molten under atmospheric conditions. The VCM samples were transferred, immediately after the preparation cycle, from the VCM tool on to the rheometer's baseplate and subsequently molten. The measurement gap was set between 1.5 and 2 mm. Excessive sample was removed by a trimming procedure with a spatula.

2.2.5 Data Fitting

For data fitting we used the Carreau-Yasuda model in Eq.2.1 [27], which is widely applied to fit rheological data of polymers since it can describe typical polymer melt flow behavior, including the zero-shear viscosity, transition region and the shear thinning region. For data evaluation, the triplicate measurements were averaged pointwise. The parameters (η_0^* , λ , a , n) were determined using the generalized-reduced gradient (GRG) algorithm implemented in Microsoft Excel®. The algorithm was applied to minimize the accumulated error between the measured data points and the fitted Carreau-Yasuda fits (Eq. 2.2).

$$|\eta^*|(\omega) = |\eta_0^*| [1 + (\lambda\omega)^a]^{\frac{(n-1)}{a}} \quad (2.1)$$

$$|\eta^*|^{FIT}(T_k, \omega_i) = |\eta_0^*(T_k)| [1 + (\lambda(T_k)\omega_i)^a]^{\frac{(n-1)}{a}} \quad (2.2)$$

In these equations, η_0^* is the complex zero shear viscosity, λ is the relaxation time, ω is the angular frequency, $(n - 1)$ represents the power-law slope, T_k is the reference temperature and the parameter a describes the transition region width between Newtonian plateau and power law behavior.

2.2.6 Time-Temperature Superposition

The shear- and temperature-dependent rheological behavior was modeled via the time-temperature superposition principle (TTS), a technique to correlate viscosity with the measurement frequency and the temperature by combining several measurements at different temperatures in a single master curve at a reference temperature. While a rheometer can only measure the frequency range within certain limits, the master curve has a wider frequency range and can be applied to describe flow behavior beyond the rheometer's measurement range by combining several measurements at different temperatures. For details of TTS refer to [28-29].

TTS was applied using the horizontal shift factor a_T and vertical shift factor b_T . The horizontal factor was calculated via the Williams-Landel-Ferry approach (Eq.2.3).

$$\ln a_T = - \frac{c_1(T - T_r)}{c_2 + T - T_r} \quad (2.3)$$

Here, c_1 and c_2 are the model constants, T_r is the reference temperature and T is the temperature. The vertical shift factor b_T was approximated using the extended Bueche-Rouse theory by Guedes (Eq. 2.4) [30].

$$b_T = 1 + \left(3\alpha_l + \frac{1}{T_r}\right)\Delta T + \left(3\alpha_l^2 + 3\frac{\alpha_l}{T_r}\right)\Delta T^2 \quad (2.4)$$

α_l is the linear thermal expansion coefficient and ΔT is the difference between the reference temperature and the actual temperature. α_l is estimated by combining the Bondi rule (Eq. 2.5) [31] and the generally known relation between the linear and volumetric thermal expansion coefficients

for isotropic materials (Eq. 2.6). Both shift factors were applied in Eq. 2.7 to obtain the TTS Carreau-Yasuda model.

$$a_v T_G \approx 0.16 \quad (2.5)$$

$$a_l = \frac{1}{3} a_v \quad (2.6)$$

$$|\eta^*|^{TTS}(T_k, \omega_i) = \frac{a_T(T_k)}{b_T(T_k)} |\eta_0^*|(T_0) [1 + (a_T(T_k) \lambda(T_0) \omega_i)^a]^{\frac{(n-1)}{a}} \quad (2.7)$$

The parameters (c_1, c_2) were determined using the generalized-reduced gradient (GRG) algorithm implemented in Microsoft Excel®. The algorithm was applied to minimize the accumulated residuals (Eq. 2.8) between the corresponding Carreau-Yasuda fits (Eq. 2.2) and the TTS Carreau-Yasuda model (Eq. 2.7).

$$\sum_{k=1}^p \sum_{i=1}^m [|\eta^*|^{TTS}(T_k, \omega_i) - |\eta^*|^{FIT}(T_k, \omega_i)]^2 \Rightarrow MIN \quad (2.8)$$

2.3 Results and Discussion

2.3.1 VCM Samples

Figure 2.3 shows a typical heating curve for a pre-set temperature of 160°C. The heating and cooling steps began at 30 seconds and 430 seconds, respectively. The heating curve follows a typical negative exponential trend, with a steep increase directly after contact and rapid flattening towards an equilibrium at 160°C. Approximately 90 percent of the target temperature during heating was reached within 1 minute. The VCM remained on the hot plate for several minutes to ensure complete melting. The cooling curve had a steep decrease during the first minute due to high temperature gradients and gradually leveled off towards room temperature. The heating and cooling cycle took less than 10 minutes.

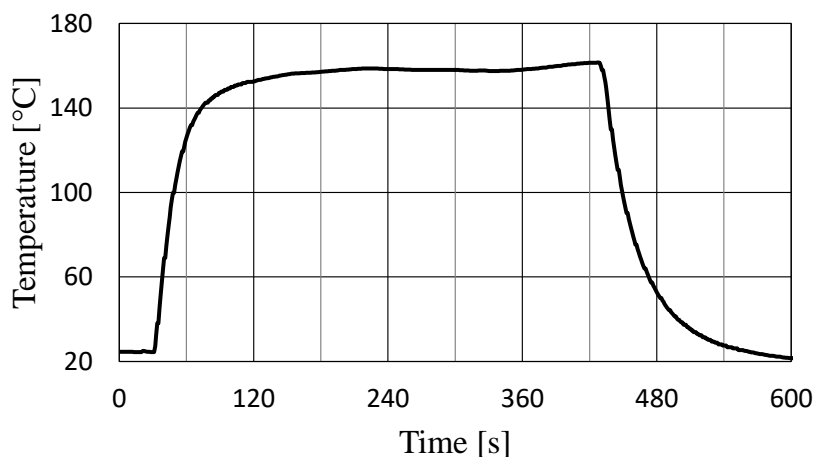


Figure 2.3: Heating and cooling curve; the heating and cooling processes begin at 30 seconds and at 430 seconds, respectively.

The samples produced for the rheological analysis are shown in Figure 2.4. They are presented on a black background with a 3 x 3 cm grid. EE samples were transparent with a slight yellowish color, S+ samples were transparent with a yellowish color and EVA were semi-transparent with a whitish color.

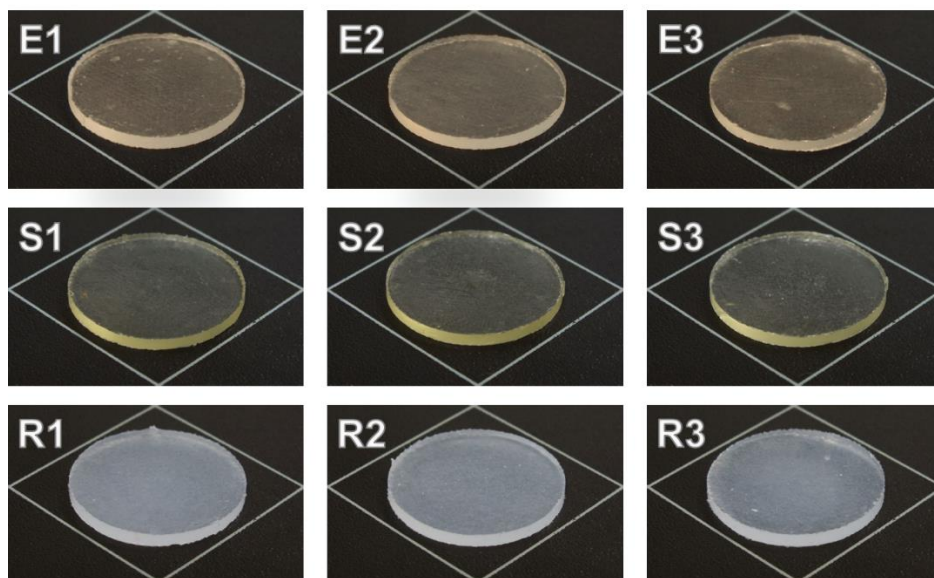


Figure 2.4: Images of samples produced via VCM (E: EE, S: S+, R: EVA).

2.3.2 Rheological Measurements

S+ is an amorphous and transparent polymer. Thus, the presence of bubbles and sample homogeneity can easily be evaluated by visual inspection. Each phase boundary between a bubble and the polymer diffracts the light and makes the sample increasingly opaque. Figure 2.6 shows snapshots of molten S+ samples of both prepared via VCM (1) and direct powder melting (2). The VCM samples showed no air inclusions or inhomogeneities, whereas the directly molten powder samples (2) contained a significant amount of air bubbles, as inter-particle air was trapped during the melting under atmospheric conditions. It is important to point out, that the VCM preparation is faster than a typical frequency sweep measurement. Thus, fresh samples are prepared for each run immediately prior the measurement and typical problems (e.g., moisture absorption) are thus prevented.

Figure 2.5 shows flow curves obtained for S+ samples prepared by both applied preparation approaches. Table 2.1 summarizes relative standard deviations (RSD), fitted zero shear viscosities η_0^* and $\eta_{\omega=526 \text{ s}^{-1}}^*$ measured complex viscosities at an angular frequency of 526 s^{-1} for all measurements shown in Figure 2.7. The reproducibility is compared by the RSD values. For powder melting the RSDs are in the range of 7% and for VCM samples below 3% which correspond

by a reduction factor (RF) of at least 2.3. The η_0^* comparison shows that all VCM measurements are approximately 30% lower than the direct powder melting. This deviation is caused by two possible interactions with the air bubbles. First, the bubbles have a large interfacial area with S+, and therefore, degradation with oxygen can be accelerated. Second, several authors reported an increase of elasticity due to relaxation of the bubbles at lower frequencies [21], [24]. This might explain the higher deviations of ~30% at the zero-shear plateau compared to only 10% at highest frequency measured. This comparison clearly shows that both the reproducibility and the absolute levels of the measurement are significantly improved by the VCM preparation.

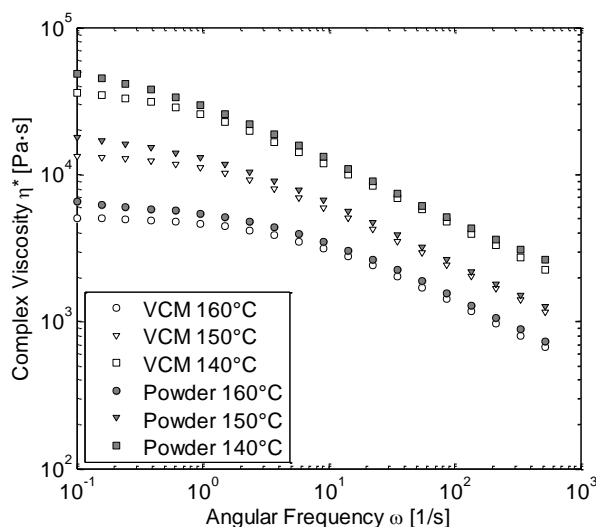


Figure 2.5: Influence of sample preparation on flow curves of S+, (VCM: prepared by novel preparation method; powder: directly molten on the rheometer's base plate under atmospheric conditions)

In the following section the chosen model substances are characterized. Figure 2.7 presents an overview of the rheological data for all three substances. The diagrams at the top show the measured flow viscosity curves and the related Carreau-Yasuda fits. All investigated samples had a typical flow behavior of polymer melts and the measurement range captured both zero-viscosity and shear-thinning regions. As a result, the parameter fitting could be performed with sufficient accuracy. All obtained model parameters are summarized in Table 2.2. The goodness of fits (Table 2.3) is expressed by the average relative residual for every combination of measurement temperature and substance. In general, the measurements were in excellent agreement with the Carreau-Yasuda fits, with all relative residuals below 1.6%.

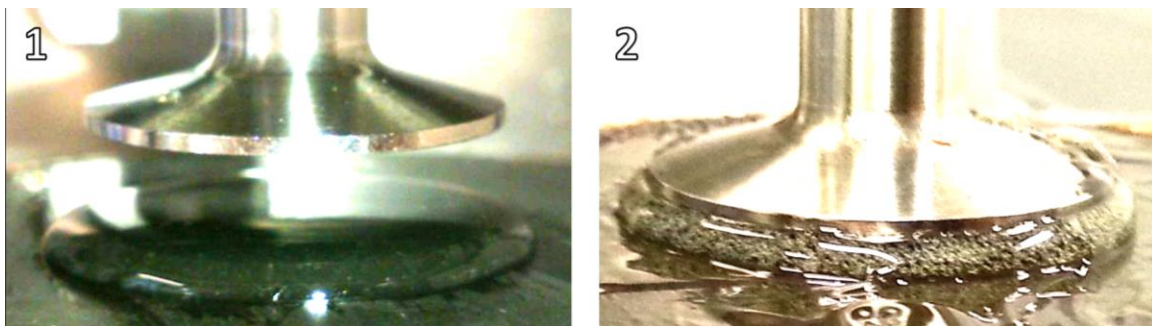


Figure 2.6: Molten samples on the rheometer base plate; 1: homogeneous VCM before measurement; 2: direct powder melting on trim position before trimming. Here the sample contains a significant amount of air bubbles.

Table 2.1: Influence of sample preparation on the S+ measurement reproducibility (T: Temperature; RSD: averaged standard deviation of all measured data points; RF: reduction factor; $|\eta_0^{*FIT}|$ fitted complex zero shear viscosity; RD: relative deviation; $\eta_{\omega=526\text{ s}^{-1}}^*$ measured complex viscosities at an angular frequency of 526 s^{-1})

T [°C]	RSD [%]		RF [-]	$ \eta_0^{*FIT} $ [Pas]		RD [%]	$\eta_{\omega=526\text{ s}^{-1}}^*$ [Pas]		RD [%]
	Powder	VCM		Powder	VCM		Powder	VCM	
160	6,37	2,83	2,3	6.560	5.070	29	733	666	10%
150	7,06	2,26	3,1	17.733	13.500	31	1.247	1.143	9%
140	7,60	2,27	3,3	48.667	37.767	29	2.630	2.387	10%

The diagrams at the bottom show the master curves obtained by TTS, as described in Section 2.2.6. The highest measurement temperature was chosen as the reference temperature for all three materials, extending the measurements range towards higher frequencies in the master curve. Similarly to the Carreau fits, TTS based on the WLF equation was in good agreement with the investigated polymers, with all curves joining reasonably well into a single master curve. The applicability was tested via the Van Gorp and Palmen method (Figure 2.8).

Based on deviations in the master curves of S+, the VGP plots confirm that its behavior can be classified as thermo-rheologically complex. Since S+ reveals deviations at high moduli, applying TTS in this case may lead to inaccurate results and should be used with caution. In contrast, since EVA and EE superimpose perfectly within the master curve and the VGP plot, they exhibit thermo-rheological simple behavior, suggesting that TTS can be applied.

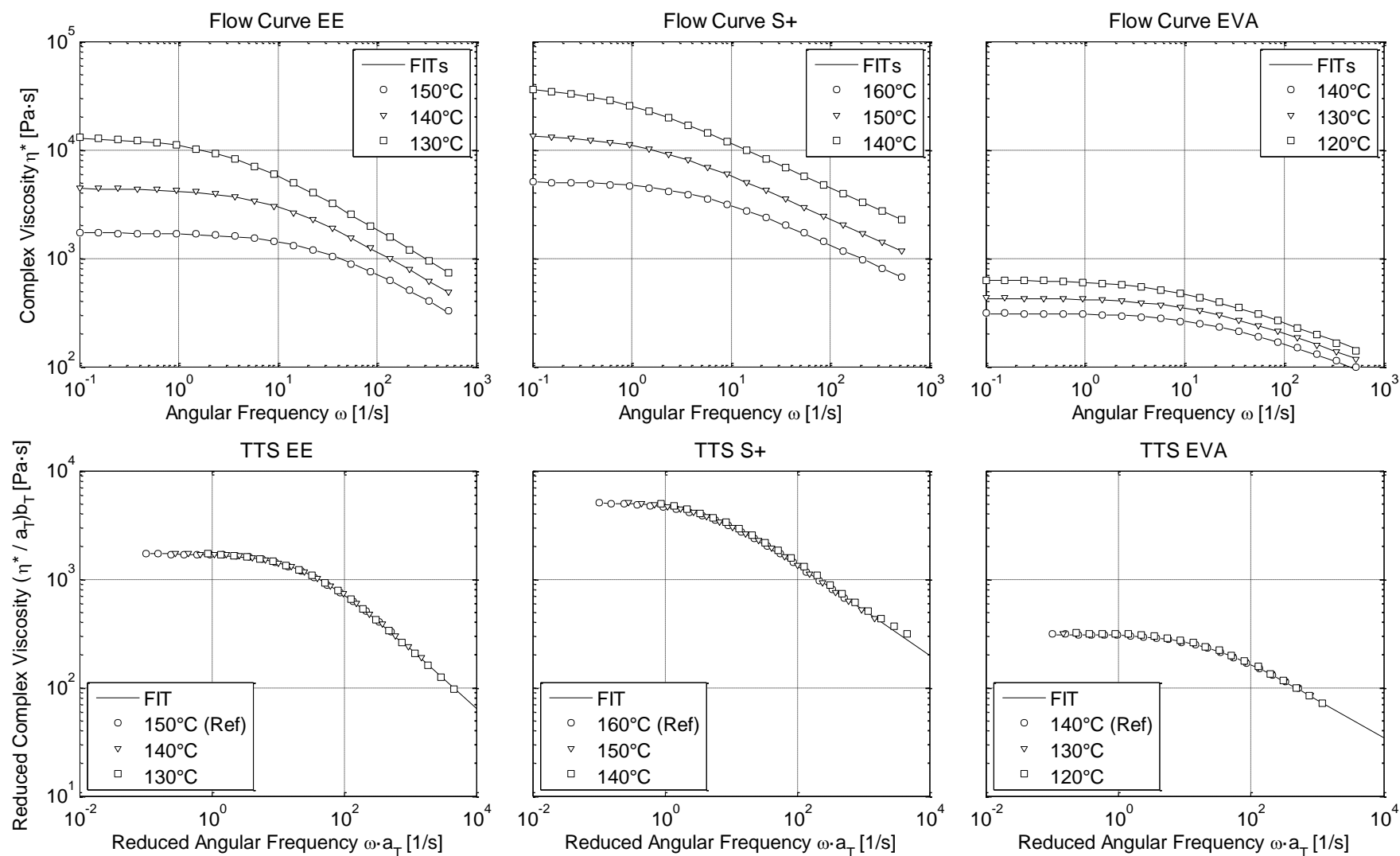


Figure 2.7: Rheological data; top row: flow curves (markers: measured data points, line: Carreau Yasuda fits), bottom row: master curve of the measured data with reference to the highest investigated temperatures (markers: shifted measured data points, line: extrapolated Carreau-Yasuda fit at reference temperature).

Table 2.2: Summarized Carreau-Yasuda and TTS Parameters (EE: $T_1=150^\circ\text{C}$, $T_2=140^\circ\text{C}$, $T_3=130^\circ\text{C}$; S+: $T_1=160^\circ\text{C}$, $T_2=150^\circ\text{C}$, $T_3=140^\circ\text{C}$; EVA: $T_1=140^\circ\text{C}$, $T_2=130^\circ\text{C}$, $T_3=120^\circ\text{C}$).

Model	Parameter	Unit	EE	S+	EVA
Carreau Yasuda	$\eta_0^*(T_0)$	$Pa \cdot s$	1.710	5.070	310
	$\eta_0^*(T_1)$		4.410	13.500	427
	$\eta_0^*(T_2)$		12.900	37.767	624
	n	-	0,4444	0,5846	0,6433
	a	-	0,9570	1,0282	0,9055
	$\lambda(T_0)$	$1/s$	0,0374	0,2429	0,0477
	$\lambda(T_1)$		0,1008	0,7056	0,0693
	$\lambda(T_2)$		0,3220	1,6763	0,0115
TTS	c_1	-	17,21	26,35	8,61
	c_2	-	178,20	261,92	227,66
	$a_T(T_1)$	-	2,5789	2,6627	1,3782
	$a_T(T_2)$	-	7,5439	7,4490	2,0129
	T_G	$^\circ\text{C}$	45	70	76
	$b_T(T_1)$	-	1,0768	1,0716	1,0763
	$b_T(T_2)$	-	1,1655	1,1535	1,1644

Table 2.3: Summarized reproducibility of the measured data (RSD: averaged standard deviation of all measured data points, Residuals: averaged relative error of all measured data points compared to the Carreau-Yasuda model data).

	EE			S+			EVA		
Temperature [°C]	150	140	130	160	150	140	140	130	120
RSD [%]	2,08	2,40	1,51	2,83	2,26	2,27	2,02	1,75	0,84
Residuals [%]	0,83	0,67	1,01	1,09	1,24	1,55	0,92	0,58	0,90

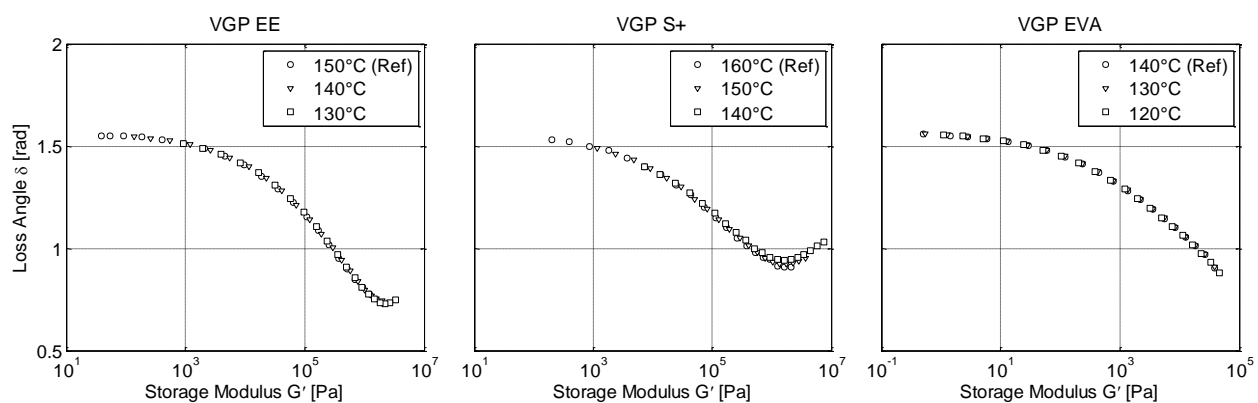


Figure 2.8: Van Gurp Palmén plots.

2.4 Conclusions

A new and straightforward thermoplastic sample production method was developed. Atmospheric pressure for sample compression and appropriately arranged separation foils resulted in a simple time- and cost-efficient design.

A rheological case study with three pharmaceutical polymers prepared with our new system was conducted. The specimens required for the investigation were 25 mm in diameter and 2 mm in height. The specimens required for the investigation were 25 mm in diameter and 2 mm in height. The preparation required short time spans at temperatures above the polymers' melting point. In addition, no significant shear forces were applied, which reduced the risk of thermo-mechanical degradation of the sample.

The VCM preparation yielded homogeneous samples of constant quality in comparison to direct powder melting. The samples were analyzed using oscillatory rheology. Since the measured data had high reproducibility (RSD<3%) in comparison to direct powder melting (RSD<8%), they were fitted to the Carreau-Yasuda model. In addition, TTS principle was highly accurate applied. Thus, it can be concluded that the gentle VCM preparation is particularly suitable for investigations on heat and shear sensitive pharmaceutical formulations.

2.5 References

- [1] J. Breitenbach, “Melt extrusion: from process to drug delivery technology,,” *Eur. J. Pharm. Biopharm.*, vol. 54, no. 2, pp. 107–17, Sep. 2002.
- [2] M. Yang, P. Wang, H. Suwardie, and C. Gogos, “Determination of acetaminophen’s solubility in poly(ethylene oxide) by rheological, thermal and microscopic methods,” *Int. J. Pharm.*, vol. 403, no. 1–2, pp. 83–89, 2011.
- [3] N. Chomcharn and M. Xanthos, “Properties of aspirin modified enteric polymer prepared by hot-melt mixing,” *Int. J. Pharm.*, vol. 450, no. 1–2, pp. 259–267, 2013.
- [4] J. G. Lyons, P. Blackie, and C. L. Higginbotham, “The significance of variation in extrusion speeds and temperatures on a PEO/PCL blend based matrix for oral drug delivery,” *Int. J. Pharm.*, vol. 351, no. 1–2, pp. 201–208, 2008.
- [5] T. Quinten, T. De Beer, F. O. Onofre, G. Mendez-Montecalvo, Y. J. Wang, J. P. Remon, and C. Vervaet, “Sustained-Release and Swelling Characteristics of Xanthan Gum/Ethylcellulose-Based Injection Moulded Matrix Tablets: in Vitro and in Vivo Evaluation,” *J. Pharm. Sci.*, vol. 100, no. 7, pp. 2858–2870, 2011.
- [6] B. Claeys, A. Vervaeck, X. K. D. Hillewaere, S. Possemiers, L. Hansen, T. De Beer, J. P. Remon, and C. Vervaet, “Thermoplastic polyurethanes for the manufacturing of highly dosed oral sustained release matrices via hot melt extrusion and injection molding,” *Eur. J. Pharm. Biopharm.*, vol. 90, pp. 44–52, 2015.
- [7] A. Goyanes, A. B. M. Buanz, A. W. Basit, and S. Gaisford, “Fused-filament 3D printing (3DP) for fabrication of tablets,” *Int. J. Pharm.*, vol. 476, no. 1–2, pp. 88–92, 2014.
- [8] S. a. Khaled, J. C. Burley, M. R. Alexander, and C. J. Roberts, “Desktop 3D printing of controlled release pharmaceutical bilayer tablets,” *Int. J. Pharm.*, vol. 461, no. 1–2, pp. 105–111, 2014.
- [9] J. Aho, J. P. Boetker, S. Baldursdottir, and J. Rantanen, “Rheology as a tool for evaluation of melt processability of innovative dosage forms,” *Int. J. Pharm.*, 2015.
- [10] J. Aho and S. Syrjälä, “On the measurement and modeling of viscosity of polymers at low temperatures,” *Polym. Test.*, vol. 27, no. 1, pp. 35–40, Feb. 2008.
- [11] K. Mattes, “Methoden zur Charakterisierung des nichtlinear viskoelastischen Verhaltens von Polymerschmelzen,” Albert-Ludwigs-Universität Freiburg, 2007.

- [12] K. M. Mattes, R. Vogt, and C. Friedrich, "Analysis of the edge fracture process in oscillation for polystyrene melts," *Rheol. Acta*, vol. 47, no. 8, pp. 929–942, Jun. 2008.
- [13] I. D. Winters, "The rheological and structural properties of blends of polyethylene with paraffin wax," Georgia Institute of Technology, 2012.
- [14] J. Férec, M. C. Heuzey, G. Ausias, and P. J. Carreau, "Rheological behavior of fiber-filled polymers under large amplitude oscillatory shear flow," *J. Nonnewton. Fluid Mech.*, vol. 151, no. 1–3, pp. 89–100, May 2008.
- [15] M. Sepehr, G. Ausias, and P. J. Carreau, "Rheological properties of short fiber filled polypropylene in transient shear flow," *J. Nonnewton. Fluid Mech.*, vol. 123, no. 1, pp. 19–32, Oct. 2004.
- [16] E. Privas, F. Leroux, and P. Navard, "Preparation and properties of blends composed of lignosulfonated layered double hydroxide/plasticized starch and thermoplastics.," *Carbohydr. Polym.*, vol. 96, no. 1, pp. 91–100, Jul. 2013.
- [17] G. Breuer and A. Schausberger, "Recovery of shear modification of polypropylene melts," *Rheol. Acta*, vol. 50, no. 5–6, pp. 461–468, May 2011.
- [18] C. Kock, M. Gahleitner, A. Schausberger, and E. Ingolic, "Polypropylene/polyethylene blends as models for high-impact propylene-ethylene copolymers, part 1: Interaction between rheology and morphology," *J. Appl. Polym. Sci.*, Jul. 2012.
- [19] J. Vermant, S. Ceccia, M. K. Dolgovskij, P. L. Maffettone, and C. W. Macosko, "Quantifying dispersion of layered nanocomposites via melt rheology," *J. Rheol.*, vol. 51, no. 3, p. 429, 2007.
- [20] C. F. Sailer, "Blends of polyamide 6 and styrenic polymers: influence of reactive compatibilization on melt rheology and morphology," ETH Zürich, 2008.
- [21] D. J. Dijkstra, "Guidelines for rheological characterization of polyamide melts (IUPAC Technical Report)," *Pure Appl. Chem.*, vol. 81, no. 2, pp. 339–349, 2009.
- [22] L. D'orazio, C. Mancarella, E. Martuscelli, G. Sticotti, and G. Cecchin, "Isotactic polypropylene/ethylene-co-propylene blends: Influence of the copolymer microstructure on rheology, morphology, and properties of injection-molded samples," *J. Appl. Polym. Sci.*, vol. 72, no. 5, pp. 701–719, May 1999.
- [23] A. U. Chaudhry and V. Mittal, "Blends of high-density polyethylene with chlorinated polyethylene: Morphology, thermal, rheological, and mechanical properties," *Polym. Eng. Sci.*, vol. 54, no. 1, pp. 85–95, Jan. 2014.

- [24] F. Wolff and H. Münstedt, “Artefacts of the storage modulus due to bubbles in polymeric fluids,” *Rheol. Acta*, vol. 52, no. 4, pp. 287–289, 2013.
- [25] F. J. Stadler, “What are typical sources of error in rotational rheometry of polymer melts?,” *Korea-Australia Rheol. J.*, vol. 26, no. 3, pp. 277–291, Aug. 2014.
- [26] R. Freisinger and P. Staudinger, “High Troughput Experimentation in Rotational Rheology for Polymer Melts Applications Description of the High Throughput,” in *SPE International Polyolefins Conference*, 2014.
- [27] K. Yasuda, R. C. Armstrong, and R. E. Cohen, “Shear flow properties of concentrated solutions of linear and star branched polystyrenes,” *Rheol. Acta*, vol. 20, no. 2, pp. 163–178, Mar. 1981.
- [28] J. M. Dealy and J. Wang, *Melt Rheology and its Applications in the Plastics Industry*. Dordrecht, Netherlands: Springer Science+Business Media B.V., 2013.
- [29] J. Dealy and D. Plazek, “Time-temperature superposition—a users guide,” *Rheol. Bull.*, vol. 78, no. 2, pp. 16–31, 2009.
- [30] R. M. Guedes, “Analysis of temperature and aging effects on biomedical ultra-high molecular weight polyethylene’s grades using a viscoelastic model,” *Polym. Test.*, vol. 30, no. 6, pp. 641–650, Sep. 2011.
- [31] D. W. van Krevelen and K. te Nijenhuis, *Properties of Polymers*, 4th ed. Elsevier, 2009.

“If I had an hour to solve a problem I'd spend 55 minutes thinking about the problem and 5 minutes thinking about solutions.”

Albert Einstein

3 Why Hot Melt Do Not Stick to Cold Surfaces?²

Abstract:

Many industrial polymer processing operations (e.g., extrusion, injection molding, etc.) include solid-to-liquid or liquid-to-solid phase changes at non-isothermal interfaces. Stickiness (tack) can occur depending on the process conditions. However, prediction of tack formation is not trivial. This work presents a hypothesis for tack formation between molten polymers and solids under non-isothermal conditions. Our hypothesis states that strong adhesion requires wetting (and thus surface creation) at the interface upon contact and, consequently, contact temperatures above the polymer's solidification point. Lower contact temperatures result in a solid-solid interface with negligible adhesion. We suggest that the contact temperature determines the existence or non-existence of surface sticking. Our hypothesis is supported by non-isothermal tack experiments, which show that the change from stickiness to non-stickiness is surprisingly pronounced with changing surface temperature of the solid material. From a practical perspective, our work may be useful both for professionals (e.g., designing new processing equipment and performing process troubleshooting) and home users (e.g., working with hot melt glue or 3d printers).

² This chapter is based on: D. Treffer and J. G. Khinast, “Why Hot Melts Do Not Stick to Cold Surfaces,” *Polym. Eng. Sci.*, 2016, accepted – in print

3.1 Introduction

In a typical plastics-manufacturing process, polymers are processed in the molten state and then solidified to obtain a final product or an intermediate. For all processes, it is critical to design the equipment in a way that allows control of sticking at defined interfaces. It can be either required or undesirable at defined non-isothermal interfaces. In 3d printing [1], polymer welding [2-3] and hot melt gluing, high levels of adhesion between the structural elements and the adhesive ensure high component strengths. In pelletizing [4], injection molding [5] and film stretching [6], sticking should be avoided, since sticking can impair the product's quality or even lead to production failure. Due to the complexity of the problem, adhesion characteristics are not well predicted in practical situations [7]. Since studies of adhesion are typically performed under isothermal conditions [8-10], results are mostly inapplicable to non-isothermal adhesion.

In general, adhesion comprises all forces between materials that are in contact. According to the seminal work by McBain and Hopkins [11], adhesive forces can be attributed to mechanical and specific adhesion. Mechanical adhesion occurs via adhesive interlocking due to the surface roughness of a substrate. Specific adhesion involves all forces occurring between perfectly flat surfaces without pores or a surface roughness based on molecular interactions. When an adhesive bond is exposed to mechanical stress, forces transferred through the interface lead to a deformation of the substrate materials and the adhesive. In that regard, one distinguishes between fundamental adhesion, which relates only to forces acting on the molecular level between the contacting phases, and practical adhesion, which is a measure of the total force that disrupts an adhesive bond [12-14], and includes fundamental adhesion and all other energy-dissipating processes during bond breaking. As such, practical adhesion is meaningful only in a specific geometry. The resistance of an adhesive bond to debonding (or bond breaking) after short contact times is termed tack (stickiness) and is pronounced for pressure sensitive adhesives (PSAs). Tack requires the right balance between the softness (low storage modulus) and ability to dissipate energy of a polymer [15].

Tack is often investigated via probe tack experiments [16–21] using a polymer melt or, more generally, an adhesive placed on a stationary plate and a vertically movable cylindrical probe on top. The experiments have two phases. First, during the bonding phase, the probe is pressed against the melt, allowing the material to wet the surface and form an adhesive bond. Second, during the debonding phase, the probe is detached under controlled conditions. The resulting force-path measurements provide information about the adhesion, cohesion, flow regime and tack failure mechanism. Isothermal tack behavior is predicted via the Dahlquist criterion [22], which states that at storage moduli below a certain threshold ($G' < 3 \cdot 10^5 Pa$ at a frequency of $1 s^{-1}$) tack (stickiness) is observed. One obvious requirement for tack is that two materials wet on contact [23]. Most tack studies are performed under isothermal conditions, investigating the effects of contact time, contact pressure, temperature, rheology, separation velocity and surface roughness [24–27]. However, since polymer processes are generally conducted under non-isothermal conditions, it is also critical to understand the mechanism of non-isothermal tack.

In our work, we describe the effect of non-isothermal conditions on tack by analyzing the heat transfer and developing a detailed contact temperature tack hypothesis. To the best of our knowledge, no controlled non-isothermal tack investigations have been described in the literature to date.

3.2 Experimental

3.2.1 Material & Sample Preparation

A polyvinyl-caprolactame polyvinyl-acetate polyethylene-glycol graft copolymer, PVCL-PVAc-PEG with the trade name Soluplus® (S+) was donated by BASF SE (Ludwigshafen, Germany). The polymer was chosen for this investigation as it shows typical PSA properties at processing temperatures. S+ is a powdery material in delivery conditions. Homogeneous solid specimens were produced via vacuum compression molding (VCM Tool, MeltPrep GmbH, Austria), resulting in cylindrical discs with a diameter of 25 mm and a thickness of approximately 2.5 mm as described in a previous publication [28]. The sample discs were manually placed onto the rheometer's ground plate, temperature controlled and molten by the rheometer's internal heating. Subsequently, the molten sample was flattened to 2 mm with a steel plate with 2 mm spacers. To ensure thermal equilibrium before performing the actual measurement, the system was kept under constant conditions for 5 minutes.

3.2.2 Differential Scanning Calorimetry (DSC)

DSC measurements (DSC 204 F1 Phoenix, Netzsch GmbH, Germany) were performed at a scanning rate of 10 K/min from 0 to 200°C. An empty aluminum pan was used as a reference, and the heat capacity result was corrected via a sapphire standard.

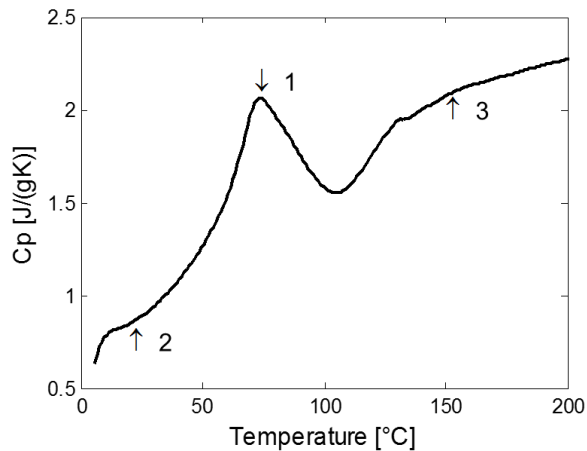


Figure 3.1: Heat capacity measurement S+. 1: $T_G = 73.2^\circ\text{C}$, 2: $c_p(20^\circ\text{C}) = 0.88 \text{ kJ}/(\text{kgK})$, 3: $c_p(150^\circ\text{C}) = 2.09 \text{ kJ}/(\text{kgK})$

Figure 3.1 shows the heat capacity curve obtained for S+. The glass transition point T_G occurred at 73.2°C , which is in good agreement with the temperature of approximately 70°C stated by the manufacturer. The heat capacities used for in calculations (see below) were $0.88 \text{ kJ}/(\text{kgK})$ and $2.09 \text{ kJ}/(\text{kgK})$ at 20°C and 150°C , respectively.

3.2.3 Non-isothermal Probe Tack Experiments

To test the influence of non-isothermal condition on tack properties, an experimental setup was developed to control the heat transfer during the probe tack experiments. The probe temperature T_P and melt temperature T_M were controlled independently. The measurements were performed with a plate-plate rheometer (MCR 301, Anton Paar GmbH, Austria) with a normal force sensor and translational moveable custom-made measurement body. A standard measurement axis holder was extended with a temperature-controlled cylindrical probe (diameter 8 mm) containing a direct current (12 V) heat cartridge, as illustrated in Figure 3.2. Both are thermally decoupled with a ceramic isolator reinforced with glass fibers. The probe was made of stainless steel (grade 1.4301) and the contact surface was polished to ensure a smooth surface ($R_a < 0.8 \mu\text{m}$). The probe was carefully cleaned with acetone as solvent and lint-free wipes after each measurement run.

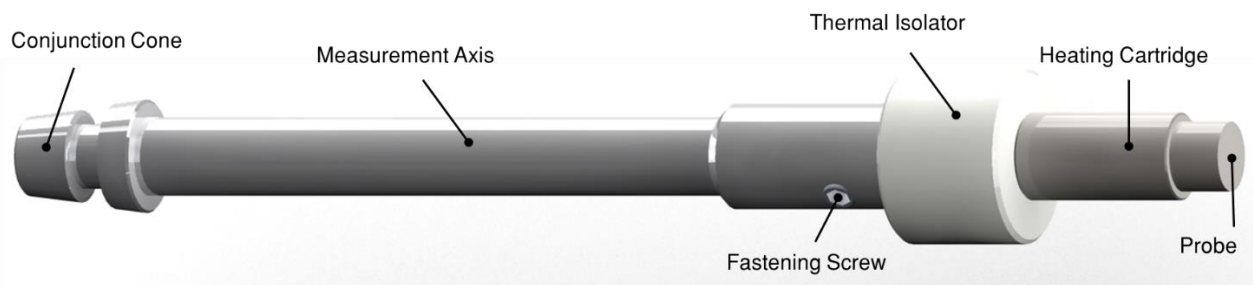


Figure 3.2: Customized measurement body.

The tack measurement cycle began at the initial height of 5 mm. During the bonding process, the probe approached the sample at a constant velocity $v_f = 1 \text{ mm/s}$, came in contact with the sample at 2 mm and proceeded until the final height of 1 mm was established. The contact continued for fixed contact times $t_{c,a} = 1 \text{ s}$ or $t_{c,b} = 5 \text{ s}$ at $H = 1 \text{ mm}$, after which the probe was detached from the sample at a constant velocity $v_s = 5 \text{ mm/s}$. The resulting path-time diagrams are presented in Figure 3.3.

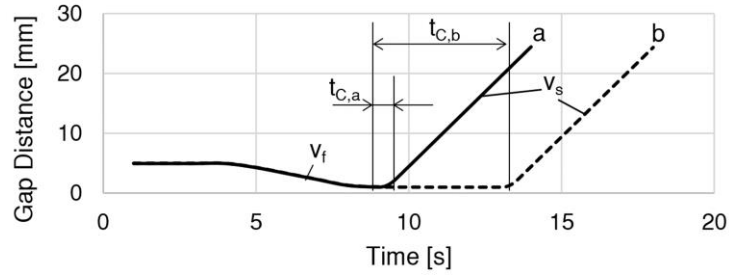


Figure 3.3: Path-time diagram of the probe tack experiments.

The ground plate had a fixed temperature. The probe temperature T_P varied from 130°C to 50°C , in 20°C steps. In order to thoroughly test the influence of heat transfer on the tack properties, we conducted three series of experiments to investigate the effects of contact time, T_M and T_P on the tack properties. Each series consisted of five measurements at all T_P levels. The first series was performed at $T_M=170^\circ\text{C}$ and $t_{C,a}$. The second series was executed at the same temperature ($T_M=170^\circ\text{C}$) but with $t_{C,b}$ to determine the influence of t_C and to test the applicability of the semi-infinite body concept. The third set was carried out at $T_M=150^\circ\text{C}$ and $t_{C,a}$ to investigate the influence of T_M .

For each experiment, a force-path diagram was captured which was transformed to σ - ε curves for easier comparison with isothermal studies in the literature. Stress was calculated by dividing the force by the cross-sectional surface area of the probe. The probe's position was described with dimensionless strain $\varepsilon=h/H-1$, indicating the relative position h compared to the compressed sample thickness H (1 mm). For both bonding and debonding, the maximum stress and the applied work $w=1/A \cdot \int F \cdot v_F \cdot dt$ were established. A is the probe's cross-sectional area, F is the applied force and v_F is the probe velocity. In addition, the rupture strain ε_r for debonding was determined from the experimental data with a threshold of -20 mN.

3.3 Results and Discussion

3.3.1 Contact Temperature Tack Hypothesis

Our hypothesis of non-isothermal tack links heat transfer and adhesion fundamentals. It states that the contact temperature T_C can serve as a criterion for the formation of a strong or weak adhesive bond since we assume that only the instantaneous conditions close to the interface upon contact are important for bond formation. As described above, adhesive forces are due either to mechanical interlocking or interacting forces on the surface, both of which require sufficient contact surface. If two solids are in contact, only a small fraction of surface molecules of either material is in contact. However, if the surface is wetted by a melt, many more molecules interact since the melt enters small notches in the solid surface creating a higher effective contact area which is a prerequisite for all specific adhesion mechanisms. Accordingly, a strong bond and stickiness exists when T_C is above a critical solidification temperature T_S of the polymer at which wetting can occur. For amorphous polymers, it is typically the glass transition temperature T_G and, for crystalline substances, it is the melting temperature. If T_C is below this critical temperature T_S , no bond is formed and the material does not stick.

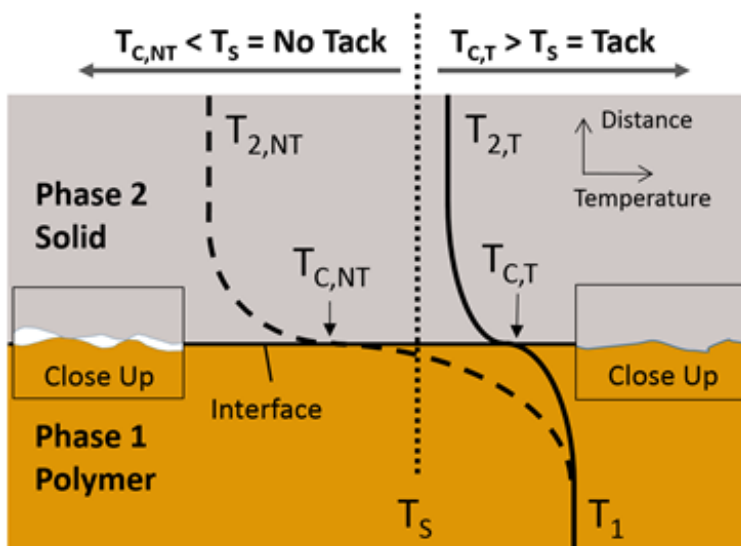


Figure 3.4: Contact temperature tack hypothesis and probe tack experiment. (A) Temperature profiles at a non-isothermal interface. Case one: Tack (solid line). Case two: No tack (dashed line); T_S solidification temperature polymer; T_1 bulk temperature polymer; $T_{2,T}$ bulk temperature solid sticky; $T_{2,NT}$ bulk temperature solid no tack; $T_{C,T}$ contact temperature tack; and $T_{C,NT}$ contact temperature no tack.

The contact temperature tack hypothesis is illustrated in Figure 3.4, which shows two temperature profiles in relationship to the distance from the interface. Phase one (a polymer) has the bulk temperature T_1 in both cases and is brought in contact with phase two (a solid) at two bulk temperatures $T_{2,T}$ (tack) and $T_{2,NT}$ (no tack). In case one, the bulk temperature $T_{2,T}$ is well above T_s . The contact temperature $T_{C,T}$ is above T_s and the material can flow and wet the interface, forming strong adhesion. In case two, the bulk temperature $T_{2,NT}$ is sufficiently below T_s . The resulting temperature profile has the interfacial temperature $T_{C,NT}$ that is lower than T_s . The polymer becomes instantaneously solid at the interface and cannot wet the solid, resulting in negligible adhesion. According to our contact temperature tack hypothesis, tack occurs when $T_C > T_s$ and tack prevention takes place when $T_C < T_s$.

3.3.2 Heat Transfer Analysis

Clearly, the local properties of the melt (such as viscosity and molecular mobility) depend on the local temperature. The local temperature at the interface is crucial for the adhesion performance as adhesion summarizes the transferred forces over the interface. The interfacial temperature can vary strongly depending on the initial bulk temperatures and thermal effusivities of the two phases in contact. When two objects with different temperatures come into contact, heat transfer or, more specifically, heat conduction occurs. To understand this process, a simplified model can be used: In our case, a system of two semi-infinite bodies is considered, which implies that the infinite bulk temperatures are constant. At times $t < 0$, the phases are not in contact and have a uniform temperature, i.e., the two infinite bulk temperatures (T_1, T_2). At time $t = 0$, the phases are brought into contact and heat transfer is initiated due to the temperature differences. The contact temperature T_C at the interface can be calculated by $T_C = e_2 T_2 / (e_1 + e_2) + e_1 T_1 / (e_1 + e_2)$. The derivation of this equation for semi-infinite bodies is described in the literature, e.g., [29]. The term $e_i = (\lambda_i c_i \rho_i)^{1/2}$ denotes thermal effusivity, which is a measure of heat conduction capacity of the material. λ_i is the heat conductivity, c_i is the heat capacity and ρ_i is the density. As highlighted by the equation, upon contact the interfacial temperature is at T_C instantly and remains constant over time.

The temperature profiles for the semi-infinite bodies are calculated using Eq. 3.1 and Eq. 3.2 for phase one and phase two, respectively [29].

$$T_{1,x} = T_C + (T_1 - T_C) \cdot \operatorname{erf}\left(\frac{x}{\sqrt{4 t a_1}}\right), \quad x \leq 0 \quad (3.1)$$

$$T_{2,x} = T_2 + (T_C - T_2) \cdot \operatorname{erf}\left(\frac{x}{\sqrt{4 t a_2}}\right), \quad x \geq 0 \quad (3.2)$$

Here, $a_i = \lambda / (\rho_i c_{p,i})$ is the thermal diffusivity in each phase. x is the coordinate in bulk direction, with x being 0 at the contact point. In addition to the semi-infinite body concept, two main assumptions were made for the purposes of this model: First, a change in the heat transfer properties was neglected. Solutions to the heat transfer problem with varying properties and phase change commonly known as the Stefan problem can be found in [30-31]. Secondly, we neglected the surface roughness that causes partial wetting and thermal contact resistance and assumed perfect surfaces and contact.

The semi-infinite bodies simplification requires a sufficient polymer layer thickness to be valid in the experiment. The thermal penetration depth in dimensionless representation $\delta = (a t c) / H^2$ can be used to check the applicability ($\delta < 1$) and it holds true for the chosen experimental parameters (Table 3.1).

Three cases with different material combinations were investigated theoretically to illustrate the influence of materials properties on the contact temperature (Figure 3.5). Case one (S+ and SS) corresponds to the material combinations applied in the experimental part of this work. The other two cases are depicted to show the impact of different material properties on the contact temperature. All essential parameters for the calculation are summarized in Table 1. The contact temperature T_C was constant over time due to the two-semi-infinite-body simplification. The initial temperature profiles are shown together with the profiles at 1 and 5s. In Figure 3.5A (S+ and SS), S+ only contributes 8.2% to the contact temperature, resulting in a temperature of 30.7°C at the interface. (Increasing S+ temperature to 170°C increases the contact temperature to 32.8°C). Both

temperatures (i.e., 30.7°C and 32.8°C) are lower than T_s (73°C) and results in instantaneous solidification at the interface and negligible adhesion.

Table 3.1: Material properties. S+ densities and thermal conductivities are taken from [32], SS: stainless steel, grade 1.4301, G: SiO₂ glass.

Property	Unit	S+			SS		G	
T	[°C]	20	150	170	20	150	20	150
ρ	[kg/dm ³]	0,87	0,92	0,92	7,92	7,90	2,2	2,2
c	[kJ/kgK]	0,88	2,09	2,17	0,47	0,50	0,73	0,91
λ	[W/mK]	0,16	0,23	0,24	14,8	17	1,36	1,53
e	[Ws ^{1/2} /(K m ²)]	0,35	0,67	0,69	7,44	8,16	1,48	1,75
Thermal Effusivity Ratio		S+			SS		G	
$e(20^\circ\text{C})/e(150^\circ\text{C})$		53%			91%		84%	
	Phase 1 / Phase 2	$\frac{e_1+e_2}{[Ws^{1/2}/(K m^2)]}$	$e_1/(e_1+e_2)$ [-]	$e_2/(e_1+e_2)$ [-]	T_c [°C]			
Case 1	S+ (150°C) / SS (20°C)	8,1	8,2%	91,8%	30,7			
-	S+ (170°C) / SS (20°C)	8,13	8,51%	91,49%	32,8			
Case 2	S+ (150°C) / G (20°C)	2,1	31,06%	68,94%	60,4			
Case 3	S+ (150°C) / S+ (20°C)	1,0	65,5%	34,5%	105,2			

In Figure 3.5B (S+ and glass), material 1 contributes more to the heat transfer since the effusivity is closer to the one of the polymer melt than in case 1. S+ bulk temperature contributes 31.1% to the contact temperature, and the resulting contact temperature of 60.4°C is higher than in case 1. In this example, the interfacial temperature is still lower than T_s (73°C) and two solids with negligible adhesion are in contact at the interface.

In Figure 3.5C (S+ and S+), the thermal effusivities are more alike. Solid S+ contributes 34.5% and the remaining part is contributed by the molten S+ to the contact temperature. The temperature at the interface is 105.2°C, indicating that material 1 remains liquid, and material 2 becomes liquid

at the interface. This may for example occur during 3d printing, resulting in good adhesion between the printed layers.

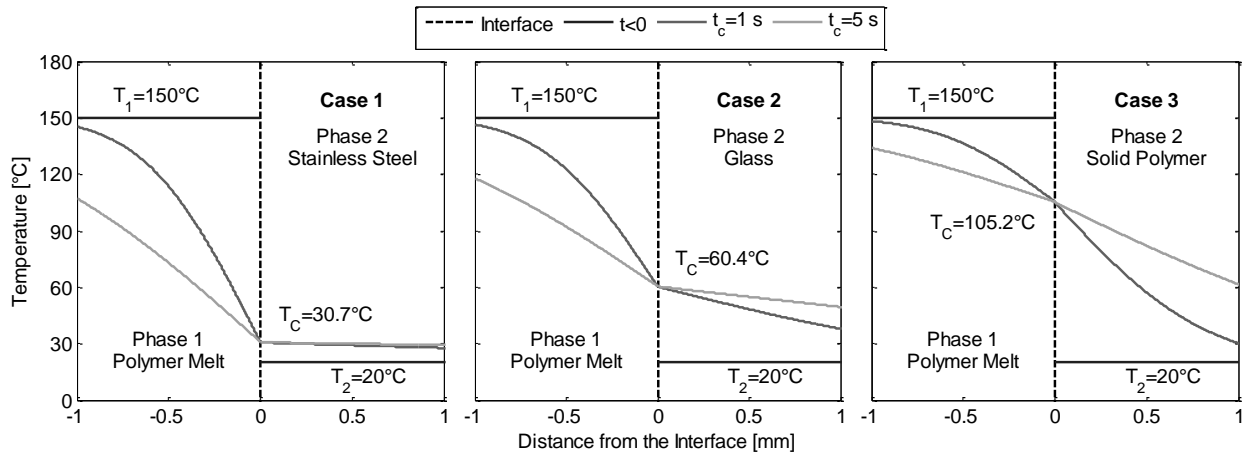


Figure 3.5: Calculated temperature profiles. Bulk temperatures are chosen for typical processing conditions: $T_1=150^\circ\text{C}$ and $T_2=20^\circ\text{C}$; (A): Polymer melt and stainless steel; (B): Polymer melt and glass; (C): Polymer melt and solid polymer

These calculations illustrate the basic effect of different thermal effusivities of the two phases on T_c . When exact T_c values are required, numerical solution to a fully parameterized heat transfer problem for a given geometry coupled with CFD simulations (to include convection) is recommended. However, we believe that our analysis captures the main effects and can explain tack behavior in various situations and for various materials combinations.

3.3.3 Non-isothermal Probe Tack Test

Figure 3.6 shows a schematic illustration of the probe tack experiments. The initial position (Figure 3.6, step 1) was used to ensure thermal equilibrium before the actual measurement. Step 2 of Figure 3.6, the bonding and contact phase is the same for all measurements in principle. However, the two following separation mechanisms were expected to be observed during the debonding phases:

- (1) Adhesive failure at the interface (Figure 3.6, step 3, no tack). $T_{C,NT}$ is below T_S of the polymer, which does not wet the probe. Only weak adhesive forces act between the phases, and during debonding the probe detaches from the sample without creating a filament, leaving an imprint on the sample

- (2) Cohesive failure in the sample material (Figure 3.6, step 4, tack). $T_{C,T}$ is well above T_C of the polymer. The adhesive forces at the interface are stronger than the flow resistance of the sample. As a result, a filament detaches from the sample that constricts until it ruptures in the constriction upon reaching a critical distance.

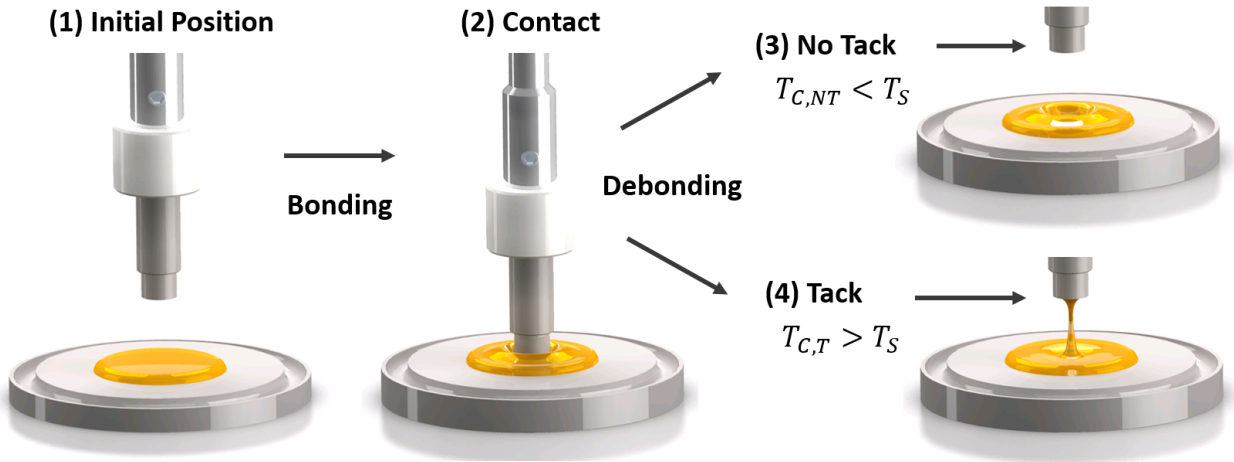


Figure 3.6: Schematic illustration of the probe tack experiment: ground plate (bottom), sample (orange), temperature controlled probe. (1) initial position; (2) position after bonding; (3) and (4) debonding with (3) no tack or adhesive failure and (4) tack or cohesive failure.

Three probe tack measurement series at different T_M , T_P and contact times t_c were performed. Figure 3.7A shows the molten samples and the cylindrical probe before the experiment. The measured stress-strain (σ - ϵ) curves for all three series are presented in Figure 3.8. In the beginning, the probe approaches the sample surface at a constant speed, without exerting force. On contact with the surface, a positive displacement force is exerted on the sample, which is compressed and squeezed under the probe until the predefined gap size $H=1\text{ mm}$ is reached.

The bonding phase has similar σ - ϵ diagrams in all experiments and also suggests good reproducibility of measurement series one and two with identical process parameters. The maximum bonding stress $\sigma_{b,max}$ increases with the decreasing T_P , which indicates that viscosity in the probe vicinity decreases due to a more intense melt cooling. In series 3, $\sigma_{b,max}$ is significantly increased due to lower T_M and higher viscosity. Trend diagrams of the bonding characteristics are shown in Figure 3.9A&C.

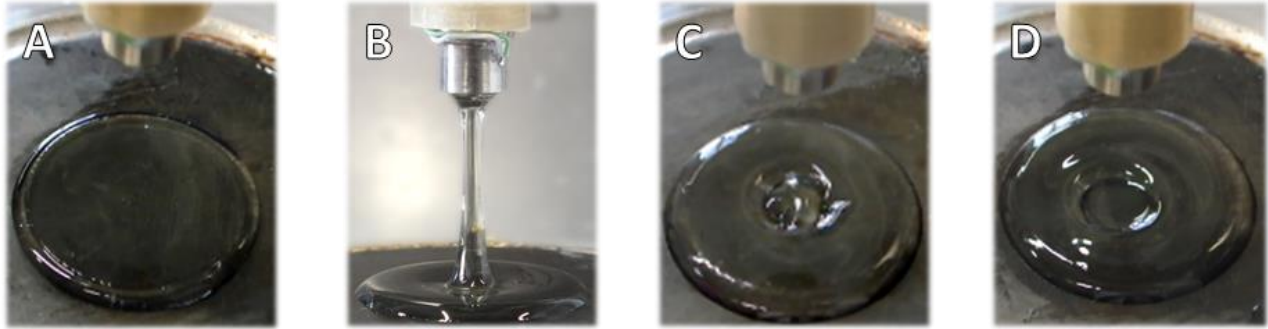


Figure 3.7: Snapshots of the probe tack experiments. Sample before bonding (A) and after debonding (B-D) at $T_M=170^\circ\text{C}$. (B) $T_P=130^\circ\text{C}$, adhesion with filament formation. (C) $T_P=110^\circ\text{C}$ initial adhesion and adhesive failure after some deformation. (D) $T_P=90\text{-}50^\circ\text{C}$ initial weak or non-adhesion and adhesive failure at the interface leaving a non-deformed imprint on the sample.

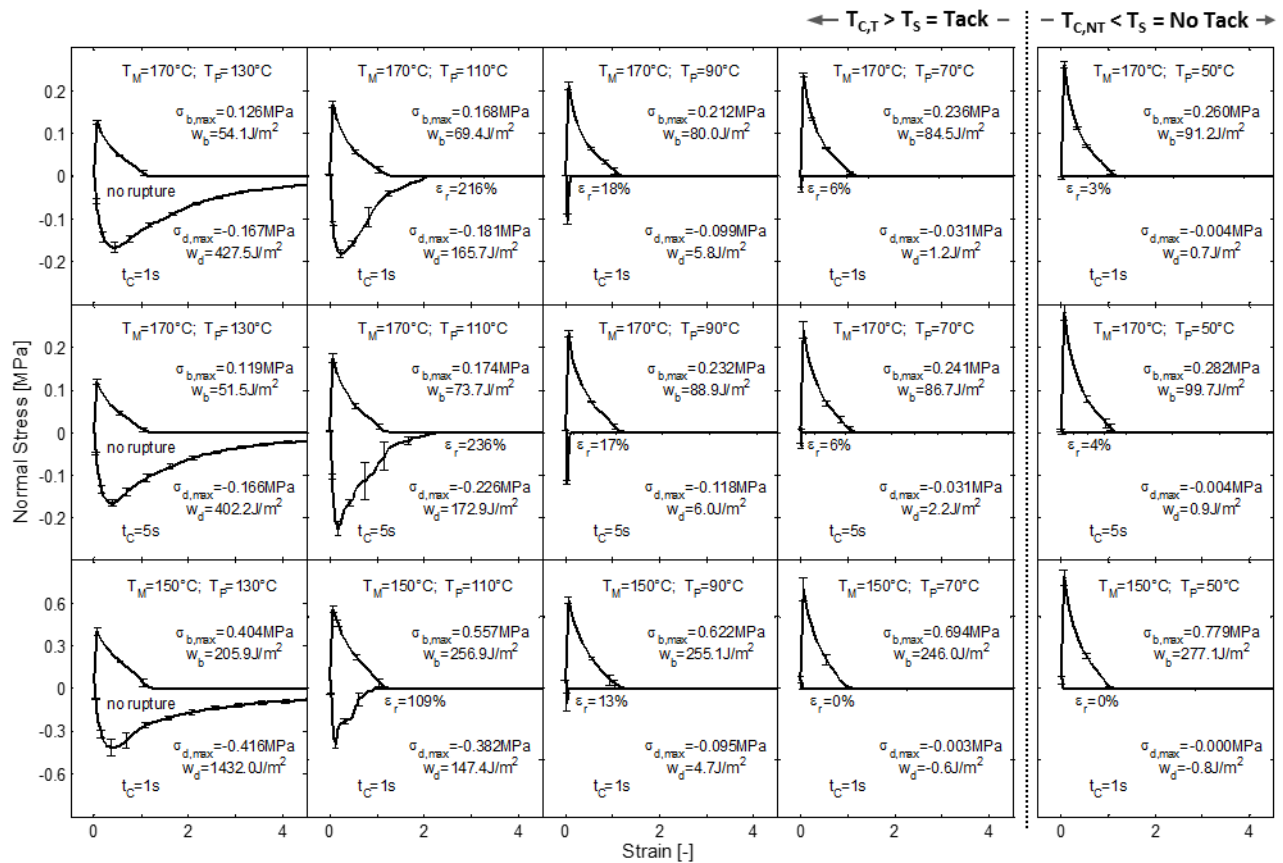


Figure 3.8: Probe tack stress-strain diagrams at different non-isothermal conditions. Positive and negative stress values correspond to bonding and debonding, respectively. Top row: series 1, $T_M=170^\circ\text{C}$, $t_c=1$ s. Middle row: series 2, $T_M=170^\circ\text{C}$, $t_c=5$ s. Bottom row: series 3, $T_M=150^\circ\text{C}$, $t_c=1$ s. T_P is decreasing from left to right (150-50°C). Glass transition of the polymer temperature is 73°C.

Measurable adhesion should be formed for $T_C > T_S$. For the polymer melt in question, T_S is approximately 73°C (Figure 3.1). The analysis of the heat transfer suggests that T_C will be slightly above T_P . As such, the formation of adhesive bonds at $T_P > 70^\circ\text{C}$ is expected and no tack should be measured at the lowest investigated $T_P = 50^\circ\text{C}$.

Debonding at the highest $T_P = 130^\circ\text{C}$ (Figure 3.8, Column 1) resulted in the formation of a single filament in all three measurement series. The filament (Figure 3.7B) did not rupture due to insufficient maximum strain and the normal stress at maximum strain did not return to 0. Since T_C is clearly above T_S , the polymer can wet the surface, forming a strong adhesive bond. Debonding work w_d and maximum debonding stress $\sigma_{d,max}$ for series one and two at equal T_P are almost identical, confirming the semi-infinite-body simplification. For measurement series three, higher $\sigma_{d,max}$ and w_d levels were observed due to increased viscosity.

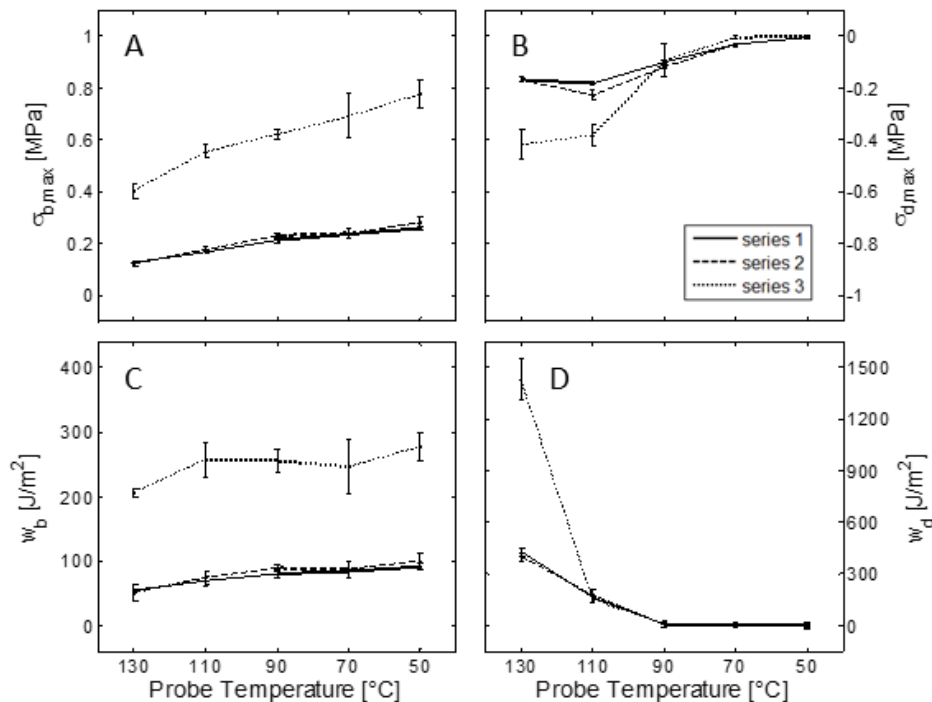


Figure 3.9: Bonding and debonding trend diagrams. (Reverse x-axis, TP probe temperature). (A): $\sigma_{b,max}$ maximum bonding stress; (B): w_b bonding work; (C): $\sigma_{d,max}$ maximum debonding stress; (D): w_d debonding work

At $T_P=110^\circ\text{C}$, which is close to the transition point between the two regimes, adhesive failure occurred after some deformation (Figure 3.7C) at rupture strains ε_r of 109-236%. Further decreasing T_P first to 90°C (Figure 3.8, column 3) and then to 70°C (Figure 3.8, column 4) decreases $\sigma_{d,max}$, w_d and ε_r further (Figure 3.7D). At the lowest $T_P=50^\circ\text{C}$ (Figure 3.8, column 5) and $T_C<T_S$, no significant $\sigma_{d,max}$ or ε_r were measured, which confirms our hypothesis. Trend diagrams for the debonding characteristics are shown in Figure 3.9B&D.

3.4 Conclusions

In this work, we proposed a contact temperature tack hypothesis and investigated the correlation between the heat transfer and tack properties of polymer melts and solid bodies. The non-isothermal probe tack measurements were in good agreement with the proposed hypothesis. Releasing the probe required significant w_d for $T_C>T_S$, little w_d for $T_C\sim T_S$ and no w_d for $T_C<T_S$. With regard to technical applications, this means that melts will stick at interfaces above T_S and that sticking can be avoided by cooling interfaces below this critical temperature. These findings support our hypothesis.

3.5 References

- [1] C. Bellehumeur, L. Li, Q. Sun, and P. Gu, “Modeling of Bond Formation Between Polymer Filaments in the Fused Deposition Modeling Process,” *J. Manuf. Process.*, vol. 6, no. 2, pp. 170–178, 2004.
- [2] R. P. Wool, B. L. Yuan, and O. J. McGarel, “Welding of polymer interfaces,” *Polym. Eng. Sci.*, vol. 29, no. 19, pp. 1340–1367, 1989.
- [3] O. A. Ezekoye, C. D. Lowman, M. T. Fahey, and A. G. Hulme-Lowe, “Polymer weld strength predictions using a thermal and polymer chain diffusion analysis,” *Polym. Eng. Sci.*, vol. 38, no. 6, pp. 976–991, 1998.
- [4] D. Treffer, P. Wahl, D. Markl, G. Koscher, E. Roblegg, and G. J. Khinast, “Hot Melt Extrusion as a Continuous Pharmaceutical Manufacturing Process,” in *Melt Extrusion: Materials, Technology and Drug Product Design*, M. A. Repka, N. Langley, and J. DiNunzio, Eds. aapspress, 2013.
- [5] J. Y. Chen and S. J. Hwang, “Investigation of adhesion phenomena in thermoplastic polyurethane injection molding process,” *Polym. Eng. Sci.*, vol. 52, no. 7, pp. 1571–1580, 2012.
- [6] W. Tillmann, L. Hagen, F. Hoffmann, M. Dildrop, A. Wibbeke, V. Schöppner, V. Resonnek, M. Pohl, C. Krumm, J. C. Tiller, M. Paulus, and C. Sternemann, “The Detachment Behavior of Polycarbonate on Thin Films Above the Glass Transition Temperature,” *Polym. Eng. Sci.*, vol. 56, no. 7, pp. 786–797, 2016.
- [7] A. Baldan, “Adhesion phenomena in bonded joints,” *Int. J. Adhes. Adhes.*, vol. 38, pp. 95–116, 2012.
- [8] A. Zosel, “Adhesion and tack of polymers: Influence of mechanical properties and surface tensions,” *Colloid Polym. Sci.*, vol. 263, pp. 541–553, 1985.
- [9] C. Creton and L. Leibler, “How Does Tack Depend on Time of Contact and Contact Pressure?,” *J. Polym. Sci. Part B Polym. Phys.*, vol. 34, pp. 545–554, 1996.
- [10] K.-Y. Bae, D.-H. Lim, J.-W. Park, H.-J. Kim, H.-M. Jeong, and A. Takemura, “Adhesion Performance and Surface Characteristics of Low Surface Energy PSAs Fluorinated by UV Polymerization,” *Polym. Eng. Sci.*, vol. 53, no. 9, pp. 1968–1978, 2013.
- [11] J. W. MCBain and D. G. Hopkins, “On adhesives and adhesive action,” *J. Phys. Chem.*, vol. 29, no. 2, pp. 188–204, 1925.
- [12] D. E. Packham, “Handbook of Adhesion,” in *Handbook of Adhesion*, Second Edi., D. E. Packham,

- Ed. Chichester: John Wiley & Sons Ltd, 2005, p. 312.
- [13] K. L. Mittal, *Adhesion Measurement of Films & Coatings*, vol. 2. Zeist: VSP BV, 2001.
- [14] K. L. Mittal, "The role of the interface in adhesion phenomena," *Polym. Eng. Sci.*, vol. 17, no. 7, pp. 467–473, 1977.
- [15] G. Crevoisier, P. Fabre, J.-M. Corpart, and L. Leibler, "Switchable Tackiness and Wettability of a Liquid Crystalline Polymer," *Science (80-.)*, vol. 285, no. 5431, pp. 1246–1249, 1999.
- [16] I. Benedek and M. M. Feldstein, *Technology of pressure-sensitive adhesives and products*. Boca Raton: CRC Press, Taylor & Francis Group, 2009.
- [17] D. A. Dillard and A. V. Pocius, Eds., *Adhesion Science and Engineering - I - The Mechanics of Adhesion*, 1st ed. Amsterdam: Elsevier Science B.V., 2002.
- [18] I. Benedek and M. M. Feldstein, *Applications of Pressure-Sensitive Products*. Boca Raton: CRC Press, Taylor & Francis Group, 2009.
- [19] C. Creton and P. Fabre, "Tack," in *The Mechanics of Adhesion*, 2002, pp. 535–575.
- [20] Y. Peykova, O. V. Lebedeva, A. Diethert, P. Müller-Buschbaum, and N. Willenbacher, "Adhesive properties of acrylate copolymers: Effect of the nature of the substrate and copolymer functionality," *Int. J. Adhes. Adhes.*, vol. 34, pp. 107–116, 2012.
- [21] N. Karyu, M. Noda, S. Fujii, Y. Nakamura, and Y. Urahama, "Effect of adhesive thickness on the wettability and deformability of polyacrylic pressure-sensitive adhesives during probe tack test," *J. Appl. Polym. Sci.*, vol. 43639, pp. 1–11, 2016.
- [22] C. A. Dahlquist, "Pressure-Sensitive Adhesives," in *Adhesion and Adhesives*, New York: Marcel Dekker Inc., 1969, pp. 219–260.
- [23] T. P. Russell and H. C. Kim, "Tack - a Sticky Subject," *Science (80-.)*, vol. 285, pp. 1219–1220, 1999.
- [24] A. Zosel, "The effect of bond formation on the tack of polymers," *J. Adhes. Sci. Technol.*, vol. 11, no. 11, pp. 1447–1457, 1997.
- [25] Y. Nakamura, K. Imamura, and K. Ito, "Contact Time and Temperature Dependencies of Tack in Polyacrylic Block Copolymer Pressure-Sensitive Adhesives Measured by the Probe Tack Test," *J. Adhes. Sci. Technol.*, vol. 26, pp. 231–249, 2012.
- [26] S. Moon, A. Chiche, A. M. Forster, W. Zhang, and C. M. Stafford, "Evaluation of temperature-

- dependent adhesive performance via combinatorial probe tack measurements,” *Rev. Sci. Instrum.*, vol. 76, p. 62210, 2005.
- [27] A. Zosel, “The effect of fibrillation on the tack of pressure sensitive adhesives,” vol. 18, no. December 1997, pp. 2–5, 1998.
- [28] D. Treffer, A. Troiss, and J. Khinast, “A novel tool to standardize rheology testing of molten polymers for pharmaceutical applications,” *Int. J. Pharm.*, vol. 495, no. 1, pp. 474–481, 2015.
- [29] H. D. Baehr and K. Stephan, *Heat and Mass Transfer*, 2nd Editio. Berlin, Heidelberg: Springer Verlag, 2006.
- [30] E.-I. Hanzawa, “Classical Solutions to the Stefan Problem,” *Tohoku Math. J.*, vol. 33, pp. 297–335, 1981.
- [31] T. Loulou and D. Delaunay, “The interface temperature of two suddenly contacting bodies , one of them undergoing phase change,” *Int. J. Heat Mass Transf.*, vol. 40, no. 7, pp. 1713–1716, 1997.
- [32] A. Eitzlmayr, J. Khinast, G. Hörl, G. Koscher, G. Reynolds, Z. Huang, J. Booth, and P. Shering, “Experimental characterization and modeling of twin-screw extruder elements for pharmaceutical hot melt extrusion,” *AIChE J.*, vol. 59, no. 11, pp. 4440–4450, 2013.

*“When everything seems to be going against you,
remember that the airplane takes off against the
wind, not with it.”*

Henry Ford

4 Enhanced Air-Cooled Die Face Pelletizing of Sticky Formulations Using a Thermally-Decoupled Die Plate

Abstract:

Hot melt extrusion is an important method for processing active pharmaceutical ingredients (API) with a carrier material and additives into a homogeneous material. After extrusion, intermediates with excellent bulk flow properties are often required, e.g., pellets sized below 1 mm manufactured via die face pelletizing (DFP). Since cutting takes place at the material’s temperatures above the extrudate’s solidification point, during transportation and cooling the newly cut pellets can be deformed into an almost spherical shape due to viscoelastic forces and surface tension. To date, air-cooled DFP has been limited to processing non-sticky formulations. This study challenges this limitation and proposes a way to prevent stickiness. We analyzed the energy balance of a conventional die plate design and knives and calculated the temperature profiles. Combined with our new contact-temperature tack hypothesis, our results were used to identify the major cause for this limitation. Thus, we re-engineered the die plate by thermally decoupling the knives’ running surface from the flow channel, creating a cold runner surface and a hot flow channel for the API-polymer mixture. The knives were actively cooled via heat exchange with the running surface of the die plate and maintained at a low temperature. The new design was implemented and successfully tested with three pharmaceutical polymers that are commonly known to be sticky. It can be concluded that a thermally decoupled die plate expands the range of processable formulations. In the future, DFP can have new applications, e. g., for producing almost spherical pellets with excellent bulk flowability, low friability and easy containment.

4.1 Introduction

Over the last years hot-melt extrusion (HME) has raised significant interest in the pharmaceutical sciences, especially with respect to the development and production of complex pharmaceutical products. It may be applied to produce various types of solid solutions and solid dispersions, can aid in increasing an API solubility and can be applied to tailor the release profiles to a certain target rate [1–6]. Nevertheless, HME is an efficient process to make pharmaceutically relevant materials in one step, combining feeding, mixing, compounding and extrusion. Thus, compared to a classical wet-granulation route with three processing steps, HME is only one step leading to more efficient processing routes. Moreover, it is an inherently continuous process, allowing for easy integration in a continuous manufacturing environment. In fact, a full pharmaceutical manufacturing environment can be realized within just a few m² of floor space by combining a continuous extruder, pelletizer and capsule filler.

In the beginning of the HME process, various powders and/or liquid materials are fed to the extruder and (mostly due to shear) a homogeneously molten material stream is created. In many cases, as final product of extrusion pellets are desired, either to be filled directly in capsules or as intermediates for tablet compaction and novel pharmaceutical processes (e.g., injection molding). Depending on a particular application, cross section of the die bores can have various shapes, ranging from cylindrical holes to thin slits. The strands are cut into small portions of identical size and shape (“pellets”). Pellets can be produced via either strand pelletizing or die face pelletizing (DFP).

Strand pelletizing (Figure 4.1A), for which a die head and a plate with several bores, a cooling section and a strand pelletizer are used, is widely applied in the plastics and pharmaceutical fields. The strand pelletizer comprises a knife roller and a bed knife and typically cuts the solidified strands into small cylinders. The strands are delivered to the knives via feeding rolls. The pellet length and diameter are determined by the feeding roll rotational speed and the mass throughput per strand, respectively.

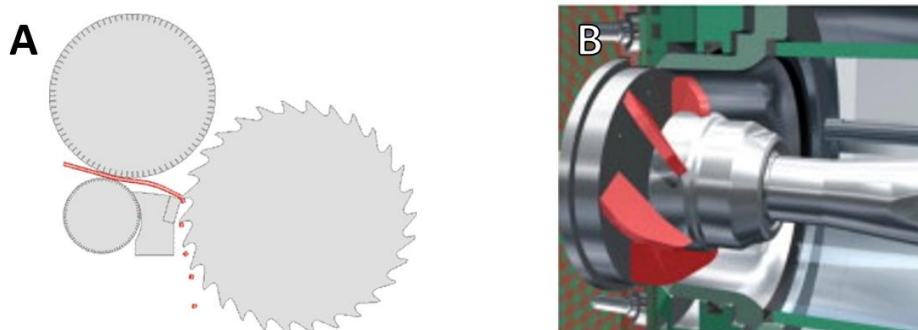


Figure 4.1: Schematics of (A) strand pelletizing and (B) die-face pelletizer (Picture courtesy: Automatik Plastics Machinery GmbH)

Although strand pelletizing is a technology that is easy to design and to apply, it is not suitable for numerous formulations due to their solidification behavior: upon cooling below the solidification temperature, some materials rapidly turn from a non-processable and highly-deformable sticky liquid into a non-processable brittle solid that breaks into small splinters, thereby creating a lot of dust and irreproducible pellet morphology. In some cases, long cooling lines may be required for sufficient quenching before cutting can take place. Generally, utilizing a cooling line increases the required floor space and the containment efforts for highly-potent products.

In contrast, during (DFP) (Figure 4.1B) cutting takes place directly on the extrusion die face, and the in-flight solidification of the particles occurs. A rotating knife presses against the die plate and cuts the emerging material in the viscous state, allowing viscoelastic forces and surface tension to render the pellets almost spherical. The pellets are forwarded to a storage bin or a subsequent processing step, solidifying during the conveying. The cooling rate depends on the cooling medium (air and water are commonly used), the flow conditions and the heat transfer properties of both, the material, and the cooling medium. Applying air or inert gas as a cooling agent is recommended since the system is solvent-free (i.e., the pellets only have to be separated from the air stream). However, the cooling intensity is significantly lower compared to water.

The advantages of DFP are twofold: (1) in one processing step, almost spherical pellets with superior bulk flow and dosing properties can be produced and (2) the system can easily be contained, since a die face cutter is typically a closed system (i.e., the cleanroom is located inside the machine). The drawback of this method, however, is that to date gas cooling can only be used for certain non-sticky formulations. For example, Case [7], Martin [8] and Treffer et al. [9] reported that many formulations cannot be processed via air-cooled DFP, since air-quenched systems tend to smear polymer on the die face. Mürb stated that cooling in the cutting chamber has a strong impact on the cuttability since it influences the rheological parameters of the freshly-emerging extrudate [10].

When water is used as a cooling agent, the process is termed underwater pelletizing. It is widely applied for high throughput production in the plastics industry. However, only few research articles on cutting and pellet formation have been published. Neubauer et al. [11] were the first that theoretically analyzed cutting. A recent publication by Kast et al. [12] relied on the basic concepts to conducted fundamental research of the influence of pellet shaping kinetics on rheology and process parameters. Yet their work did not address the effects of smearing, sticking and agglomerate formation. Most non-aqueous systems (e.g., oil) are combustible and require appropriate equipment (e.g., ex-proof). Typically, liquid cooling fluids are not suitable for pharmaceutical applications. Since APIs and the matrix material are typically water-soluble (or at least they are intended to be soluble in bio-relevant media), water can change the pellet properties. What is more, the remaining liquid could cause certain problems, e.g., in terms of stability issues and flowability. Thus, mostly air-cooled systems are used in pharmaceutical manufacturing.

Pelletizing is only feasible when the pellets detach from the cutting tool after being cut. When sticky formulations are processed, the material tends to stick to the back of the knife or the extrudate is smeared across the die face. Large agglomerates can accumulate on the blade before detaching due to centrifugal forces and/or the smeared extrudate can form a film on the die face. Such materials cannot yet be processed via DFP.

Sticking of the material on the knife is termed ‘tack’, which is defined as the work required for release a bond between two materials after a short, defined contact time and pressure. Although most tack studies on adhesives were performed under isothermal conditions, a recent publication [13] reported on an investigation of the influence of heat transfer on tack properties and established that tack is formed only when the immediate contact temperature at the interface is above the solidification point of the adhesive polymer. In this case, the polymer is liquid at the interface and can wet the micro-rough substrate surface, forming a strong adhesive bond. At contact temperatures below the solidification point, the polymer is solid at the interface and cannot wet the substrate (i.e., penetrate into microscopic surface irregularities), leading to a strongly reduced direct contact between metal and polymer molecules, thus effectively preventing adhesion. This is also the main reason why DFP is limited to non-tacky formulations. According to this contact-temperature tack hypothesis, the surface temperature of the knives under processing conditions may be too high, and cooling of the knives could solve the problem. Strong experimental evidence for high temperature levels at the knives was obtained when annealing colors were observed on the high-speed steel (HSS) knives after processing, which only occur at temperatures above 200°C on HSS surfaces.

The problem with using conventional die plates for DFP is that the bore holes conveying the melt must have a wall temperature above the melting or, rather, the solidification point in order to avoid blocking the die by solidified material (die freeze-off). Therefore, the bore holes are well-heated and can only process materials that are not too sticky (e.g., PVC) or the surface is permanently cooled beneath the solidification temperature by the cooling agent. A minimum throughput of the material is required to carry the heat with the flow of material, and sufficient frictional heating must be established to keep the orifices open.

A previous work of our group [9] suggested that the stability of a pelletizing process can be increased by thermally decoupling the melt temperature in the die zone and the pelletizer to prevent strong interactions between them. For example, during the start-up phase, when the pelletizer is

docked to the extruder's die plate, the melt temperature drops noticeably and may lead to die freeze-off and emergency shutdowns.

The current study goes beyond this idea and presents an investigation of thermally decoupling the extruder's die head and the pelletizer. The goal is to reduce the cutting tool temperature to prevent sticking and to increase the processability window of DFP also to sticky materials. Thus, process stability is enhanced by decreasing the interactions between the two units. First, we analyzed the energy balance of a conventional DFP system applied for HME in the pharmaceutical industry. Next, an implementation with a thermally decoupled die plate was carried out and analyzed following the approach that exists for conventional die plate designs. Finally, we compared both designs and provided an application, demonstrating the suitability of the thermally decoupled die plate prototype for sticky polymers.

4.2 Materials and Methods

4.2.1 Materials

Experiments with the extrusion equipment were performed with three pharmaceutical polymers.

1. Eudragit®E (EE) (Evonik Industries AG, Darmstadt, Germany) is a cationic copolymer based on dimethyl-aminoethyl-methacrylate, butyl-methacrylate and methyl-methacrylate with a glass transition temperature of $\sim 45^{\circ}\text{C}$.
2. Kollidon® VA64 (K64) (BASF SE, Ludwigshafen, Germany) is a vinylpyrrolidone-vinyl acetate copolymer and has a glass transition temperature of $\sim 100^{\circ}\text{C}$.
3. Soluplus® (S+) (BASF SE, Ludwigshafen, Germany) is a polyvinyl-caprolactam-polyvinyl acetate-polyethylene-glycol graft-copolymer and has a glass transition temperature of $\sim 70^{\circ}\text{C}$.

All three polymers were donated by their respective manufacturers.

4.2.2 Extrusion Line Setup

The extrusion line comprised an 18 mm co-rotating twin-screw extruder (ZSK 18, Coperion GmbH) and a hot die face pelletizer (SPHERO®-THA, Automatik Plastics Machinery GmbH). Feeding was performed with a twin-screw loss in weight feeder (K-Tron K-PH-KT20, Niederlenz, Switzerland). The extruder/pelletizer setup is described in more detail in the previous publications of our group [14-16].

4.2.3 Heat Transfer Analysis

Heat transfer was analyzed using the software PTC Creo Simulate 2.0, which solves the partial differential equation describing heat conduction using the FE-Method. Convective heat transfer was considered at the boundary conditions. The heat transfer coefficient for natural convection was averaged as $\alpha_{NC} = 20 \text{ W/m}^2\text{K}$, and forced convection as it occurs on the die face was averaged as $\alpha_{FC} = 150 \text{ W/m}^2\text{K}$. In both cases, room temperature $T_R = 25^{\circ}\text{C}$ was used to calculate the temperature gradient. The material used in the simulations were stainless steel (SS), copper (Cu),

PTFE and hard metal alloy tungsten carbide (TC). The material properties applied in the calculations are summarized in Table 4.1.

Table 4.1: Applied material properties

	SS	Cu	PTFE	TC
Thermal conductivity $\lambda_i \left[\frac{W}{mK} \right]$	15	300	0.25	75.3
Density $\rho_i \left[\frac{kg}{m^3} \right]$	7,8	8,2	2,2	14
Heat capacity $c_p \left[\frac{J}{kgK} \right]$	400	385	1300	155

The boundary conditions at the interfaces between the die plate, the DFP and the extruder were identical in both of the investigated cases. The extruder /die adapter plate (“8-0-piece”) had a uniform surface temperature of $T_{8-0} = 200^\circ C$, and the water cooled THA housing temperature was $T_{THA} = 20^\circ C$. All interfaces were treated without accounting for thermal contact resistance.

4.3 Results and Discussion

4.3.1 Energy Balance - Modeling and Simulation

4.3.1.1 Conventional Design

Figure 4.2 illustrates the various contributions and effects that need to be included in the energy balance of a conventionally designed die plate, showing every heat flow within the boundary region between the die plate and the knives. Heat sources and heat sinks are colored red and blue, respectively. The die plate is temperature-controlled via heat conduction from an electrically or oil-heated 8-0 adapter. Here, the so-called “8-0 adapter” is the transition from the 8-shaped twin-screw channel to a circular melt flow channel. The die plate has a second contribution to the energy balance, i.e., the rotating knife is pressed against the die plate and thus, frictional heating occurs that depends on the rotational speed, contact pressure and friction coefficient. The frictional heating is superimposed to the thermal conduction from the knife’s head.

The system has four heat sinks: (1) forced convection induced by the cooling air stream, (2) conduction across the thermally insulating PTFE seal into the DFP housing, (3) conduction into the knife shaft and (4) natural convection on the lateral surface of the die plate.

The knife (where melt-sticking issues are most relevant) is shown in Figure 4.3. The knife has two heat sources and two heat sinks: the sources are due to frictional heating and conduction from the die plate, and the heat sinks are due to forced convection from the cooling air stream and conduction towards the knife’s head and shaft. Cutting occurs in the vicinity of the contact area between the knife and the die plate. The temperature in this region is above that of the die plate since conduction and frictional heating are superimposed. Figure 4.4 shows the calculated temperature profiles of a conventional die plate design. The running (cutting) surface has temperatures between 100-180°C. This high temperature is required to ensure a minimum extrudate temperature and steady extrusion without die freeze-off. However, such high temperatures cause sticking in case of sticky materials. Thus, sticky materials would require a certain minimum die temperature (to avoid freeze-off), yet a cold knife to reduce sticking. However, both requirements cannot be satisfied with the standard

design and the limited cooling provided by an air-cooled system. Thus, the equipment design must be revised to implement both, a heated flow channel and a cold running surface.

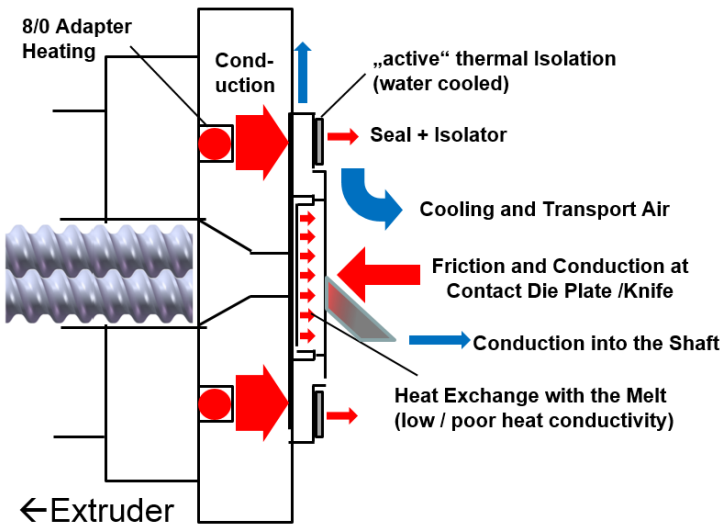


Figure 4.2: Illustration of the contributions that need to be considered in the energy balance of a conventional die plate

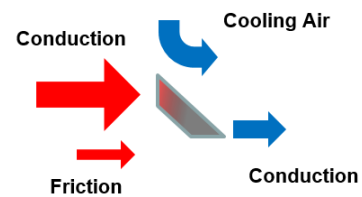


Figure 4.3: Contributions to the energy balance for a knife used on a conventional die plate

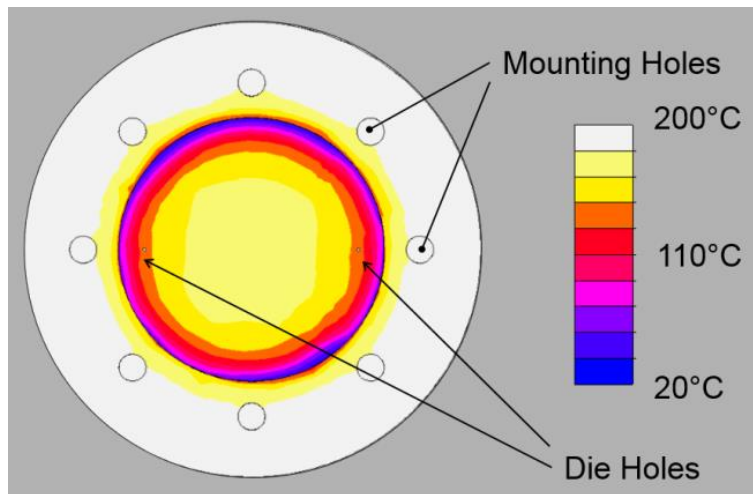


Figure 4.4: Calculated temperature profile of a conventional die plate (2 die holes with a 1 mm bore diameter).

4.3.1.2 Novel Thermally-decoupled Design

Achieving a high temperature difference between the flow channel and the sliding surface of the die plate requires their thermal decoupling. Thermally decoupling the flow channel and the rest of the die plate comprises both (passive) insulation and active heating and cooling. The insulation simply minimizes the heat exchange between the decoupled parts.

Figure 4.5 shows the contributions to the energy balance of the thermally decoupled die plate and the 8-0 adapter. The flow channel can be temperature controlled using an appropriate heating system (e.g., electrical heating or circulating heat transfer medium such as oil) in a double jacket nozzle system or can be coupled with the 8-0 adapter heating. The heat exchanged between the die plate and the flow channel can be minimized via thermally decoupling of both, using an air gap or a thermally insulating structure. The applied cooling significantly decreases the running surface temperature. The thermally-insulating seal used in the conventional design is replaced by a thermally conductive seal (e.g., copper based) in order to maximize conduction into the water-cooled THA housing.

The energy balance for the knife in the novel design is shown in Figure 4.6. It consists of the same contributions as for the conventional design. However, the conduction term changes sign as the knife loses heat via conduction to the cold die plate, which is the dominant contact most of the time during one revolution. When the knife is in contact with the hot parts of the flow channel, the heat flows in the opposite direction, towards the knife. This contribution, however, is small. Thus, effective knife cooling via conduction can be achieved using die plates whose cold area is much larger than the warm area [17].

Figure 4.7 shows the calculated temperature profiles of the thermally decoupled die plate design. The running surface is at an almost constant temperature of 20°C. Only in the vicinity of the flow channels temperatures of ~180°C are observed. In this calculation, about 99% of the running surface are cold and only a very small portion (1%) is warm. As such, the decoupled design

promotes the knife's cooling via heat conduction into the die plate, significantly reducing the knife's temperature and ensuring better processability of sticky materials.

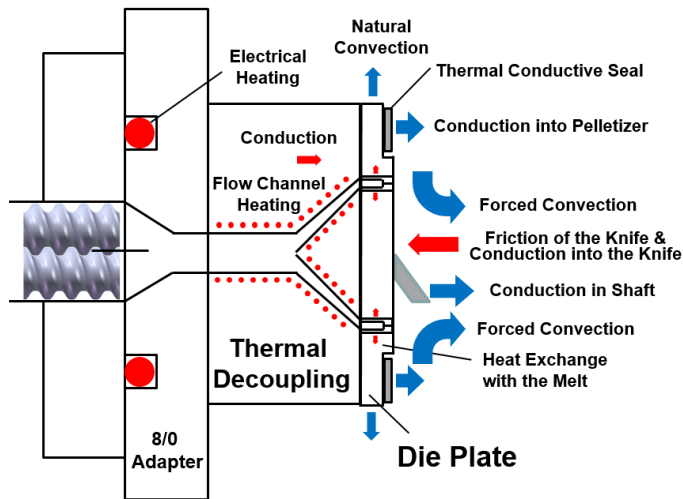


Figure 4.5: Illustration of the contributions to the energy balance of the thermally decoupled design

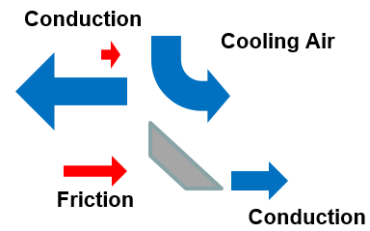


Figure 4.6: Extracted knife heat balance in combination with the thermally decoupled die plate

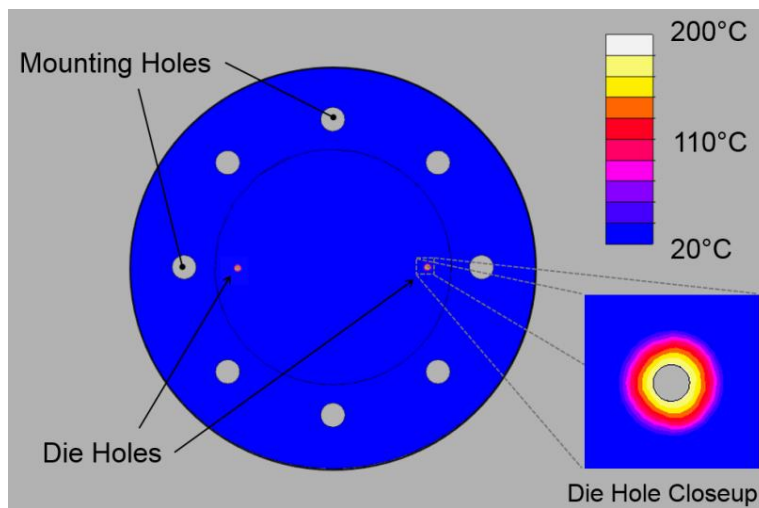


Figure 4.7: Calculated temperature profile of the thermally decoupled design (2 die holes with 1 mm bore diameter)

4.3.2 Prototype

The prototype was designed in a modular manner to assure a high degree of flexibility and to fit into the same space as available for the conventional design. No further modifications of the adapter plates were required. A sectional view of the construction is shown in Figure 4.8. The flow channels are formed by the distributor plate and the exchangeable nozzles. The running surface is made of TC and is part of the perforated body. The alignment between single components is performed using spacers and centering pins. Thermal decoupling between the cold and warm sides is achieved via an air gap in large areas. Since direct contact occurs in small areas where the centering pins and spacers are located (close to the THA cooling), the transferred heat is drained away without excessively heating the running surface. The nozzle region is covered with an elastic silicone-based seal, preventing the material from entering the gap. A close-up of the nozzle region is shown in Figure 4.9. Material entry would impact the heat transfer between actual decoupled components and could cause process stability issues. Thus, uniform contact with the seals is preferred although it cools the flow channel slightly.

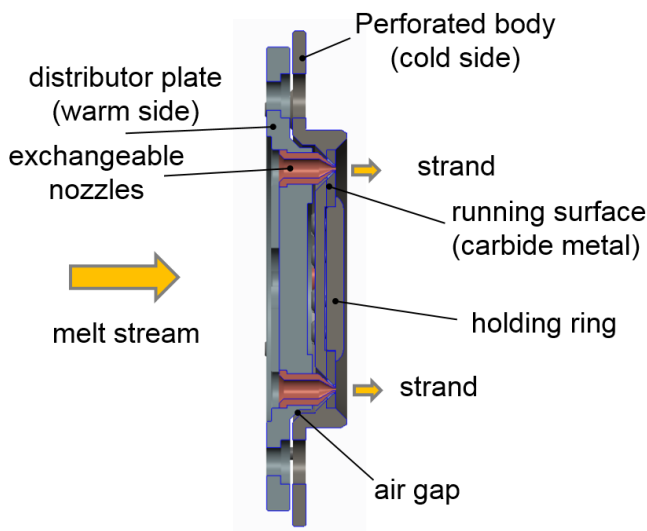


Figure 4.8: Sectional view of the modular thermally decoupled die plate

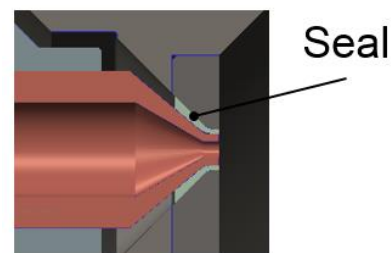


Figure 4.9: Close-up of the die hole

The exchangeable nozzles allow to change the die plate configuration with little effort. The number of die holes can be altered by installing blind plugs. Nozzle configuration (e.g., cylindrical length and bore diameter) can be adapted by simply manufacturing small lathed parts according to the individual requirements. As such, a broad spectrum of throughputs and pellet dimensions can be produced using the same die plate.

4.3.3 Pelletizing Experiments

In the initial experiments, the energy balance calculations of the real prototype were validated. The system was preheated, and the pelletizer was coupled with the extrusion line and started. All heat sources and sinks were active, and the system was allowed to reach a steady state. Next, the system was stopped and the cutting chamber was opened. Temperatures of the sliding surface, flow channel and knives were measured manually using a surface temperature probe or a cylindrical probe that fit closely into the flow channel. These simple measurements matched the calculated temperature profiles presented in the previous section reasonably well. As predicted, high temperature differences between running surface and flow channel were successfully achieved.

For extrusion experiments, the start-up procedure for processing was similar to the one applied during the validation runs. The extrusion line was heated to set temperatures, and the pelletizer was docked with the extrusion line and started. Again, for a smooth startup the system was allowed to reach the steady state. Subsequently, the materials were fed into the prototype, and after a certain start-up phase constant pellet properties were achieved.

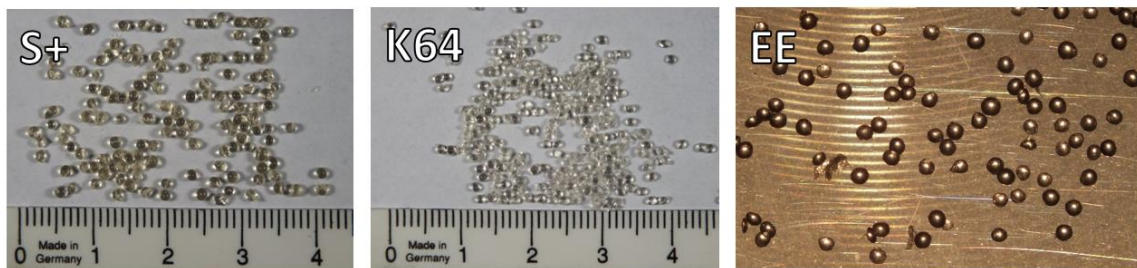


Figure 4.10: Pictures of the pellets produced by DFP and the thermal decoupled die plate prototype (EE pellet diameter 0.8 mm)

This fully-contained extrusion line is easy to implement and a high degree of process stability can be achieved. Experimental runs to demonstrate the concept were performed using three polymers. Photographs of the pellets produced with the new prototype die plate are shown in Figure 4.10. As can be seen, various types of pure pharma polymers, which cannot be handled by conventionally-designed die plates, can be processed using this die plate.

4.4 Conclusions

The recently introduced contact-temperature tack hypothesis suggests that tacking can be prevented by lowering the cutting tool temperature. An energy balance analysis of the conventional die plate design indicated that the flow channel and the knife temperatures cannot be set independently. Lowering the temperature requires thermal decoupling of the flow channel and the sliding surface of the die plate. This realization inspired a novel thermally-decoupled die plate design. Its modular structure allows to satisfy a broad range of requirements using the same die plate. The prototype was successfully developed and applied to pelletizing three polymers known to be highly sticky. As such, more formulations can be processed by DFP and can benefit from the advantages of this technology (e.g., easy containment and spherical pellets with optimal bulk flowability).

4.5 References

- [1] E. Roblegg, E. Jäger, A. Hodzic, G. Koscher, S. Mohr, A. Zimmer, and J. Khinast, “Development of sustained-release lipophilic calcium stearate pellets via hot melt extrusion.,” *Eur. J. Pharm. Biopharm.*, vol. 79, no. 3, pp. 635–45, Nov. 2011.
- [2] S. Bialleck and H. Rein, “Preparation of starch-based pellets by hot-melt extrusion.,” *Eur. J. Pharm. Biopharm.*, vol. 79, no. 2, pp. 440–448, Oct. 2011.
- [3] T. Kipping and H. Rein, “A new method for the continuous production of single dosed controlled release matrix systems based on hot-melt extruded starch: analysis of relevant process parameters and implementation of an in-process control.,” *Eur. J. Pharm. Biopharm.*, vol. 84, no. 1, pp. 156–71, May 2013.
- [4] F. Zhang and J. W. McGinity, “Properties of sustained-release tablets prepared by hot-melt extrusion.,” *Pharm. Dev. Technol.*, vol. 4, no. 2, pp. 241–50, May 1999.
- [5] C. De Brabander, C. Vervaet, and J. . Remon, “Development and evaluation of sustained release mini-matrices prepared via hot melt extrusion,” *J. Control. Release*, vol. 89, no. 2, pp. 235–247, Apr. 2003.
- [6] N. Follonier, E. Doelker, and E. T. Cole, “Various ways of modulating the release of diltiazem hydrochloride from hot-melt extruded sustained release pellets prepared using polymeric materials,” *J. Control. Release*, vol. 36, no. 3, pp. 243–250, Oct. 1995.
- [7] C. C. Case, “Melt Pelletization,” in *Pharmaceutical Extrusion Technology*, New York: Marcel Dekker Inc., 2003, p. 400.
- [8] C. Martin, “Twin Screw Extrusion for Pharmaceutical Processes,” in *Melt Extrusion: Materials, Technology and Drug Product Design*, M. A. Repka, N. Langley, and J. DiNunzio, Eds. New York, Heidelberg, Dordrecht, London: Springer, 2013.
- [9] D. Treffer, P. Wahl, D. Markl, G. Koscher, E. Roblegg, and G. J. Khinast, “Hot Melt Extrusion as a Continuous Pharmaceutical Manufacturing Process,” in *Melt Extrusion: Materials, Technology and Drug Product Design*, M. A. Repka, N. Langley, and J. DiNunzio, Eds. aapspress, 2013.
- [10] R.-K. Mürb, “Kunststoff granulieren und/oder pelletieren?,” *Chemie Ing. Tech.*, vol. 84, no. 11, pp. 1885–1893, Nov. 2012.
- [11] A. C. Neubauer, S. J. Rhee, and G. L. Smitherman, “Troubleshooting underwater pelletizing processes,” no. 4, pp. 241–245, 2003.

- [12] O. Kast, K. Geiger, E. Grünschloss, and C. Bonten, “Analysis of Pellet Shaping Kinetics at the Die Opening in Underwater Pelletizing Processes,” *Polym. Eng. Sci.*, vol. 55, no. 5, pp. 1170–1176, 2015.
- [13] D. Treffer and J. G. Khinast, “Why Hot Melts Do Not Stick to Cold Surfaces,” *Polym. Eng. Sci.*, 2016.
- [14] P. R. Wahl, D. Treffer, S. Mohr, E. Roblegg, G. Koscher, and J. G. Khinast, “Inline monitoring and a PAT strategy for pharmaceutical hot melt extrusion.,” *Int. J. Pharm.*, Jul. 2013.
- [15] D. Treffer, P. R. Wahl, T. R. Hörmann, D. Markl, S. Schrank, I. Jones, P. Cruise, R.-K. Mürb, G. Koscher, E. Roblegg, and J. G. Khinast, “In-line implementation of an image-based particle size measurement tool to monitor hot-melt extruded pellets.,” *Int. J. Pharm.*, vol. 466, no. 1–2, pp. 181–9, May 2014.
- [16] E. Roblegg, S. Ulbing, S. Zeissmann, and A. Zimmer, “Development of lipophilic calcium stearate pellets using ibuprofen as model drug.,” *Eur. J. Pharm. Biopharm.*, vol. 75, no. 1, pp. 56–62, May 2010.
- [17] D. Treffer, J. Khinast, J. Grubbauer, A. Eitzlmayr, G. Koscher, and T. Klein, “Hot viscous raw material leaving a cooler perforated body cooling a cutter,” 2013.

“Always deliver more than expected.”

Larry Page

5 In-line Implementation of an Image-based Particle Size Measurement Tool to Monitor Hot-melt Extruded Pellets³

Abstract:

This work focuses on the implementation and application of an in-line particle measurement tool to monitor particle properties of hot melt extruded pellets. A novel image analysis system (Eyecon) is used to analyze pellets with a size of approximately 1 mm. The method is based on photometric stereo imaging, which is achieved by three different-colored light sources arranged circularly around the lens. Several implementations, whereby the product stream was led through the optical sampling volume, have been tested. The advantages and disadvantages of each implementation are discussed and evaluated. The most suitable implementation was applied to an extrusion run with constant throughput and different cutting frequencies resulting in different pellet sizes. A particle size distribution comparison between the image analysis system and an off-line reference particle analysis (QICPIC) showed good agreement although only a small fraction of the particles were analyzed in-line. Additionally, some illustrative examples for process development are given. With this approach the capability of hot-die face pelletizing to manufacture nearly-spherical pellets with a narrow size distribution is proven.

³ This chapter is based on: D. Treffer, P. R. Wahl, T. R. Hörmann, D. Markl, S. Schrank, I. Jones, P. Cruise, R.-K. Mürb, G. Koscher, E. Roblegg, and J. G. Khinast, “In-line implementation of an image-based particle size measurement tool to monitor hot-melt extruded pellets,” *Int. J. Pharm.*, vol. 466, no. 1–2, pp. 181–189, 2014.

5.1 Introduction

Hot-melt extrusion is a continuous manufacturing process with increasing importance for the pharmaceutical industry. It offers a robust manufacturing alternative for solid solutions and solid dispersions, which are used to increase the bioavailability of poorly soluble drugs [1-2] or to achieve sustained-release behavior [3–5], respectively.

An extruder processes a formulation comprising of powders, pellets or liquids to form homogeneous strands of molten material. The molten material can be formed into various shapes, such as pellets, tablets or implants. In this work the strands are intended to be shaped into spherical pellets, which are used as intermediates for capsule filling [6-7], tablet compaction [8-9] or other processing steps. A typical way of achieving spherical pellets is extrusion-spheronization [10–12]. Here, after extrusion, the pellets are irregularly shaped (e.g., strands or cylinders) and need to be spheronized in an extra spheronization step. During spheronization the material is heated up to soften it and rounded by collisions with each other and the equipment walls. Highly uniform and spherical pellets are desired as this increases dosing precision (e.g., in pellet-dosing processes) and improves flowability.

However, this additional downstream process can be avoided by using hot-die face pelletizing that combines pelletizing and spheronization in one processing step. Figure 5.1 illustrates the described process. Hot-die face pelletizing is a method where cutting of the extrudate strands takes place above the softening point of the material. Thus, surface tension acts on the viscous pellets after cutting as a driving force for spheronization. Several authors found that the pellet morphology depends on formulation and process parameters and reported the production of nearly-spherical pellets by hot-die face pelletizing [13-14]. The obtained sphericity with an aspect ratio of 1 to 1.1 is superior to typical spheronization results. Additionally, the particle size distribution (PSD) can be much narrower. An extensive overview of the available pelletizing methods can be found in [15].

The downstream processes after pelletizing require constant pellet quality to obtain a robust process with high dosing accuracy. In order to ensure a certain quality, a suitable monitoring approach needs to be applied.

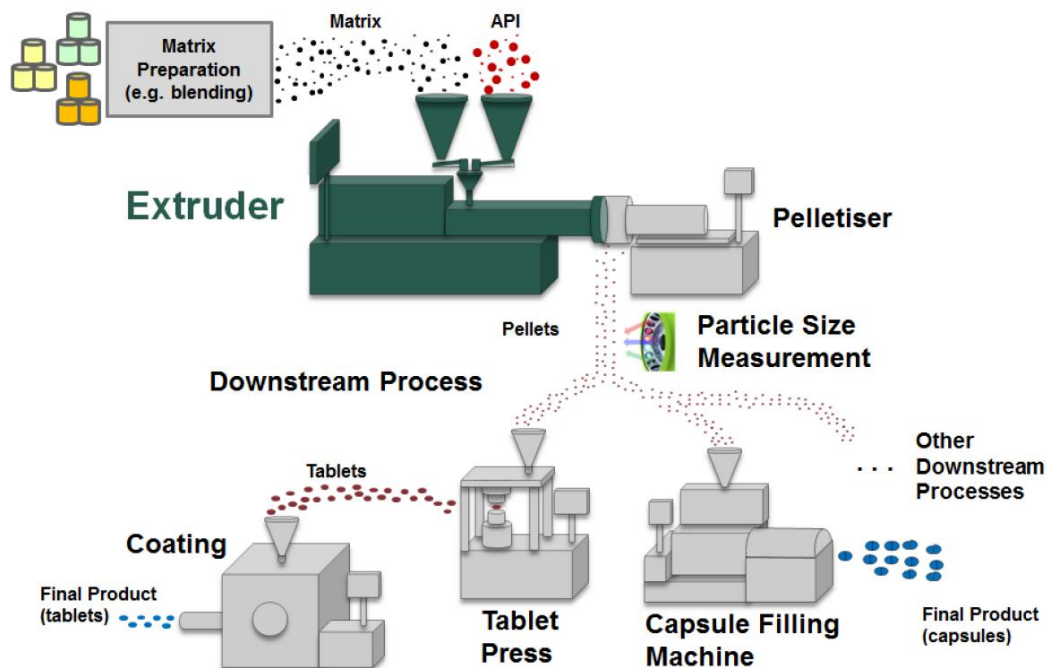


Figure 5.1: Process options in combination with a die-face pelletizing step

The pellet quality can be monitored with two main approaches [16]. First, in off-line monitoring [17] the samples are taken from the product stream at regular intervals and analyzed in the laboratory. Second, in/on-line monitoring [18]: for on-line monitoring a small bypass stream of the product stream is lead through the measurement device and analyzed in real time. In contrast, in-line analyzers are situated in the main product stream. The distinct advantage of in/on-line approaches is real-time information. In case of out-of-spec products, the operator or an automated process control system can react immediately, so that only small amounts of waste arise from a single process disturbance and the whole batch does not have to be disposed of or reworked.

Several techniques are available for in-line particle size measurement, of which focused beam reflectance (FBRM), spatial filter velocimetry, laser diffraction and various image analysis

methods are common [16]. In the pharmaceutical context, they are mainly used for fluid bed granulation, crystallization and spheronization.

In this work an image-based analysis method has been chosen to acquire visual information of shape and surface morphology besides pellet dimensions. Specifically, we focus on the implementation of a novel in-line photometric stereo image analyzer for production of nearly-spherical pellets. The analyzer uses photometric stereo techniques to derive 3D information based on 2D images to accurately measure particle size and shape. By monitoring production of pellets by hot-melt extrusion and hot-die face pelletizing the capabilities of manufacturing nearly-spherical pellets by this downstream method will be presented.

5.2 Materials and methods

5.2.1 Materials

The model matrix carrier for the hot-melt extrusion was calcium stearate CaSt (Werba-Chem GmbH, Austria; mean particle size 16.62 μm). The use of calcium stearate as a carrier matrix was recently introduced by Roblegg et al. [14]. The model active pharmaceutical ingredient (API) was paracetamol, donated by GL Pharma GmbH, Austria (mean particle size 139.2 μm). Glycerol-mono-stearate (GMS) was used as a plasticizer to lower the viscosity, and thus, the required process temperature. All CaSt-based experiments were performed with a formulation consisting of 75% CaSt, 20% Paracetamol and 5% GMS.

In addition, two different types of pellets, based on pure ethylene-vinyl-acetate EVA Ateva®1807EG (Celanese, USA) and based on a formulation consisting of 40% Eudragit RS, 40% Eudragit PO (Evonik Industries, Germany) and 20% Talcum (donated by GL Pharma GmbH, Austria) were used in the experiments.

5.2.2 Methods

5.2.2.1 Hot-melt extrusion

The extrusion line consists of a co-rotating twin-screw extruder ZSK 18 (Coperion GmbH, Germany) and a novel hot-die face pelletizer Sphero®-THA (Automatik Plastics Machinery GmbH, Germany). Both systems are implemented into a SIPAT system (Siemens AG, Belgium) for process control and monitoring. The extrusion line is also capable of monitoring the API content of the produced melt as described in [19-20].

Figure 5.2 shows a photograph of the pelletizing equipment and provides a detailed view of the cutting chamber. It is based on a rotor knife, which cuts the strands to form pellets of a predefined size, i.e., the emerging strands are cut into pellets directly at the hot die face. A previous study showed that almost spherical pellets can be obtained via hot-die face pelletizing [14].

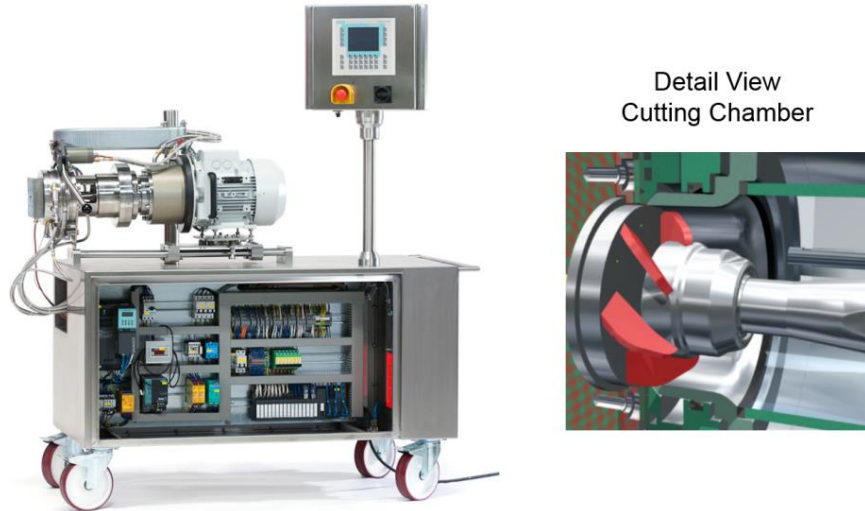


Figure 5.2: Picture of the Sphero®-THA and a detailed 3D illustration of the cutting chamber (Picture courtesy: Automatik Plastics Machinery GmbH).

5.2.2.2 In-line monitoring of pellet size properties

The pellet monitoring method is based on image analysis. The Eyecon™ particle characterizer technology uses concepts from 3D machine vision. It enables capturing both the size and shape of particles between 50 and 3000 microns. A CCD camera is used to capture a continuous image sequence of the particles every 600 ms, using pulses of direct illumination with a length of between one and five microseconds. This brief pulse avoids motion blurring of particles, which may be moving at speeds of up to ten meters per second. The illumination is arranged according to the principle of photometric stereo for capturing the 3D features of the particles in addition to a regular 2D image (Figure 5.3A).

The particle size is estimated from the images using the 2D and 3D information, applying novel image analysis methods and direct geometrical measurement [21-22]. The color information improves the edge detection. In case of overlapping or touching particles, the particles can be distinguished by color change, while conventional methods have problems with this situation and often overestimate the particle dimensions, as two particles are counted as one. Only fully captured particles are analyzed by the system. Partially captured particles, occurring at the image boundaries and in case of overlapping by overlying particles, are not analyzed. Each particle detected within

an image is first identified, and then described in terms of a best-fit ellipse (Figure 5.3B). The maximum and minimum diameters of this ellipse are used to calculate the volume of the particle. By combining all of the measured particle volumes the x_{10} , x_{50} and x_{90} values for the analyzed sample can be computed. The sample size can be adjusted from a single image to multiple images (e.g., to determine a x_{50} time course) up to the entire sampling period to obtain representative information for all particles.

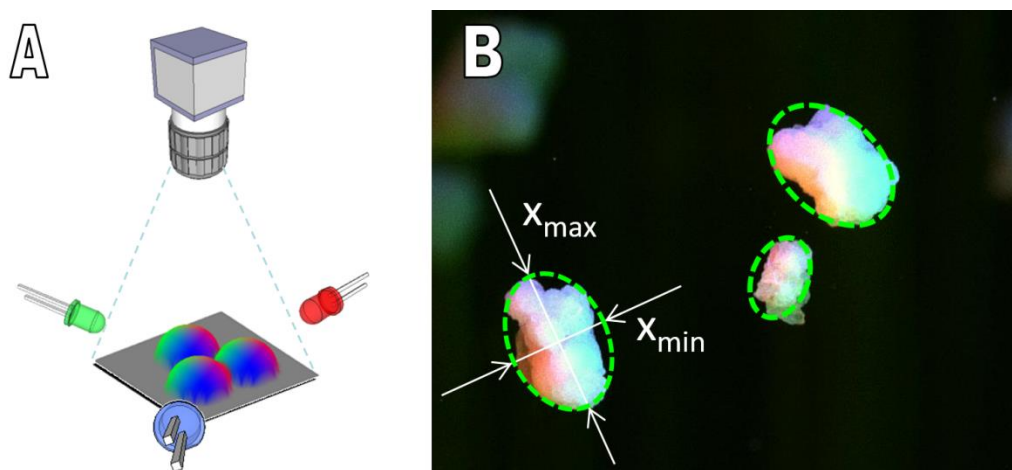


Figure 5.3: A: photometric stereo illumination arrangement (3 RGB LEDs); B: ellipses fitted to detected particles (Picture courtesy: Innopharma Labs Ltd.)

As the technology is based on direct measurement instead of indirect, such as laser diffraction, there is no need for material-based calibration. In addition, the method is a non-contact methodology and uses RGB LEDs to illuminate the field of view (9x6.5mm), so that no specific background is necessary. Thus, it can be applied externally to a process, e.g., through a glass window. However, there are some restrictions: the principle is based on diffuse reflected light, thus it cannot correctly detect black, strongly reflecting or transparent particles. Examples for the two later cases are shown in the results section. Applicability must be tested case by case, yet can be done off-line. The data are processed in real-time and the time evolution of the characteristic diameters are displayed, e.g. x_{10} , x_{50} , x_{90} . In addition, the data are stored as a number-based density distribution (q_0). This information can be used to derive the more common cumulative volume-based particle size distribution (Q_3) by applying basic conversion rules [23-24].

5.2.2.3 Area fraction calculation

The area fraction is used for a quantitative evaluation of the applied implementation approaches. It is an indication of the amount of particles within the optical sampling volume. The calculation of the area fraction is performed with the open source software ImageJ (National Institutes of Health (NIH), USA) [25]. The images are processed in the following sequence. First, the color images are converted into 8-bit grayscale images. Subsequently, the grayscale is inverted and the pellets are separated with a suitable threshold. The area fraction is obtained by averaging 20 images. To prevent distortion of the result, e.g. caused by dust on the measurement window, only particles greater than 1000 pixel² are included in the calculation. This pixel area corresponds to an actual area of ~0.04 mm² or ~0.11 mm diameter of a circle of equal projection area (EQPC).

5.2.2.4 Reference particle analysis

For reference particle analysis, an off-line image analysis tool (QICPIC, Sympatec GmbH, Germany) is used. The high-speed imaging tool is based on shadow projection. The sample is dispersed in a controlled way by means of a RODOS dry disperser and a VIBRI vibrational conveyor. At this configuration, the system is capable of capturing particles in the range of 1 µm to 6 mm. The particle size is determined by EQPC. Analysis using this method is carried out with at least 50,000 particles. Measurements were always done in triples.

5.2.3 Implementation

The in-line measurement tool has a field of view of 9x6.5 mm and depth of focus of 1.4 mm. The rather small optical sampling volume required some effort during the implementation to the pelletizer because of two reasons: First, the mean particle size in general is in the range of 1 mm, which is in the range of the depth of focus. Thus, for ideal recognition the pellets should pass the sampling volume in a monolayer arrangement. Second, the particles are conveyed by a cooling air stream at low volume concentrations.

A low volume concentration with a large particle diameter gives a very low particle amount. Assuming a pellet diameter of 1 mm and an air volume stream of 500 l/min, resulting in 63 pellets

per liter cooling air. The optical sample volume is approximately 0.23 ml, which would lead to a 593-fold exchange of the sample volume per second by direct implementation into the pelletizing system. Therefore, different implementation approaches with partial and full separation of the cooling air were developed and compared. The extruder was operated at constant throughput of 0.8 kg/h. The analysis was carried out with regard to the particle count per image, particle orientation and area fraction (a/a) of the analyzed particles. The values of area fraction and particle count per image have been analyzed for 20 consecutive images of each implementation approach.

In general, the main criterion for particle measurement by image analysis is to have focused images and a sufficient number of particles in each image. Apart from pellets, dust may be generated during cutting and transportation of the pellets which may influence the measurement. In this section two different implementation approaches regarding separation of the pellets and dust from the conveying air are described (Figure 5.4). Corresponding experimental results and their evaluation are discussed in detail in the Section 3.2.

5.2.3.1 Partial separation of the transportation gas

The pellet outlet of the Sphero®-THA is a cylindrical pipe 44.3 mm in diameter. The exit velocity depends on the cooling air stream that is required to render the pellets non-sticky and has typical values between 2.7–10.8 m/s for air flow rates of 250–1000 l/min. Figure 5.4.1 shows the investigated direct implementation approach.

The maximum velocity of the pellets is assumed to be the average outlet velocity of the exiting air flow. Furthermore, the pellets have velocity components in all directions due to turbulent eddy flow. Therefore, the outlet stream is guided into a funnel made of transparent glass and Plexiglas. The camera is located behind the glass plate, due to better optical properties compared to Plexiglas. Furthermore, the glass plate protects the lenses against dust. The major part of the gas flow is separated and exists at the top funnel inlet. The particles collide with the wall and fall subsequently through the funnel. The in-line measurement captures the particles at the rectangular funnel outlet

which has the dimensions of 8x6x20 mm. The narrow gap is designed to transport a sufficient amount of particles into the measurement area.

5.2.3.2 Complete pellet separation and camera position

The pellets are first completely separated from the air stream. Two different types of separation units are investigated. First, a centrifugal separator, i.e., a cyclone and, second, an impact separator with a subsequent classifier. The cyclone separates the solid particles from the air including dust that arises during cutting or transportation from the air stream.

Contrarily, the impact separator offers the option of separating dust and air stream from the pellets. This is performed by gravity separation against the air stream in a vertical pipe with an appropriate diameter. In both cases, the separated pellets drop on a chute of a vibrating conveyor. Two different measurement positions are investigated. First, the camera is located above the chute and captures the vibrating pellets during transportation (Figure 5.4.2a). Second, the camera is placed in front of the vibrating conveyor and captures the pellets immediately after dropping off the edge of the vibrating chute (Figure 5.4.2b).

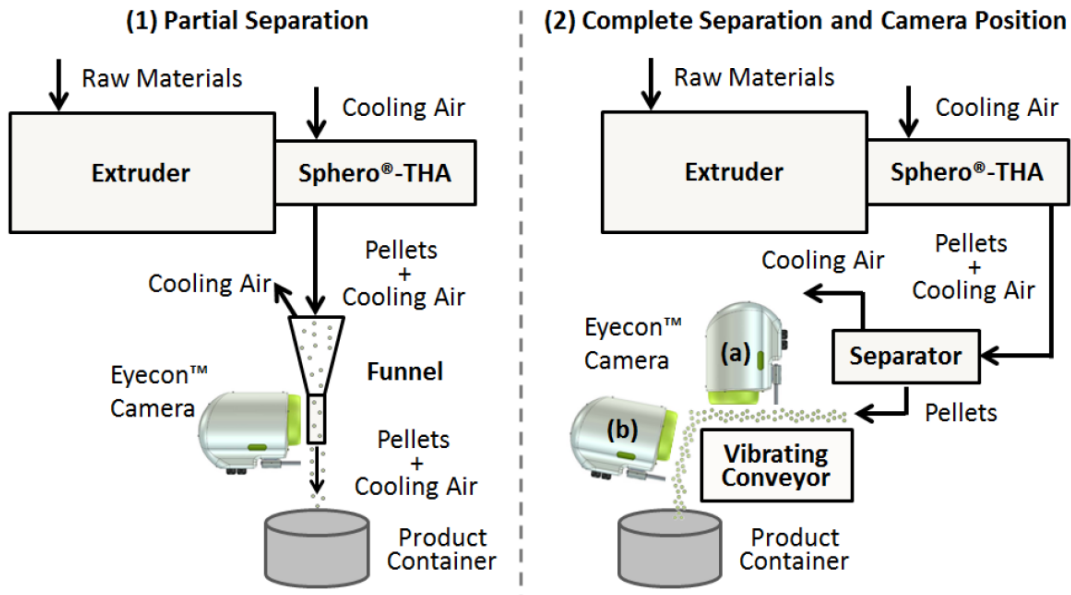


Figure 5.4: Implementation approaches

5.3 Results and discussion

All presented snapshots show the entire field of view (9x6.5 mm) of the in-line measurement tool. They are taken in-line and are representative of the described configuration except for where otherwise specified.

5.3.1 Applicability to pellet analysis

First, the applicability to the investigated material was tested by off-line analysis. The stereo photometric system was operated in an off-line bench-top mode and the pellets were located on a moveable stage. Figure 5.5A shows an image of CaSt pellets. The opaque white pellets reflected the light uniformly (diffuse) and all three RGB colors can be identified on the image. The pellets were placed as a monolayer with some overlying particles. However, the measurement system cannot handle every type of material, as shown in Figure 5.5(B-D). Figure 5.5B shows the pellets composed of EVA, which is a transparent material. The transparency is apparent by looking at the upper layer pellets: the borders of the hidden particles can be seen through them. One of the borders is highlighted with a dashed white line as an example and a detail view of the white solid box is shown in Figure 5.5C. The light can pass through the transparent material and is partially scattered at the surface. In addition, the particle edges are brighter on the images. This situation cannot be handled by the implemented detection algorithm. Thus, measurements were not possible. Figure 5.5D shows free-falling EVA pellets. Here, the light is to some extent specularly reflected by the particles. One can see the reflections of the individual LEDs, which are circularly arranged around the lens. This is due to either over-illumination or a change of optical properties caused by the elevated material temperatures as the measurement was performed in-line and the pellets were not at room temperature.

In summary, it has been shown that the system is applicable to CaSt pellets due good diffuse reflection. However, the system is not applicable to transparent EVA pellets.

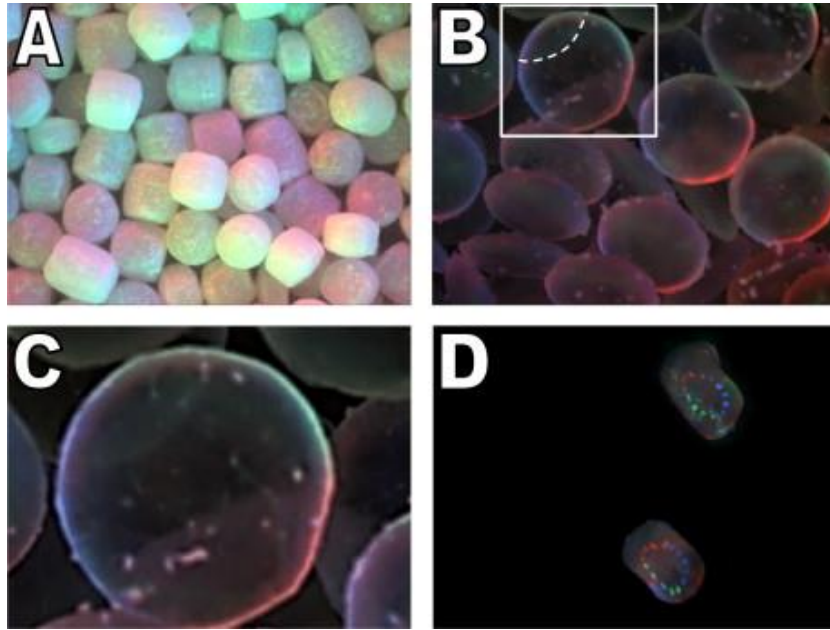


Figure 5.5: Snapshots of pellets with different optical properties. A: diffuse reflecting CaSt pellets; B: transparent EVA pellets (note the RGB light sources); C: detail view of the highlighted region in Image B; D: reflecting EVA pellets (in-line)

5.3.2 Implementation evaluation

The number of analyzed particles impacts the reliability of the PSD. In this section the implementations are evaluated through a comparison of the quantity of captured particles and their orientation. The particle volume concentration at the pelletizer exit has been calculated with the following assumptions: air volume stream = 500 l/min; particle mass stream = 1 kg/h, density = 1 kg/dm³, resulting in a very low particle volume concentration of $c = 0.0033\%$ (v/v). Thus, an increase in concentration is necessary to enable the measurements.

5.3.2.1 Partial separation of the transportation gas

Figure 5.6 shows two typical snapshots from the partial air separation implementation. The particle orientation in the optical sampling volume is random due to the freely falling pellets. As can be seen, a very low particle count is observed. On average only 1.5 particles were captured per image, which corresponds to an area fraction of 3.5% (a/a). This is even more problematic as only fully captured particles are analyzed. Particles which cross the image border are not evaluated.

Moreover, small dust particles settle on the funnel walls and disturb the image capturing process. This effect can be compensated by the evaluation algorithm by defining a particle detection range so that small dust particles are not evaluated, e.g., a minimum detection range of 300 μm .

In summary, this implementation is prone to errors if used in relation to non-stationary production (e.g., start up, shut down, disturbances) and the production of larger particles. Such particles could easily block the funnel and would need to be removed manually.

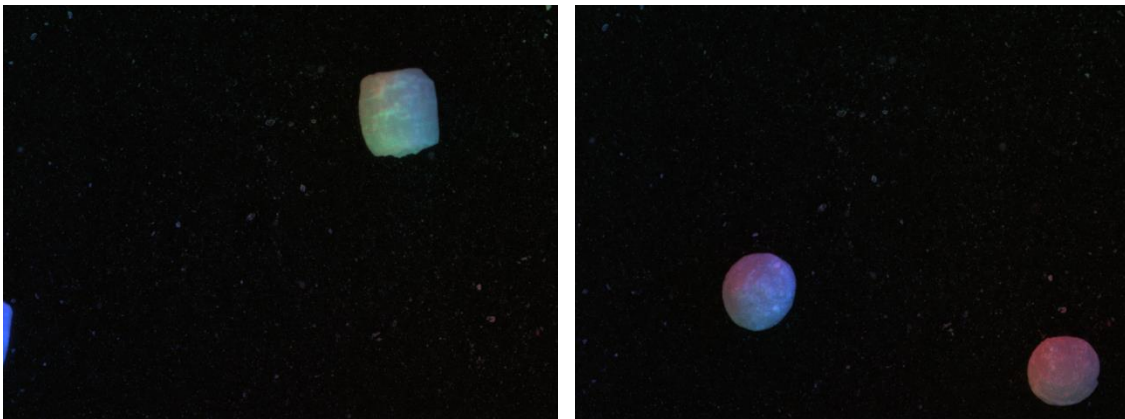


Figure 5.6: Snapshots the partial separation implementation

5.3.2.2 Complete air separation and camera in top view position

In this case the evaluation of particle concentration was performed by image analysis and area fraction and calculation of the area fraction (a/a) only.

In the experiments, the cutting frequency of the hot-die face pelletizer was varied from low to middle to high, resulting in three different types of pellets. Figure 5.7 shows snapshots at each operating point. The shape of the pellets was cylindrical with different length to diameter (L/D) ratios: first, at the low cutting frequency an L/D ratio of approximately 1.5 (left snapshot), at the middle cutting frequency an L/D ratio of close to one, and at the high cutting frequency an L/D ratio of approximately 0.5 were obtained, i.e., in the last case pellets resembled disks.

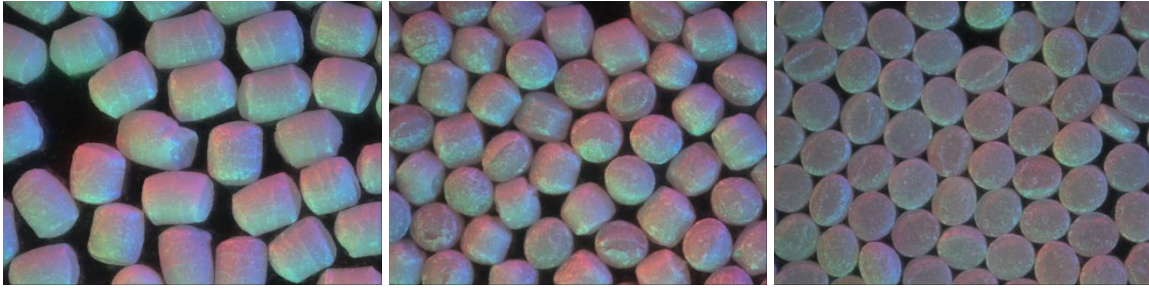


Figure 5.7: Snapshots of pellets obtained with complete air separation and camera position above the vibrating conveyor (cutting frequency; left-low; center-middle; right-high)

The use of a vibrating chute results in a preferred orientation of particles. The pellet rotation axis for an L/D ratio greater than one is parallel to the chute surface, while for L/D ratios smaller to one it is normal to the chute surface, leading to an overestimation of the pellet volume. This is a significant drawback for this implementation approach. For L/D close to one, the vibration energy is sufficient to establish a random representation of the pellets.

The evaluation of the area fraction resulted in values from 87% for the left and middle pellet dimensions and 90% for thin plates: the number of particles was depending on the actual size between 15-30 particles per image. For this implementation multi-sampling of the same pellet was possible, which could distort the results. The residence time within the optical sampling volume and thus the chance of multi-sampling depends on the particle properties like weight and shape.

5.3.2.3 Complete pellet separation and lateral camera position

The pellets were separated from the air stream using the same method as described above. However, the camera was located right after the edge of the chute. The pellets were captured while dropping into the storage bin following a parabolic trajectory. Therefore, the camera was tilted by a few degrees to maximize the optical sampling volume, as indicated in Figure 5.4.2b. The area fraction was used to describe the quantity of particles captured by the camera. The average particle count was 4.5 particles per image and the area fraction was 7.2% (a/a) on average.

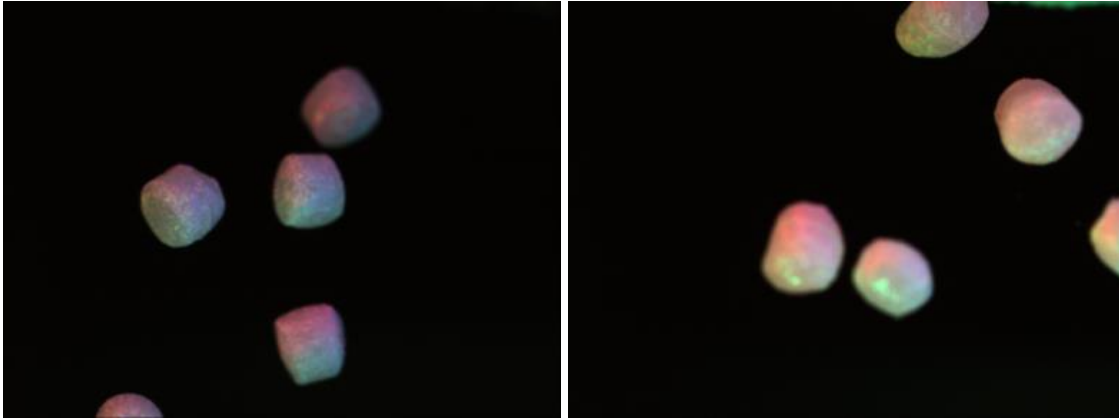


Figure 5.8: Snapshots of the implementation with complete pellet separation and lateral camera position

Figure 5.8 shows two representative snapshots for this implementation. The left image shows four pellets which are located farther away, while the right image shows pellets closer to the camera. If pellets are too close the size may be overestimated and vice versa, if pellets are too far way an underestimation may occur or pellets may become invisible. This source of error has a minor impact, as the depth of focus is narrow and particles far outside focus are not illuminated via the LED flash, and thus are not visible. Therefore, accurate alignment of the sampling volume is important for measurement reliability.

5.3.2.4 Comparison of the implementation approaches

In this section the results for the three different setups are compared and a recommendation for the most suitable approach is given. In Table 5.1 the results of the three setups are summarized. The first approach with partial separation has an advantage in terms of random particle orientation. However, the risk of blockage and a low number of particles for a reliable determination of the PSD are reasons for excluding this approach. The second setup approach has been developed to increase the number of analyzed particles. The area fraction was approximately increased by a factor of 30. However, the particle orientation was not random, effectively presenting the largest area in the image plane. This fact biased the PSD dramatically. Thus, this approach was also not deemed accurate enough for quality control of pellets.

Table 5.1: Overview of the image analysis relevant results for the three setups

Setup	Area Fraction (a/a)	Volume Fraction (v/v)	Number of Particles per Image [-]	Particle Orientation [-]
Partial Separation	3	0.0033%	1.5	Random
Complete Separation & Above Camera Position	88	-	30	Oriented
Complete Separation & Lateral Camera Position	7.2	-	4.5	Random

The aim of the last approach was to combine the advantages of the previous implementation while minimizing its drawbacks. The resulting statistics lie between the first two approaches. However, the clear advantages of this implementation are the statistically random pellet representation, the background-free images (no dust) and the single capturing. The number of particles is 4.5 which is still at the lower limit for efficient quality analysis; however, in a production environment higher throughputs are normal and would lead to a higher number of pellets per image. As a result, a clear recommendation for the last implementation can be given. This setup was further tested by in-line monitoring of an actual manufacturing process of pellets. The results are shown in Section 3.3.

5.3.3 Application to in-line process monitoring

The final setup of the analysis system was applied to in-line monitor the pellet size distributions during an extrusion process with subsequent hot-die face pelletizing. The objective was to show a comparison between in-line PSD data and the reference method. First, an experimental design to obtain pellets at different sizes was chosen. The material throughput of 0.8 kg/h was kept constant and the cutter speed was changed from 2000 rpm to 3600 rpm in 400 rpm steps. Thus, five settings were investigated. The cutter setup consisted of two die holes and two knives. Thus, cutting frequencies of 133 to 240 pellets per second were achieved. A sampling period of 10 minutes was chosen. The in-line PSD data have been extracted for investigated sampling of each log file entry and averaged over the sampling period. The off-line analysis has been applied to all produced

pellets for each investigated set of parameters, which corresponds to sample sizes between 80 and 140 thousand pellets.

Figure 5.10 shows the PSD data obtained from the experiment, both from the in-line measurement system and the reference measurements. The in-line data are shown as solid lines and the reference data as dashed. Clearly, a decreasing pellet size with increasing cutting frequency can be seen, as the curves are shifted from right to left. The results have also been verified against a theoretical size ratio estimation for average pellets obtained from the highest (3600 rpm) and lowest (2000 rpm) cutting frequencies. Clearly, the ratio of cutting frequencies of 1.8 should be identical to the volume ratio of ideal spherical pellets, resulting in a theoretical ratio of the diameters of 1.21. The measured ratio of 1.24 between the $x_{50}=1480 \mu\text{m}$ at 2000 rpm and $x_{50}=1198 \mu\text{m}$ at 3600 rpm corresponds well with the theoretical diameter ratio for ideal spherical pellets. The small deviation was probably caused by the non-spherical shape of the pellets.

The comparison between the off-line and in-line approach showed - in general - good agreement (see Table 5.3). The x_{50} and x_{90} values were almost identical (deviations $< 5\%$) and the shape of the curve was quite similar. Differences, as observed for x_{10} , might be explained by the different measurement approach of 3D diffuse reflected light vs. 2D shadow projection and the small number of pellets analyzed by the in-line measurement in this setup. The system analyzed approximately 50 pellets per minute, whereas the reference method analyzed the entire bulk produced during the 10 minutes sampling time. Thus, the in-line analysis considered only 0.3 to 0.6% of the total number of pellets to calculate the PSD. Despite the low particle count, the comparison suggested that the results were quite accurate, with some deviations towards smaller particle sizes.

In general, the more narrow a distribution the fewer particles are required for a reliable PSD analysis [23]. A simple approach to describe the width of a distribution is to calculate the x_{90} to x_{10} ratio, i.e., the span of the distribution. At normal operating conditions the pellets produced by hot-die face pelletizing show a ratio well below 1.5, which corresponds to a narrow PSD according to the classification shown in

Table 5.2 [23]. By comparing the PSD width ($x_{90}-x_{10}$, Table 5.3) one can see that the width became narrower with increasing cutting frequency (Figure 5.9), with a slight minimum at 2800 rpm. The reason for a narrower PSD was identified by analyzing the aspect ratio in Table 5.4. Both in-line and reference analytics show the lowest aspect ratios (a_{50}), i.e., the roundest pellets, for rotational speeds of 2800 rpm and 3200 rpm. These pellets also showed the lowest span of the aspect ratio distribution (a_{90}/a_{10}).

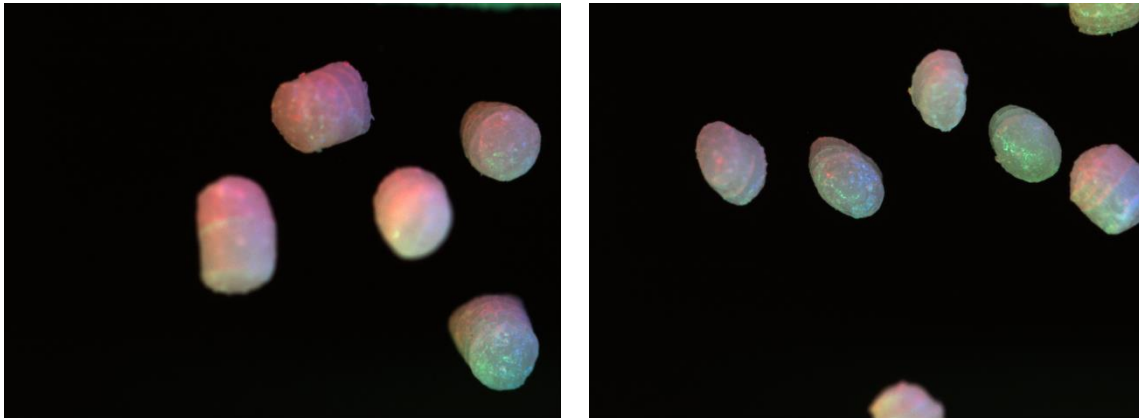


Figure 5.9: Snapshots at 2000 rpm (left) and 3600 rpm (right). Note the different length to diameter ratio of the pellets.

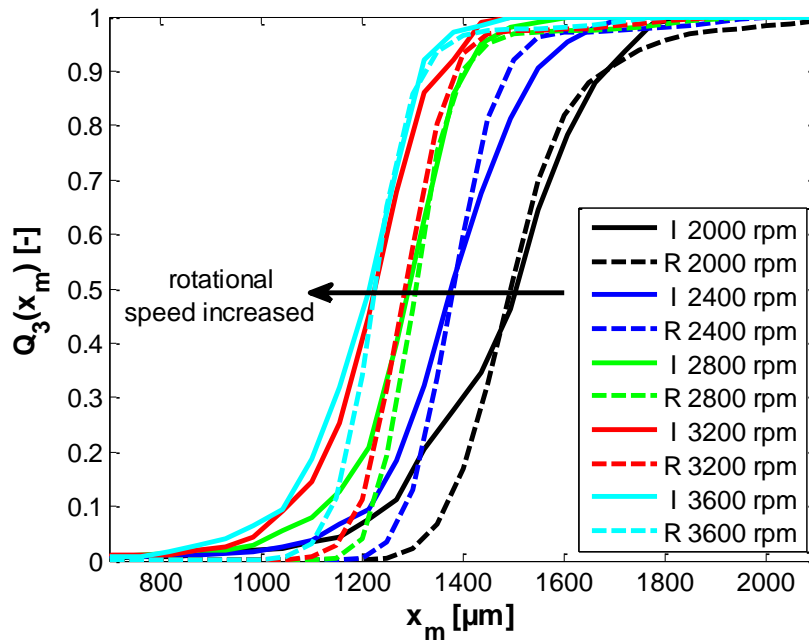


Figure 5.10: Comparison of the in-line PSD data to the reference method (I: In-line measurement; R: Reference measurement)

At lower cutting frequencies the pellets became more elongated with a higher length to diameter ratio. This resulted, due to the random orientation of the pellets in the observation window, in a broadened PSD, as well as larger aspect ratios and a broadened distribution of the aspect ratios. Thus, the broadening did not necessarily correspond to physical deviations between the pellets. In that sense, the same non-spherical particle captured multiple times in a random orientation would result in a particle size distribution and different aspect ratios due to the 2D analysis method. This fact has to be taken into account when regularly shaped particles are analyzed. Thus, additional parameters, such as shape factors, are important to be considered.

Table 5.2: PSD width classification [23]

	x_{90}/x_{10} [-]
Monosized	<1.02
Ultra-narrow	1.02-1.05
Narrow	1.05-1.5
Medium	1.5-4
Broad	4-10
Very Broad	>10

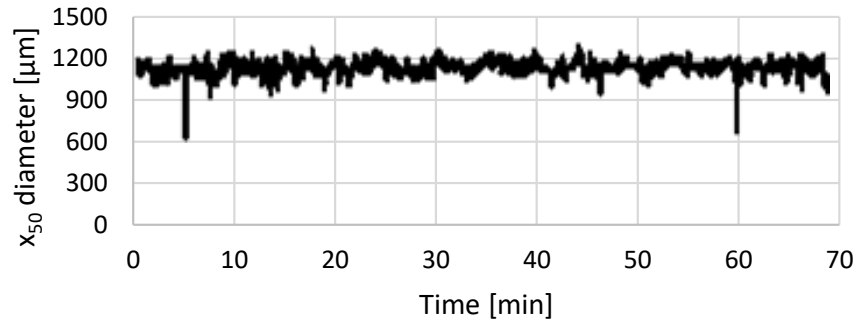
Table 5.3: Comparison of important PSD measures of Figure 5.10 (I: In-line measurement; R: Reference measurement)

RPM	x_{10} [μm]			x_{50} [μm]			x_{90} [μm]			x_{90}/x_{10} [-]		$x_{90}-x_{10}$ [μm]	
	I	R	Dev.	I	R	Dev.	I	R	Dev.	I	R	I	R
2000	1250	1366	9%	1506	1494	-1%	1685	1682	0%	1.35	1.23	435	316
2400	1217	1284	6%	1378	1381	0%	1548	1490	-4%	1.27	1.16	331	206
2800	1124	1219	8%	1294	1306	1%	1408	1399	-1%	1.25	1.15	283	180
3200	1052	1192	13%	1225	1286	5%	1362	1388	2%	1.29	1.16	310	195
3600	1047	1141	9%	1214	1226	1%	1320	1327	1%	1.26	1.16	273	186

Table 5.4: Comparison of particle shape measures of Figure 5.10 (I: In-line measurement; R: Reference measurement)

RPM	a_{50} [-]			a_{90}/a_{10} [-]
	I	R	Dev.	R
2000	1.27	1.35	6%	1.30
2400	1.21	1.25	3%	1.19
2800	1.20	1.20	0%	1.16
3200	1.20	1.19	-1%	1.17
3600	1.24	1.23	0%	1.27

In most in-line applications, the monitoring of the entire PSD over time leads to an unmanageable amount of information. Therefore, only a single parameter of the PSD can be extracted and monitored together with the real-time snapshots. An example is shown in Figure 5.11.

Figure 5.11: x_{50} time curve in-line monitoring (10 seconds averaging window)

5.3.4 Application in process development

In general, pelletizing is performed as the last step of a hot-melt extrusion process, with formulations comprising a carrier matrix, an API and possible functional additives. The material properties (rheology, heat capacity, heat conductivity...) of such mixtures are difficult to measure. In some cases, the properties are also time dependent, i.e., they depend on the processing history in the extruder as well. Thus, the prediction of a process window is difficult due to the complex interactions. A common approach is to start with known parameters, e.g., for a similar formulation or pure components and to stepwise adjust the process towards an optimum setup with satisfactory product quality criteria. This approach can be sped up by providing real-time information.

Figure 5.12 shows four examples of visual real-time information. The Eudragit pellets (A) were acorn-shaped. This shape was probably obtained by a predominant elastic behavior. The pellets were teed off like a golf ball by momentum transfer of the impacting knife during cutting. Thereby, the material in the die plate section was expanded and contracted until it ruptured. The CaSt pellets (B) show occasional voids or shrinking holes in the pellets, which occurred when gas was entrapped in the melt passing the die section or volume contraction during cooling. Here, information about the surface texture can be obtained, which can exhibit various forms for complex systems, e.g., CaSt with liquid crystal meso-phases. Image (C) shows elongated pellets, which are sometimes termed longs, elbows or sausages. Furthermore, it shows another surface texture of CaSt, namely a glossy appearance. Image (D) shows almost spherical pellets after adjustment of the process parameters.

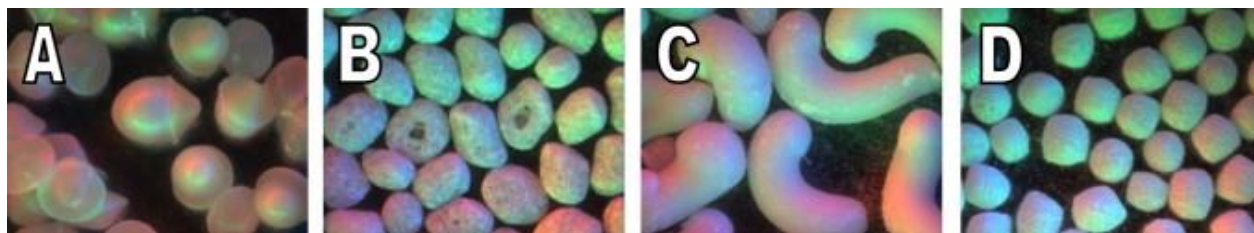


Figure 5.12: Off-line snapshots of pellets consisting of (A) Eudragit, (B) CaSt with rough surface and shrinking holes, (C) CaSt with glossy surface texture and (D) almost spherical CaSt pellets

These examples demonstrate that an imaging method based on diffusive light can provide, besides the PSD, important visual properties, such as surface texture, void detection and information about shape. However, the qualitative visual information is not further processed by the applied in-line measurement system. Thus, additional analysis tools are required to transform this visual information into quantitative measures for quality assessment.

Finally, it is recommended to implement a separation mechanism to separate the product into acceptable or unacceptable quality, e.g., by using a switch for the product stream. In this case, a suitable residence time between the image analysis and the switch must be chosen.

5.4 Conclusion

It has been shown that photometric stereo image analysis is a suitable tool to monitor particle size distribution and shape of pellets produced by hot melt extrusion with hot–die face pelletizing. Challenges concerning the limitations of a very low volume fraction of particles in the transportation air had to be overcome. Additionally, random orientation of the particles was necessary, in order to obtain statistically valid data. The selected measurement setup included an impact separator to split pellets from the transportation gas and measurement of the pellets directly after a vibratory chute in a lateral position. After optimization, the amount of measured pellets was still only about 500 for 10 min sample time, compared to around 10^5 pellets for off-line analysis.

The reduction in the x_{50} of the pellets by increasing the pelletizer rotational speed could be accurately monitored and was verified off-line by reference measurements. Despite the small amount of pellets measured in-line, good agreement in x_{50} for both methods was found. Image shape information was found to be a significant advantage of the diffusive light methodology. It allowed capturing of in-line information about surface texture and shape. This is of particular importance for development purposes, when for example, the interactions of a process parameter with a specific product property or set of properties is subject to research.

Based on the results, photometric stereo image analysis appears to be a suitable tool for in-line measurement of particle size and shape. A drawback of the current image analysis algorithm is the restriction to diffusive-reflective materials.

5.5 Acknowledgements

This work has been funded by the Austrian COMET Program by the Austrian Federal Ministry of Transport, Innovation and Technology (bmvit), the Austrian Federal Ministry of Economy, Family and Youth (bmwfj) and by the State of Styria (Styrian Funding Agency SFG). We thank our colleagues from the extrusion group at the Research Center Pharmaceutical Engineering for making this work possible.

5.6 Reference

- [1] J. Breitenbach, "Melt extrusion: from process to drug delivery technology," *Eur. J. Pharm. Biopharm.*, vol. 54, no. 2, pp. 107–117, Sep. 2002.
- [2] D. A. Miller, J. T. McConville, W. Yang, R. O. Williams III, and J. W. McGinity, "Hot-melt extrusion for enhanced delivery of drug particles," *J. Pharm. Sci.*, vol. 96, no. 2, 2007.
- [3] N. Follonier, E. Doelker, and E. T. Cole, "Various ways of modulating the release of diltiazem hydrochloride from hot-melt extruded sustained release pellets prepared using polymeric materials," *J. Control. Release*, vol. 36, no. 3, pp. 243–250, Oct. 1995.
- [4] F. Zhang and J. W. McGinity, "Properties of sustained-release tablets prepared by hot-melt extrusion," *Pharm. Dev. Technol.*, vol. 4, no. 2, 1999.
- [5] C. De Brabander, C. Vervaet, and J. . Remon, "Development and evaluation of sustained release mini-matrices prepared via hot melt extrusion," *J. Control. Release*, vol. 89, no. 2, pp. 235–247, Apr. 2003.
- [6] F. Podczeck and B. Jones, "Dry Filling of Hard Capsules," in *Pharmaceutical Capsules*, PhP Pharmaceutical Press, 2004, p. 288.
- [7] R. Chopra, F. Podczeck, J. M. Newton, and G. Alderborn, "The influence of pellet shape and film coating on the filling of pellets into hard shell capsules," *Eur. J. Pharm. Biopharm.*, vol. 53, no. 3, pp. 327–333, May 2002.
- [8] S. Abdul, A. V Chandewar, and S. B. Jaiswal, "A flexible technology for modified-release drugs: multiple-unit pellet system (MUPS)," *J. Control. Release*, vol. 147, no. 1, pp. 2–16, Oct. 2010.
- [9] D. Ghanam and P. Kleinebudde, "Suitability of κ -carrageenan pellets for the formulation of multiparticulate tablets with modified release," *Int. J. Pharm.*, vol. 409, no. 1–2, pp. 9–18, May 2011.
- [10] C. Vervaet, L. Baert, and J. P. Remon, "Extrusion-spheronisation A literature review," *Int. J. Pharm.*, vol. 116, no. 2, 1995.
- [11] C. Lustig-Gustafsson, H. Kaur Johal, F. Podczeck, and J. M. Newton, "The influence of water content and drug solubility on the formulation of pellets by extrusion and spheronisation," *Eur. J. Pharm. Sci.*, vol. 8, no. 2, 1999.
- [12] C. R. Young, J. J. Koleng, and J. W. McGinity, "Production of spherical pellets by a hot-melt

- extrusion and spheronization process,” *Int. J. Pharm.*, vol. 242, no. 1–2, 2002.
- [13] S. Bialleck and H. Rein, “Preparation of starch-based pellets by hot-melt extrusion.,” *Eur. J. Pharm. Biopharm.*, vol. 79, no. 2, pp. 440–448, Oct. 2011.
- [14] E. Roblegg, E. Jäger, A. Hodzic, G. Koscher, S. Mohr, A. Zimmer, and J. Khinast, “Development of sustained-release lipophilic calcium stearate pellets via hot melt extrusion.,” *Eur. J. Pharm. Biopharm.*, vol. 79, no. 3, pp. 635–45, Nov. 2011.
- [15] R.-K. Mürb, “Kunststoff granulieren und/oder pelletieren?,” *Chemie Ing. Tech.*, vol. 84, no. 11, pp. 1885–1893, Nov. 2012.
- [16] A. F. T. Silva, A. Burggraeve, Q. Denon, P. Van der Meeren, N. Sandler, T. Van Den Kerkhof, M. Hellings, C. Vervaet, J. P. Remon, J. A. Lopes, and T. De Beer, “Particle sizing measurements in pharmaceutical applications: comparison of in-process methods versus offline methods.,” *Eur. J. Pharm. Biopharm.*, Apr. 2013.
- [17] K. Lövgren and P. J. Lundberg, “Determination of sphericity of pellets prepared by extrusion/spheronization and the impact of some process parameters,” *Drug Dev. Ind. Pharm.*, vol. 15, no. 14–16, 1989.
- [18] A. Burggraeve, N. Sandler, J. Heinämäki, H. Räikkönen, J. P. Remon, C. Vervaet, T. De Beer, and J. Yliruusi, “Real-time image-based investigation of spheronization and drying phenomena using different pellet formulations.,” *Eur. J. Pharm. Sci.*, vol. 44, no. 5, pp. 635–42, Dec. 2011.
- [19] P. R. Wahl, D. Treffer, S. Mohr, E. Roblegg, G. Koscher, and J. G. Khinast, “Inline monitoring and a PAT strategy for pharmaceutical hot melt extrusion.,” *Int. J. Pharm.*, Jul. 2013.
- [20] D. Treffer, P. Wahl, D. Markl, G. Koscher, E. Roblegg, and G. J. Khinast, “Hot Melt Extrusion as a Continuous Pharmaceutical Manufacturing Process,” in *Melt Extrusion: Materials, Technology and Drug Product Design*, M. A. Repka, N. Langley, and J. DiNunzio, Eds. aapspress, 2013.
- [21] R. J. Woodham, “Photometric Method for determining Surface Orientation from Multiple Images.,” *Opt. Eng.*, vol. 19, no. 1, 1980.
- [22] P. Hansson and J. Fransson, “Color and shape measurement with a three-color photometric stereo system,” *Appl. Opt.*, vol. 43, no. 20, 2004.
- [23] H. G. Merkus, *Particle Size Measurements*. Springer Science+Business Media B.V., 2009.
- [24] M. Stieß, “Partikelmesstechnik,” in *Mechanische Verfahrenstechnik - Partikeltechnologie 1*, 2009,

pp. 161–260.

- [25] W. S. Rasband, “ImageJ: Image processing and analysis in Java,” *Astrophys. Source Code Libr. Rec. ascl1206.013*, vol. 6, 2012.

*“You can’t climb the ladder of success with your
hands in your pockets”*

Arnold Schwarzenegger

6 Findings and Future Directions

6.1 Findings

The main finding of chapter 2 is the so called VCM tool, which is a novel approach for rapid sample preparation and screening of pharmaceutical formulations. It is the result of a combination of existing technologies, into a new and straight forward sample preparation method. The inventive step to cover the lateral surface of the sample chamber, by simply wrapping up a PTFE foil, laid the foundation for the adaptive geometry of the VCM tool. This adaptability makes it capable to compensate volume changes (due to temperature and phase changes) of the sample material during the preparation. In addition, the vacuum compaction enables small dimensions of the VCM tool and enclosed phase boundary free samples within short cycle times. The applicability for pharmaceutical substances was demonstrated in a rheological study, which resulted in accurate and precise results.

In chapter 3, one of the major problems in melt processing, undesired sticking to parts of the processing equipment, was investigated. The major finding of this part of the thesis is the contact temperature tack hypothesis. To our best knowledge, this hypothesis relates, for the first-time adhesion properties and heat transfer. Fascinatingly, the contact temperature (which is also referred to as the interfacial temperature), jumps to a constant temperature and remains at this temperature over time, when both phases can be assumed as semi-infinite bodies. The contact temperature can serve as criterion for sticking. Sticking occurs when at least one phase remains liquid at the interface. Liquids are able to wet surfaces, which is the main requirement for sticking. When the interfacial temperature is too low, both phases are instantaneously solid on contact, no wetting

occurs and sticking is avoided. Experimental data from probe tack experiments on samples prepared using the VCM tool (from chapter 2) supports the hypothesis.

In chapter 4 the redesign of the heat balance of a die face pelletizer is described. Die face pelletizing is a downstream option to pharmaceutical hot melt extrusion. The redesign was made to broaden the processing window to sticky pharmaceutical formulations. The idea emerged when the contact temperature tack hypothesis was born and one thing led to another. It was understood that cold surfaces are required to solve the sticking issues in melt processing. The heat transfer of the conventional system was analyzed and necessary changes were made. The main finding is the thermal decoupling of cutting tools from the flow channel, which is required to obtain different temperature levels at both components. Subsequently, a prototype with a thermally decoupled design was developed and successfully tested. Substances which were formerly classified as “not processable” or “to be sticky” by the users, as only empirical knowledge existed, were now successfully processed by the novel equipment.

In chapter 5 of this thesis, the implementation of an analyzing imaging method to monitor pellets, revealed the importance of random pellet orientation to obtain statistically valid data. In die face pelletizing, the shaping mechanisms are not fully understood, and spherical, regular shaped cylinders, or irregular pellet shapes can occur, depending on the formulations flow behavior and processing parameters. This makes the implementation difficult, while spherical particles are easy to monitor, because the necessary information can be derived from a two-dimensional image. Regular (e.g. flat cylinders) and irregular shaped particles require either a fully resolved three-dimensional analysis, or statistical random representation of the measurement zone of an image based method. An implementation with free falling particles in the measurement zone was identified as the most promising approach to achieve reliable pellet monitoring results with the tested photometric stereo imaging method.

6.2 Future Directions

The VCM approach [1] has great potential to empower scientists to reach their requested results faster. Numerous applications are currently under investigation; one obvious application is to extend the concept from the rheological application towards dynamical mechanical thermal analysis (DMTA). The required measurement bodies are in DMTA of rectangular shape (e.g. 10x40x1 mm) and require dedicated VCM tools, which are under development in a joint research project at the MeltPrep GmbH and RCPE GmbH. Both the rectangular and the circular shapes can be useful for various pharmaceutical applications. New formulations can be prototyped without extruder, and within a couple of hours, which is an enormous saving in time compared to the conventional mini-extrusion approaches. In addition, multilayer structures with different formulation elements can simply be prototyped and evaluated regarding their properties, for example their dissolution profiles. Even though not-obvious at first sight, there are fascinating applications of the VCM tool to be found in the field of spectroscopy. Phase boundaries within the investigated samples are problematic, as the radiation beam scatters at interfaces and the signal is distorted or weakened. The VCM approach can help to get rid of phase boundaries and provide the optimal solution for sample preparation of the thermoplastic materials in spectroscopy.

The developed contact temperature tack hypothesis [2] provides a fundamental basis for understanding why polymer melts may stick to hot surfaces, while they do not stick to cold surfaces. However, there are also substances (e.g. purge materials) that do not stick to warm surfaces either. As outlined in the publication, this phenomenon is not fully understood and is probably linked to the Dahlquist criteria [3-4], or the occurrence of a yield-point of non-sticky materials. The in-depth investigation of the correlations between rheological parameters, adhesion, wetting and heat transfer will be an exciting area for further research.

In die face pelletizing, the processing window was significantly increased within this work [5]. Almost all thermoplastic substances with suitable viscosity levels can be processed by the novel thermally decoupled die plate design. However, as investigated by the pellet monitoring

publication, the shaping process of the pellets is not fully understood. Only empirical knowledge on the pellet shaping process existed until recently, first publications appeared, describing concepts in a similar technology, the underwater pelletizing [6-7], which could be transferred to the air-cooled die face cutting. The task is challenging, as the influencing factors are manifold: heat transfer, fluid mechanics, surface properties, kinetics, tribology, complex rheology, as well as phase changes. All factors are relevant at two different time scales: firstly, within a few milliseconds, when the actual cutting takes place, and secondly within seconds, when the pellets are conveyed until they reach the product container. The complex task could be approached with first principle models, similarly described by Kast [6] and require validation experiments with well-characterized materials and process parameters. A comprehensive material properties database and high speed imaging as well as an in-line monitoring tool [8] are a prerequisite for the validation. This field of research will be exciting to participate and to follow in the future.

6.3 References

- [1] D. Treffer, A. Troiss, and J. Khinast, “A novel tool to standardize rheology testing of molten polymers for pharmaceutical applications,” *Int. J. Pharm.*, vol. 495, no. 1, pp. 474–481, 2015.
- [2] D. Treffer and J. G. Khinast, “Why Hot Melts Do Not Stick to Cold Surfaces,” *Polym. Eng. Sci.*, 2016.
- [3] C. A. Dahlquist, “Tack,” in *Adhesion: fundamentals and practice: a report of an international conference held at the University of Nottingham, England, 20-22 September 1966*, 1969.
- [4] B. E. Gdalin, E. V. Bermesheva, G. A. Shandryuk, and M. M. Feldstein, “Effect of Temperature on Probe Tack Adhesion: Extension of the Dahlquist Criterion of Tack,” *J. Adhes.*, vol. 87, pp. 111–138, 2011.
- [5] D. Treffer, G. Koscher, and J. G. Khinast, “Die Face Pelletizing of Sticky HME Formulations,” in *AIChE Annual Meeting Conference Proceedings*, 2014.
- [6] O. Kast, K. Geiger, E. Grünschloss, and C. Bonten, “Analysis of Pellet Shaping Kinetics at the Die Opening in Underwater Pelletizing Processes,” *Polym. Eng. Sci.*, vol. 55, no. 5, pp. 1170–1176, 2015.
- [7] O. Kast, M. Musialek, K. Geiger, and C. Bonten, “Influences on particle shape in underwater pelletizing processes,” vol. 20, pp. 20–23, 2014.
- [8] D. Treffer, P. R. Wahl, T. R. Hörmann, D. Markl, S. Schrank, I. Jones, P. Cruise, R.-K. Mürb, G. Koscher, E. Roblegg, and J. G. Khinast, “In-line implementation of an image-based particle size measurement tool to monitor hot-melt extruded pellets,” *Int. J. Pharm.*, vol. 466, no. 1–2, pp. 181–189, 2014.

7 Appendix

7.1 List of Figures

Figure 1.1: Illustration of the HME Process (reproduced with kind permission [3])	8
Figure 1.2: Overview of common downstream processes (reproduced with kind permission [3]) .	8
Figure 2.1: Sectional view of the vacuum compression tool; left: 3d explosion view, right: assembled front view.....	19
Figure 2.2: VCM Setup	21
Figure 2.3: Heating and cooling curve; the heating and cooling processes begin at 30 seconds and at 430 seconds, respectively.	25
Figure 2.4: Images of samples produced via VCM (E: EE, S: S+, R: EVA).....	26
Figure 2.5: Influence of sample preparation on flow curves of S+, (VCM: prepared by novel preparation method; powder: directly molten on the rheometer's base plate under atmospheric conditions)	27
Figure 2.6: Molten samples on the rheometer base plate; 1: homogeneous VCM before measurement; 2: direct powder melting on trim position before trimming. Here the sample contains a significant amount of air bubbles.....	28
Figure 2.7: Rheological data; top row: flow curves (markers: measured data points, line: Carreau Yasuda fits), bottom row: master curve of the measured data with reference to the highest investigated temperatures (markers: shifted measured data points, line: extrapolated Carreau-Yasuda fit at reference temperature.	29
Figure 2.8: Van Gurp Palmen plots.....	31
Figure 3.1: Heat capacity measurement S+. 1: $T_G = 73.2^\circ\text{C}$, 2: $c_p(20^\circ\text{C})=0.88 \text{ kJ}/(\text{kgK})$, 3: $c_p(150^\circ\text{C})=2.09 \text{ kJ}/(\text{kgK})$	39
Figure 3.2: Customized measurement body.....	40
Figure 3.3: Path-time diagram of the probe tack experiments.	41
Figure 3.4: Contact temperature tack hypothesis and probe tack experiment. (A) Temperature profiles at a non-isothermal interface. Case one: Tack (solid line). Case two: No tack	

- (dashed line); T_s solidification temperature polymer; T_1 bulk temperature polymer; $T_{2,T}$ bulk temperature solid sticky; $T_{2,NT}$ bulk temperature solid no tack; $T_{C,T}$ contact temperature tack; and $T_{C,NT}$ contact temperature no tack.....42
- Figure 3.5: Calculated temperature profiles. Bulk temperatures are chosen for typical processing conditions: $T_1=150^\circ\text{C}$ and $T_2=20^\circ\text{C}$; (A): Polymer melt and stainless steel; (B): Polymer melt and glass; (C): Polymer melt and solid polymer46
- Figure 3.6: Schematic illustration of the probe tack experiment: ground plate (bottom), sample (orange), temperature controlled probe. (1) initial position; (2) position after bonding; (3) and (4) debonding with (3) no tack or adhesive failure and (4) tack or cohesive failure.....47
- Figure 3.7: Snapshots of the probe tack experiments. Sample before bonding (A) and after debonding (B-D) at $T_M=170^\circ\text{C}$. (B) $T_P=130^\circ\text{C}$, adhesion with filament formation. (C) $T_P=110^\circ\text{C}$ initial adhesion and adhesive failure after some deformation. (D) $T_P=90-50^\circ\text{C}$ initial weak or non-adhesion and adhesive failure at the interface leaving a non-deformed imprint on the sample.....48
- Figure 3.8: Probe tack stress-strain diagrams at different non-isothermal conditions. Positive and negative stress values correspond to bonding and debonding, respectively. Top row: series 1, $T_M=170^\circ\text{C}$, $t_c=1$ s. Middle row: series 2, $T_M=170^\circ\text{C}$, $t_c=5$ s. Bottom row: series 3, $T_M=150^\circ\text{C}$, $t_c=1$ s. T_P is decreasing from left to right ($150-50^\circ\text{C}$). Glass transition of the polymer temperature is 73°C48
- Figure 3.9: Bonding and debonding trend diagrams. (Reverse x-axis, T_P probe temperature). (A): $\sigma_{b,max}$ maximum bonding stress; (B): w_b bonding work; (C): $\sigma_{d,max}$ maximum debonding stress; (D): w_d debonding work49
- Figure 4.1: Schematics of (A) strand pelletizing and (B) die-face pelletizer (Picture courtesy: Automatik Plastics Machinery GmbH)56
- Figure 4.2: Illustration of the contributions that need to be considered in the energy balance of a conventional die plate.....63

Figure 4.3: Contributions to the energy balance for a knife used on a conventional die plate63

Figure 4.4: Calculated temperature profile of a conventional die plate (2 die holes with a 1 mm bore diameter).....63

Figure 4.5: Illustration of the contributions to the energy balance of the thermally decoupled design65

Figure 4.6: Extracted knife heat balance in combination with the thermally decoupled die plate 65

Figure 4.7: Calculated temperature profile of the thermally decoupled design (2 die holes with 1 mm bore diameter)65

Figure 4.8: Sectional view of the modular thermally decoupled die plate.....66

Figure 4.9: Close-up of the die hole.....66

Figure 4.10: Pictures of the pellets produced by DFP and the thermal decoupled die plate prototype (EE pellet diameter 0.8 mm)67

Figure 5.1: Process options in combination with a die-face pelletizing step73

Figure 5.2: Picture of the Sphero®-THA and a detailed 3D illustration of the cutting chamber (Picture courtesy: Automatik Plastics Machinery GmbH).....76

Figure 5.3: A: photometric stereo illumination arrangement (3 RGB LEDs); B: ellipses fitted to detected particles (Picture courtesy: Innopharma Labs Ltd.).....77

Figure 5.4: Implementation approaches80

Figure 5.5: Snapshots of pellets with different optical properties. A: diffuse reflecting CaSt pellets; B: transparent EVA pellets (note the RGB light sources); C: detail view of the highlighted region in Image B; D: reflecting EVA pellets (in-line).....82

Figure 5.6: Snapshots the partial separation implementation83

Figure 5.7: Snapshots of pellets obtained with complete air separation and camera position above the vibrating conveyor (cutting frequency; left-low; center-middle; right-high).....84

Figure 5.8: Snapshots of the implementation with complete pellet separation and lateral camera position85

Figure 5.9: Snapshots at 2000 rpm (left) and 3600 rpm (right). Note the different length to diameter ratio of the pellets.88

Figure 5.10: Comparison of the in-line PSD data to the reference method (I: In-line measurement; R: Reference measurement)88

Figure 5.11: x50 time curve in-line monitoring (10 seconds averaging window)90

Figure 5.12: Off-line snapshots of pellets consisting of (A) Eudragit, (B) CaSt with rough surface and shrinking holes, (C) CaSt with glossy surface texture and (D) almost spherical CaSt pellets.....91

7.2 List of tables

Table 2.1: Influence of sample preparation on the S+ measurement reproducibility (T: Temperature; RSD: averaged standard deviation of all measured data points; RF: reduction factor; η_0 * <i>FIT</i> fitted complex zero shear viscosity; RD: relative deviation; $\eta\omega = 526 \text{ s}^{-1}$ * measured complex viscosities at an angular frequency of 526 s^{-1})	28
Table 2.2: Summarized Carreau-Yasuda and TTS Parameters (EE: $T_1=150^\circ\text{C}$, $T_2=140^\circ\text{C}$, $T_3=130^\circ\text{C}$; S+: $T_1=160^\circ\text{C}$, $T_2=150^\circ\text{C}$, $T_3=140^\circ\text{C}$; EVA: $T_1=140^\circ\text{C}$, $T_2=130^\circ\text{C}$, $T_3=120^\circ\text{C}$).	30
Table 2.3: Summarized reproducibility of the measured data (RSD: averaged standard deviation of all measured data points, Residuals: averaged relative error of all measured data points compared to the Carreau-Yasuda model data).	31
Table 3.1: Material properties. S+ densities and thermal conductivities are taken from [32], SS: stainless steel, grade 1.4301, G: SiO ₂ glass.....	45
Table 4.1: Applied material properties.....	61
Table 5.1: Overview of the image analysis relevant results for the three setups	86
Table 5.2: PSD width classification [23]	89
Table 5.3: Comparison of important PSD measures of Figure 5.10 (I: In-line measurement; R: Reference measurement)	89
Table 5.4: Comparison of particle shape measures of Figure 5.10 (I: In-line measurement; R: Reference measurement)	90

7.3 List of publications

7.3.1 Peer reviewed papers

Treffer, D. F., Khinast, J.: *Why hot melts do not stick to cold surfaces*, - in: Polymer Engineering & Science (2016), in press - accepted manuscript

Witz, C.; Treffer, D.; Hardiman, T.; Khinast, J.; *Local gas holdup simulation and validation of industrial-scale aerated bioreactors*, - in: Chemical Engineering Science (2016), 152, 636 - 648

Eggenreich, K.; Windhab, S.; Treffer, D.; Juster, H.; Steinbichler, G.; Laske, S.; Koscher, G.; Roblegg, E.; Khinast J.: *Injection molding as a one-step process for the direct production of pharmaceutical dosage forms from primary powders*, - in: International journal of pharmaceutics (2016), 1-2, 341 - 351

Treffer, D. F.; Troiss, A.; Khinast, J.: *A Novel Tool to Standardize Rheology Testing of Molten Polymers for Pharmaceutical Applications*, - in: International journal of pharmaceutics (2015), 1, 474 - 481

Treffer, D. F.; Wahl, P.; Hörmann, T. R.; Markl, D.; Schrank, S.; Jones, I.; Cruise, P.; Mürb, R.-K.; Koscher, G.; Roblegg, E.; Khinast, J.: *In-line implementation of an image-based particle size measurement tool to monitor hot-melt extruded pellets*. - in: International journal of pharmaceutics (2014) 2, 181 – 189

Wahl, P.; Treffer, D. F.; Mohr, S.; Roblegg, E.; Koscher, G.; Khinast, J.: *Inline monitoring and a PAT strategy for pharmaceutical hot melt extrusion*. - in: International journal of pharmaceutics (2013) 455, 159 – 168

7.3.2 Book Chapters:

Treffer, D. F.; Wahl, P.; Markl, D.; Koscher, G.; Roblegg, E.; Khinast, J.: *Hot Melt Extrusion as a Continuous Pharmaceutical Manufacturing Process*. - in: Melt Extrusion. (2013), 363 – 396

7.3.3 Patent Applications:

Treffer, D. F.; Grubbauer, J. Koscher, G.; Khinast, J.: *Apparatus, method and system for moulding a thermoplastic material by vacuum compression moulding*, PCT/EP2015/064547, 2014

Treffer, D. F.; Eitzlmayr, A.; Grubbauer, J.; Koscher, G.; Khinast, J.: *Hot viscous raw material leaving a cooler perforated plate cooling a cutter*, PCT/EP2014/067449, 2013

7.3.4 Conference Talks:

Treffer, D. F.; Hörmann, T.; Koscher, G.; Khinast, J.; *Prozessentwicklung zur Herstellung schmelzextrudierter pharmazeutischer Produkte*, - in 41. Deutsche Compoundiertagung - Prozessoptimierung an Compoundieranlagen, Nuremberg, Germany, 03.12.2015

Witschnigg, A.; Koscher, G.; Treffer, D.F.; Mürb, R.K.; Laske, S.; Khinast, J; *Micro-pelletizing of pharmaceutical HME formulations using a die face pelletizer*, - in Polymer Processing Society Conference, Graz, Austria, 24.09.2015

Treffer, D. F.; Troiss, A.; Khinast, J.: *Novel Vacuum Compression Molding as a Tool for Sample Preparation in Rotational Melt Rheology*, - in Polymer Processing Society Conference, Graz, Austria, 24.09.2015

Treffer, D. F.; Troiss, A.; Khinast, J.: *Novel Vacuum Compression Molding as a Tool for Sample Preparation in Rotational Melt Rheology*, - in 24th Nordic Rheology Conference, Karlstad Sweden, 19.08.2015

Treffer, D. F.; Koscher, G.; Khinast, J.: *Die Face Pelletizing of Sticky HME Formulations*. - in: AIChE 2014 - Annual Meeting. Atlanta: 16.11.2014

Treffer, D. F.; Koscher, G.; Khinast, J.: *Die Face Pelletizing of Sticky HME Formulations*. - in: ICPE 6th international Congress on Pharmaceutical Engineering 2014 - Graz: 16-17.6.2014

Wahl, P.; Markl, D.; Treffer, D. F.; Sacher, S.; Koscher, G.; Roblegg, E.; Khinast, J.: *PAT for Pharmaceutical Extrusion: In-line Monitoring of Drug Content with NIR*. - in: PAT & QbD Meeting 2013. Dresden: 10.06.2013

Treffer, D. F.: *Rheological Measurements in the Field of Pharmaceutical Hot Melt Extrusion - from user's point of view*. - in: Rheology Workshop in Ghent. Ghent: 18.09.2013

Treffer, D. F.; Eggenreich, K.; Schrank, S.; Koscher, G.; Roblegg, E.; Khinast, J.: *Injection Moulding as a One-Stop-Production to Produce Pharmaceutical Dosage Forms*. - in: 2013 AIChE Annual Meeting. San Francisco: 03.11.2013

Treffer, D. F.; Eitzlmayr, A.; Smola, C.-M.; Koscher, G.; Roblegg, E.; Khinast, J.: *Continuous Pharmaceutical Hot-Melt Extrusion & Hot-Die Face Pelletizing*. - in: AIChE Annual Meeting 2012. Pittsburgh: 28.10.2012

Wahl, P.; Markl, D.; Treffer, D. F.; Sacher, S.; Menezes, J. C.; Koscher, G.; Roblegg, E.; Khinast, J.: *PAT for Pharmaceutical Extrusion Monitoring and Supervisory Control*. - in: AIChE 2012 Annual Meeting. Pittsburgh: 28.10.2012

Eitzlmayr, A.; Treffer, D. F.; Hörl, G.; Windhab, S.; Koscher, G.; Khinast, J.: *Predictive Modeling of Hot Melt Extruders*. - in: 2012 AIChE Annual Meeting. Pittsburgh, PA: 28.10.2012

Eitzlmayr, A.; Treffer, D. F.; Jedinger, N.; Koscher, G.; Roblegg, E.; Khinast, J.: *Hot Melt Extrusion: Product and Process Development*. - in: 6th Annual PSSRC Symposium. Lisbon: 26.08.2012

Wahl, P.; Markl, D.; Treffer, D. F.; Koscher, G.; Roblegg, E.; Khinast, J.: *PAT Solution for Inline Content Homogeneity Monitoring with NIR for Pharmaceutical Hot Melt Extrusion*. - in: 8. Minisymposium der Verfahrenstechnik.: 02.05.2012

Wahl, P.; Markl, D.; Treffer, D. F.; Koller, D. M.; Koscher, G.; Roblegg, E.; Khinast, J.: *Full PAT Solution for Real-Time Process Control of a Pharmaceutical Hot Melt Extruder (HME)*. - in: 8th

World Meeting on Pharmaceutics, Biopharmaceutics and Pharmaceutical Technology. Istanbul:
19.03.2012

7.3.5 Posters:

Treffer, D. F.; Troiss, A.; Khinast, J.; *Melt Rheology of Selected Pharmaceutical Polymers for Hot Melt Extrusion*, - in Polymer Processing Society Conference, Graz Austria, 24.09.2015

Treffer, D. F.; Troiss, A.; Khinast, J.; *Melt Rheology of Selected Pharmaceutical Polymers for Hot Melt Extrusion*. – in 24th Nordic Rheology Conference, Karlstad Sweden, 19.08.2015 – rewarded with the best poster award

Treffer, D. F.; Wahl, P.; Hörmann, T. R.; Markl, D.; Eitzlmayr, A.; Schrank, S.; Koscher, G.; Roblegg, E.; Khinast, J.: *Implementation of a Novel Particle Size Measurement Tool to Monitor Pellet Produced by Hot Melt Extrusion and Die Face Pelletizing*. - in: AIChE Annual Meeting 2013. San Francisco: 03.11.2013

Treffer, D. F.; Koscher, G.; Roblegg, E.; Khinast, J.: *Application of Hot-Die Face Pelletizing for Downstream Processing of Pharmaceutical Hot-Melt Extrusion*. - in: 9. Minisymposium der Verfahrenstechnik. Leoben: 17.04.2013

Treffer, D.; Mürb, R.-K.; Koscher, G.; Khinast, J.: *Pharmaceutical Hot-Melt Extrusion and Novel Hot-Die Face Pelletizing*. - in: APV Workshop: Continuous Manufacturing. Graz, Austria am: 26.09.2012

Wahl, P.; Treffer, D.; Markl, D.; Koscher, G.; Roblegg, E.; Khinast, J.: *Developing a PAT Strategy for Pharmaceutical Hot Melt Extrusion*. - in: EuPAT 5 Continuous Innovation in Process Analytics & Control. Ghent, Belgium am: 09.05.2012

Treffer, D. F.; Sungkorn, R.; Khinast, J; *High Sensitivity Conductivity Probe for Measurement of Gas Hold-up and Mixing Time*, in - Jahrestreffen der Fachausschüsse Computational Fluid Dynamics und Mischvorgänge, Dortmund, Germany 21.02.2011

7.3.6 Degree Thesis:

Master Thesis, *Development of a measurement technique to investigate mixing behavior and gas hold-up distribution in a multi-phase reactor*; Supervisor: Johannes Khinast, Co-Supervisor: Radompon Sungkorn; 04.05.2011

Bachelor Thesis, *Auslegung, Aufbau und Inbetriebnahme eines Teststandes zur Wasserstoffproduktion nach dem Eisen-Dampf-Prozess*; Supervisor: Viktor Hacker, Co-Supervisor: Markus Thaler; 10.03.2009

7.4 Curriculum Vitae



Personal details:

Name: Daniel Franz Treffer

Nationality: Austrian

Date of Birth: 24 February 1985

Place of Birth: Wolfsberg

Address: 9413 St. Gertraud, St. Gertraud 20

Marital Status: single

E-mail: daniel.treffer@gmx.at

Mobile: +436502248027

Education:

09/2011 – 01/2017 Graz University of Technology
Doctoral School Chemical Engineering

08/2009 – 01/2010 School of Engineering Jönköping, Sweden
Erasmus Program

10/2005 – 05/2011 Graz University of Technology,
Chemical Engineering (Bachelor/Master)

1999 – 2004 HTL - Wolfsberg for Mechanical Engineering
Focus: Automation

1995 – 1999 Secondary School, St. Gertraud

1991 – 1995 Elementary School, St. Gertraud

Work experience:

03/2016 – present	CEO and Partner roombiotic GmbH
03/2015 – present	Founder and CEO MeltPrep GmbH
09/2015 – 08/2016	Project Collaborator Institute for Process and Particle Engineering Graz University of Technology
09/2011 – 08/2016	Scientist Area III: Process and Manufacturing Science Research Center Pharmaceutical Engineering
09/2011 – 08/2015	University Assistant Institute for Process and Particle Engineering Graz University of Technology
07/2010 – 05/2011	Project Collaborator, Design Study and Master Thesis, Institute for Process and Particle Engineering, Graz University of Technology
02/2010 – 06/2010	Project Collaborator, Fuel Cell Laboratory, Graz University of Technology
07/2007 – 06/2009	Project Collaborator, CD-Laboratory for Fuel Cell Systems, Graz University of Technology
11/2004 – 06/2005	Military Service

Personal skills and competences:

- Software skills: ProEngineer, Creo Simulate, Visual Basic, Labview, Matlab, Mathcad, Gimp
Fundamental CFD Experience
Excellent MS Office skills
- Languages: English, German (mother tongue)
- Associations: Alumni of the TERA – TU-Graz,
Active Member 2009-2012
We have built the most fuel-efficient vehicle,
Fennek 2010, 0.05 L Benzin / 100 km,
tera.tugraz.at

Graz, 16th December 2016